

The Pennsylvania State University

The Graduate School

College of Engineering

**THE EFFECT OF BUFFER CHARGE AND BUFFER RETENTION ON
BIOELECTROCHEMICAL SYSTEMS AND POST-TREATMENT FOR MICROBIAL
FUEL CELL EFFLUENT WITH FLUIDIZED BED MEMBRANE BIOREACTORS**

A Dissertation in

Environmental Engineering

by

Yaoli Ye

© 2017 Yaoli Ye

Submitted in Partial Fulfillment
of the Requirements
for the Degree of

Doctor of Philosophy

December 2017

The dissertation of Yaoli Ye was reviewed and approved* by the following:

Bruce E. Logan
Kappe and Evan Pugh University Professor of Environmental Engineering
Dissertation Advisor
Chair of Committee

Michael A. Hickner
Associate Professor of Materials Science and Engineering

Rachel A. Brennan
Associate Professor of Environmental Engineering

Christopher A. Gorski
Assistant Professor of Environmental Engineering

William D. Burgos
Professor of Environmental Engineering
The Graduate Program Chair

*Signatures are on file in the Graduate School

ABSTRACT

Microbial fuel cells (MFCs) and microbial electrolysis cells (MECs) are very promising technologies for simultaneous wastewater treatment and energy recovery. In MFCs, buffers are typically used to improve performance by stabilizing the electrode pH and increasing the electrolyte conductivity, but the importance of the buffer net charge at current densities typical of MFCs on cathode performance has received little attention. Current production in MFCs produces an electric field that drives cations towards the cathode, and anions to the anode. A series of biological buffers were selected with positive, negative, and neutral charges that had pK_as ranging from 5 to 10.8. Cathodic current production using these different buffers in solutions with different pHs and conductivities was compared using linear sweep voltammetry (LSV). At lower pHs, buffers with positive charge increased cathodic current by as much as 95% within certain ranges (potential windows) of cathode potentials. No difference in cathodic current was shown in current for buffers with neutral or negative charge. The reason for this increase with the net positive charge buffers was likely due to a more stable electrode pH produced by electric field driving the positively charged ions towards the cathode. The potential window for the positively charged buffers was positively correlated to the concentration of cationic buffer in the electrolyte. At a pH higher than 9, no improvement in cathodic current was shown for buffers with positive charge, indicating at these higher pHs diffusion dominated buffer transport.

In two-chamber microbial electrolysis cells (MECs) with anion exchange membranes (AEMs), a phosphate buffer solution (PBS) is typically used to avoid increases in catholyte pH as Nernst equation calculations indicate that high pHs adversely impact electrochemical performance. However, ion transport between the chambers will also impact performance, which is a factor not included in those calculations. To separate the impacts of pH and ion transport on MEC performance, a high molecular weight polymer buffer (PoB), which was retained in the

catholyte due to its low AEM transport and cationic charge, was compared to PBS in MECs and abiotic electrochemical half cells (EHCs). In MECs, catholyte pH control was less important than ion transport. MEC tests using the PoB catholyte, which had a higher buffer capacity and thus maintained a lower catholyte pH (<8), resulted in a 50% lower hydrogen production rate (HPR) than that obtained using PBS (HPR=0.7 m³-H₂ m⁻³ d⁻¹) where the catholyte rapidly increased to pH=12. The main reason for the decreased performance using PoB was a lack of hydroxide ion transfer into the anolyte to balance pH. The anolyte pH in MECs rapidly decreased to 5.8 due to a lack of hydroxide ion transport, which inhibited current generation by the anode, whereas the pH was maintained at 6.8 using PBS. In abiotic tests in ECHs, where the cathode potential was set at -1.2 V, the HPR was 133% higher using PoB than PBS due to catholyte pH control, as the anolyte pH was not a factor in performance. These results show that hydroxide ion transport through AEM to control anolyte pH is more important than obtaining a more neutral pH catholyte.

MFCs cannot effectively treat wastewater with low a COD, so a post-treatment is usually needed for polishing MFC effluent. Anaerobic fluidized bed membrane bioreactors (AFMBRs) use granular activated carbon (GAC) particles suspended by recirculation to effectively treat low strength wastewaters (~100–200 mg L⁻¹, chemical oxygen demand, COD), including MFC effluent, but the effluent contains dissolved methane. An aerobic fluidized bed membrane bioreactor (AOFMBR) was developed to avoid methane production and the need for wastewater recirculation by using rising air bubbles to suspend GAC particles. The performance of the AOFMBR was compared to an AFMBR and a conventional aerobic membrane bioreactor (AeMBR) for domestic wastewater treatment over 130 d at ambient temperatures (fixed hydraulic retention time of 1.3 h). The effluent of the AOFMBR had a COD of 20 ± 8 mg L⁻¹, and a turbidity of <0.2 NTU, for low-COD influent (153 ± 19 and 214 ± 27 mg L⁻¹), similar to the AeMBR and AFMBR. For the high-COD influent (299 ± 24 mg L⁻¹), higher effluent CODs

were obtained for the AeMBR ($38 \pm 9 \text{ mg L}^{-1}$) and AFMBR ($51 \pm 11 \text{ mg L}^{-1}$) than the AOFMBR ($26 \pm 6 \text{ mg L}^{-1}$). Transmembrane pressure of the AOFMBR increased at 0.04 kPa d^{-1} , which was 20% less than the AeMBR and 57% less than the AFMBR, at the low influent COD. Scanning electron microscopy (SEM) analysis indicated a more uniform biofilm on the membrane in AOFMBR than that from the AeMBR biofilm, and no evidence of membrane damage. High similarity was found between communities in the suspended sludge in the AOFMBR and AeMBR (square-root transformed Bray–Curtis similarity, SRBCS, 0.69). Communities on the GAC and suspended sludge were dissimilar in the AOFMBR (SRBCS, 0.52), but clustered in the AFMBR (SRBCS, 0.63).

Although the production of dissolved methane can be avoided in AOFMBR, the process is energy intensive due to the large air flowrates. In addition, ammonia nitrogen is not effectively biologically removed in either AFMBRs or AOFMBRs. Membrane aerators were added into an AFMBR to form an aerated membrane fluidized bed membrane bioreactor (AeMFMBR) capable of simultaneous removal of organic matter and ammonia without production of dissolved methane. Good effluent quality was obtained for domestic wastewater ($193 \pm 23 \text{ mg/L}$ and $49 \pm 5 \text{ mg-N/L}$) treatment, with non-detectable suspended solids ($< 2 \text{ mg/L}$), $93 \pm 5\%$ of chemical oxygen demand (COD) removal to $14 \pm 11 \text{ mg/L}$, $89 \pm 7\%$ of soluble COD removal to $13 \pm 11 \text{ mg/L}$, and $74 \pm 8\%$ of total nitrogen (TN) removal to $12 \pm 3 \text{ mg-N/L}$. Nitrate and nitrite concentrations were always low ($< 1 \text{ mg-N/L}$) during continuous flow treatment. The ammonia removal rate (AR) was higher with continuous flow treatment than fed batch operation, higher for a synthetic wastewater compared to a domestic wastewater, but independent of the hydraulic retention time. Membrane fouling was well controlled by fluidization of the granular activated carbon (GAC) particles as shown by a low transmembrane pressure ($< 3 \text{ kPa}$). No methane was detected in the treated effluent ($< 0.5 \text{ mg/L}$). Analysis of the microbial communities suggested that the nitrogen removal

was due to nitrification and denitrification based on the presence of microorganisms associated with these processes.

TABLE OF CONTENTS

LIST OF FIGURES	x
LIST OF TABLES	xiv
ACKNOWLEDGEMENTS	xv
Chapter 1 Introduction	1
1.1 Energy demand and challenge of environmental issues.....	1
1.2 Energy demand for wastewater treatment.....	1
1.3 Bioelectrochemical and membrane systems for wastewater treatment and energy recovery.....	2
1.4 Objectives.....	3
1.5 Outline of Dissertation	4
1.6 Literature cited	6
Chapter 2 Literature Review	8
2.1 BES for energy recovery from wastewater	8
2.1.1 MFC, electricity production and wastewater treatment	9
2.1.2 MEC, hydrogen production.....	22
2.1.3 MxC.....	28
2.2 Membrane bioreactor	29
2.2.1 Membrane fouling	29
2.2.2 Membrane configuration	33
2.2.3 Aerobic membrane bioreactor	33
2.2.4 Anaerobic membrane bioreactor	35
2.2.5 Anaerobic fluidized bed membrane bioreactor	37
2.3 Membrane aerators.....	39
2.3.1 Oxygenation	40
2.3.2 Hydrogen pressurized in the lumen.....	41
2.4 Literature cited	41
Chapter 3 Effect of buffer charge on performance of air-cathodes used in microbial fuel cells	59
3.1 Introduction.....	60
3.2 Methods.....	63
3.2.1 Buffer selection and solution preparation	63
3.2.2 Electrochemical analyses	66
3.3 Results.....	66
3.3.1 Impact of buffer charge for a pH similar to the buffer pKa	66
3.3.2 Buffer tests with the pH shifted away from the pKa.....	68
3.3.3 Dominant buffer species and potential window	70
3.4 Discussion	72

3.4.1 Enhanced transport by migration	72
3.4.2 Comparison with other buffer studies	74
3.5 Conclusions.....	75
3.6 References.....	76
 Chapter 4 The importance of OH ⁻ transport through anion exchange membrane in microbial electrolysis cells.....	 79
4.1 Introduction.....	80
4.2 Material and Methods	82
4.2.1 PoB synthesis and preparation	82
4.2.2 Buffer retention and buffer capacity tests	83
4.2.3 MEC operation and hydrogen test.....	84
4.2.4 Electrochemical tests.....	85
4.2.5 Calculations.....	86
4.3 Results and discussion	87
4.3.1 Characterization of PoB and buffer retention test	87
4.3.2 Hydrogen production in MECs with AEM after 1 cycle.....	89
4.3.3 Hydrogen production in MECs with AEM in 3 cycles	91
4.3.4 Hydrogen production tests in EHCs with AEM.....	93
4.3.5 MECs with PoB without catholyte over 15 cycles.....	95
4.3.6 Outlook.....	96
4.4 Conclusions.....	98
4.5 References.....	99
 Chapter 5 An aerated and fluidized bed membrane bioreactor for effective wastewater treatment with low membrane fouling	 103
5.1 Introduction.....	104
5.2 Materials and Methods.....	106
5.2.1 Reactor design	106
5.2.2 Reactor operation	107
5.2.3 Measurement and analysis	108
5.3 Results.....	110
5.3.1 Effluent quality and COD removal	110
5.3.2 Effluent Turbidity.....	113
5.3.3 Transmembrane pressures	114
5.3.4 SEM imaging.....	115
5.3.5 Microbial community analysis	117
5.3.6 Energy production and consumption.....	118
5.4 Discussion	121
5.4.1 Enhanced effluent quality and membrane fouling control	121
5.4.2 Microbial community analysis	124
5.4.3 Energy consumption.....	125
5.5 Conclusions.....	127
5.6 References.....	128

Chapter 6 Simultaneous nitrogen and organics removal using membrane aeration and effluent ultrafiltration in an anaerobic fluidized membrane bioreactor	133
6.1 Introduction.....	133
6.2 Material and Methods	136
6.2.1 Reactor setup.....	136
6.2.2 Operation.....	137
6.2.3 Analytical methods.....	139
6.3 Results and Discussion.....	141
6.3.1 Nitrogen removal with COD-free synthetic wastewater	141
6.3.2 COD and nitrogen removals using synthetic wastewater.....	143
6.3.3 COD and nitrogen removal using diluted domestic wastewater	145
6.3.4 Transmembrane pressure, DO and dissolved methane.....	146
6.3.5 Microbial community analyses	149
6.3.6 Overall assessment and future studies.....	150
6.4 Conclusions.....	151
6.5 References.....	152
Chapter 7 Future studies	157
Appendix A Effect of buffer charge on performance of air-cathodes used in microbial fuel cells	160
Appendix B The importance of OH ⁻ transport through anion exchange membrane in microbial electrolysis cells.....	163
Appendix C An aerated and fluidized bed membrane bioreactor for effective wastewater treatment with low membrane fouling	167
Appendix D Simultaneous nitrogen and organics removal using membrane aeration and effluent ultrafiltration in an anaerobic fluidized membrane bioreactor	174

LIST OF FIGURES

Fig. 2-1 Possible anode and cathode reactions in BESs (9).....	9
Fig. 2-2 Extracellular electron transfer mechanisms. From top to bottom, direct electron transfer, nanowire and mediator (31).....	13
Fig. 2-3 The air cathode structure with a catalyst layer facing the solution side, and a carbon layer and diffusion layer facing the air side (49).....	16
Fig. 2-4 Membrane fouling mechanism (a) pore blocking and (b) cake layer (107).....	30
Fig. 2-5 Three common membrane configurations: (a) external flow membrane; (b) submerged membrane; (c) external submerged membrane (119).....	32
Fig. 2-6 The schematic diagram of the MABR (155).....	39
Fig. 3-1 Diagram of (A) a positively charged and (B) a neutrally charge buffer interfacing with cathode in an MFC.....	68
Fig. 3-2 A. Comparison of LSVs of three different buffers (with the charge of +, -, 0) with and pH 5 in a high concentration (HC) solution (7 mS/cm). For comparisons of different buffers at different pHs, the current is compared at two different potentials: current production corresponding to cathode potential and conductivity of B. 0 V and 7 mS/cm (HC), C. -0.1 V and low conductivity (LC), D. 0 V and LC, E. -0.1 V and LC. The electrolyte conductivity for each low conductivity condition are at the top of bars.....	69
Fig. 3-3 Current production obtained from LSVs at the potential of A. 0 V and B. -0.1 V through adjusting buffers from pKa 8 to pH 7, 8, 9 with conductivity of 5.5 mS/cm (LC).....	71
Fig. 3-4 Current obtained in LSVs at the potential of A.0 V and B. -0.1 V, using diethanolamine and CAPS (pKa 10.8) at pHs of 9.8, 10.8, and 12 in low conductivity electrolyte (LC, 4.9 mS/cm).....	71
Fig. 3-5 Adjusting buffers with pKa 8 to pH 7 and comparing with buffers with pKa 7 (pH 7) under the same conductivity of 6.5 mS/cm	72
Fig. 4-1 The percentage of PoB or phosphate (PBS) buffers retained in (A) diffusion tests using an AEM (without current) and (B) in MECs. The dashed line (minimum) shows the result that would be based on equilibrium between the two chambers each time the counter electrolyte solution was changed (eq. 4-1). (B) The retention of PBS in MEC with AEM.....	88
Fig. 4-2 (A) Current (C, open symbols) and hydrogen production (H, filled symbols) using PoB or phosphate (PBS) buffers in MECs with AEMs in three, one-day cycles.	

- The anolyte was replaced daily, while the catholyte was not. (B) the anode potential of the MECs with PoB and PBS 89
- Fig. 4-3** (A) Changes in the pH of the anolytes (-An) and catholytes (-Cat) in MECs with AEMs. Schematic showing the main ions that are expected to be transported through the AEM with (B) PBS and (C) PoB. 91
- Fig. 4-4** (A) Hydrogen production (H, filled symbols) and current (C, open symbols) in an electrochemical cell separated using an AEM, with PoB and PBS as catholyte, at a fixed cathode potential of -1.2 V. The negative current indicates a reduction reaction. (B) Changes in pH of the anolytes (An) and catholytes (Cat) in electrochemical half cells with PoB or phosphate (PBS) buffers. 93
- Fig. 4-5** Conductivities of the anolytes (An) and catholyte (Cat) over three days with one day cycles, with anolyte replaced daily in (A) MECs and (B) EHCs. 95
- Fig. 4-6** Current and the anode potentials of MECs with PoB over a single, 24-h cycle after 15 cycles without catholyte replacement. 96
- Fig. 5-1** Average CODs and SCODs in the effluents of the AFMBR (AF), AOFMBR (AO), and AeMBR (MBR) in four Phases of operation. The standard deviations for COD is in black and for SCOD is in blue. The corresponding removal efficiencies are shown above the bar chart. The thick lines below each designation indicate whether the effluent of one reactor has significantly different average COD compared with others. If the colors are the same, the average CODs are not significantly different, while if the colors are different, the average COD are different based on analysis using the Student's T-test. 111
- Fig. 5-2** Effluent turbidity over time measured for the three different types of membrane bioreactors. The inset shows the low turbidity range. 114
- Fig. 5-3** Transmembrane pressure over time with the flux of 11.6 L/m²-membrane-h. The lines were obtained by linear fitting of the TMP over the first two phases, where the slopes were 0.04 (AOFMBR), 0.05 (MBR), and 0.09 (AFMBR) kPa/d. 114
- Fig. 5-4** SEM images with the magnitude of $10,000 \times$ (A–D) and $125 \times$ (E – H) for the surfaces of the membranes in the reactor of AFMBR (A and E), AOFMBR (B and F), AeMBR (C and G) and abiotic membrane (D and H). 116
- Fig. 5-5** (A) Similarity among the GAC or suspended biomass samples in the different reactors presented as an mMDS plot. (B) Analysis of the microbial communities in the solution (S) and on the GAC (G) in the AOFMBR (AO), AFMBR (AF) and AeMBR (MBR) reactors based on relative abundance at the genera level. Only genera with a relative abundance $>1\%$ were included, Unclassified sequences and minor genera (relative abundance $<1\%$) were summarized at the phylum level. Vertical lines with different colors separate bacteria into 7 phyla. Archaea is shown as a kingdom. 119

Fig. 6-1 Schematic of the AeMFMBR showing locations of the aeration and filtration membranes.	136
Fig. 6-2 Comparison of ammonia removal rate (AR) in each of the six phases of operation (phase 1B-HN, 2B-LN, 3B-SG, 4C-SGU, 5C-WGU and 6C-WGUP).	142
Fig. 6-3 (A) Total ammonia (TA) concentration of the influent, effluent, and the mixed liquor during continuous mode operation (phase 4C-SGU, 5C-WGU and 6C-WGUP); (B) TCOD, SCOD, HBOD, and TSS of the influent, effluent and the mixed liquor. Two different HRTs were used in phase 4C-SGU with 4a (20.5 h) and 4b (41 h).	144
Fig. 6-4 Transmembrane pressure and mixed liquor suspended solids in phase 4C-SGU, 5C-WGU and 6C-WGUP. Two different HRTs were used in phase 4C-SGU with 4a (20.5 h) and 4b (41 h).	147
Fig. 6-5 Community analysis of membrane aerator in phase 2B-LN (Aer_2) and GAC, mixed liquor (ML), and the membrane aerator in phase 4C-SGU (Aer_4). (A) Principal component analysis based on OTUs relative abundance. Microbial community presented with first two principal components with OTUs relative abundance >5% shown as the axes. The axes pointing at the sample indicates the high relative abundance; (B) microbial community analysis based on the relative abundance on the genus level. Only the genera with a relative abundance higher than 1% were shown (with pattern), while the other genera were included based on phylum level (pure color and vertical lines). Archaea (<0.01%) and Eukaryota were shown at the Kingdom level.	148
Fig. A-S1 LSVs for buffers of three groups with pKa and pH 5, 7, 8, 9, 10.8. The conductivity of the buffer solution is A. 7 mS/cm, B. LC (at the lower right corner)	160
Fig. A-S2 The relationship between diffusivity and cathodic current	161
Fig. A-S3 LSVs for cathode buffered by buffers with A. pKa 8, pH adjusting to 7, 8, and 9, and conductivity of 5.5 mS/cm; B. pKa 10.8, pH adjusting to 9.8, 10.8 and 12, and conductivity of 4.9 mS/cm.	162
Fig. B-S1 (A) the structure for MEC (4 cm wide) with 2 cm electrode spacing, resulting in anode and cathode volume of 13 mL; (B) electrochemical half cells with anode chamber of 13 mL and cathode chamber of 26 mL. The cathode was incised to ventilate produced hydrogen gas from reference electrode chamber to the chamber with anaerobic tube for gas sample collection.	163
Fig. B-S2 Titration curves showing the buffer capacities of the PBS and PoB solutions.	164
Fig. C-S1 Reactor configuration A. AFMBR, B. AOFMBR and AeMBR. AeMBR and AOFMBR had the same reactor configuration except no GAC was added into AeMBR	167

Fig. C-S2 The effluent COD and SCOD over time	168
Fig. C-S3 Analysis of the microbial communities in the solution (S) and on the GAC (G) in the AOFMBR (AO), AFMBR (AF) and AeMBR (MBR) reactors based on relative abundance at the genus level (removing genera at <1% abundance).....	169
Fig. D-S1 The ammonia, nitrate and nitrite concentration in phase 1B-HN (batch mode repeated two times, synthetic wastewater with 236 ± 9 mg-N/L).....	174
Fig. D-S2 Ammonia, nitrate and nitrite concentration in phase 2B-LN (batch mode repeated two times, COD-free synthetic wastewater with 79 ± 11 mg-N/L).....	175
Fig. D-S3 Ammonia, nitrite and nitrate concentration in phase 3B-SG (batch mode repeated three times, synthetic wastewater with 73 ± 7 mg-N/L).....	176
Fig. D-S4 Triplicate COD removal test in phase 3B-SG.....	177
Fig. D-S5 Nitrite and nitrate concentrations in the effluent and mixed liquor (ML) during continuous flow operation (phases 4C-SGU, 5C-WGU and 6C-WGUP).....	178
Fig. D-S6 Bubbleless and bubble abiotic air stripping test.....	179

LIST OF TABLES

Table 2-1 Contribution of each sludge fraction to membrane fouling during membrane filtration of sludge suspension (reconstructed) (107).....	31
Table 3-1 Buffer selected from biologically compatible buffers. Abbreviations used for some buffers are defined in the text. The charged dissociation ligand (L) species is shown for each buffer. All the buffer pKa are given at 30 °C.....	62
Table 3-2 Buffer common name, chemical structure and molecular weight.....	64
Table 5-1 Wastewater characteristics (influent) and membrane condition.	108
Table 5-2 Estimates of energy consumption for AOFMBR compared to the AFMBR.	120
Table 6-1 Operational conditions of the reactors for the six phases.	137
Table 6-2 Nitrate and nitrite concentration, total ammonia removal and TCOD/SCOD removal during the six phases of operation.....	143
Table C-S1 The effluent COD, SCOD and removal efficiencies (average \pm SD) for the three reactors in the 131-day of operation for the four phases.....	173
Table C-S2 Examination of whether the effluent CODs among the reactors (AF-AFMBR, AO-AOFMBR, MBR-AeMBR) were significantly different. When p values (based on the Student's T-test) were smaller than 0.03, the effluents were not considered to be significantly different. Comparisons are made on the data shown in Figure 5-1.....	173

ACKNOWLEDGEMENTS

Many thanks to my advisor, Dr. Bruce E. Logan, for offering me this chance to work with him and learn from him. I think I cannot ask for a better advisor, who is so supportive, patient, skilled in writing and socializing, hardworking and, most importantly of all, willing to share his wisdom with us. He encourages me to challenge research topics that I thought I could never accomplish. His patience in research and hardworking inspired me to make my own study more rigid and persuasive. He contributes so much to help me improve my English writing skill, once criticized as a “tough writer”. I am truly honored to have worked closely with him to share his understanding and passion in doing research, and I think this experience will be a priceless treasure for my future career. I would also like to thank the other committee members, Dr. Michael A. Hickner, Dr. Rachel A. Brennan and Dr. Christopher Gorski, for their time and support in evaluating this research. I am also thankful to Kaust for funding me.

I would like to express my gratitude to everybody who have worked with me throughout my Ph.D study. Special thanks to Nicole, Kyoung-Yeol, Hiroyuki, Xiuping, Emily and Andrew for their contribution in the works presented in this dissertation. Thanks to David Jones for letting my work here so much easier. I really enjoy the research atmosphere in this group, and I think I will definitely miss this organized working environment.

Last but not least, I would like to thank my parents for being so supportive in these years financially and mentally. Without your understanding, I can never achieve this accomplishment of becoming Ph.D. In addition, I also very grateful to all my friends here, my teammates in Penn State table tennis team, and the head coach Henry McCollum. You have made my spare life so colorful and meaningful, which has helped me get through many difficulties.

Chapter 1

Introduction

1.1 Energy demand and challenge of environmental issues

According to the US Energy Information Administration report, the electricity generation from all fuels in 2016 is 4079 million megawatt hours, in which fossil fuel is the major energy source to produce electricity.(1) The consumption of electricity in 2016 is 3710 million megawatt hours, which is believed to be further growing in the future. The increase in energy demand accelerates the depletion of non-renewable fossil fuels, which has been produced from animal biomass and plants over millions of years. The energy crisis is at the corner, since an estimation by CIA World Factbook showed our oil deposits will be gone by 2052.(2) In addition, the use of fossil fuels is leading to severe environmental problems, such as global warming and acid rain, due to the release of carbon dioxide, nitrogen oxides, and sulfate oxide. The emission of fossil fuels increased by 29% between 2000 and 2008. The concentration of carbon dioxide in the atmosphere is found to be 36% higher than that before industrial revolution, even though a large amount of carbon dioxide can be taken up by the oceans.(3) The limited uptake of carbon dioxide resulted in 43% of carbon dioxide emitted remaining in the atmosphere on average each year.(4) Renewable, sustainable and clean energy sources will be needed in the future to mitigate the energy crisis and related climate issues.

1.2 Energy demand for wastewater treatment

Water and wastewater treatment systems are an important energy consumers of electricity, accounting for 3-5% of electricity consumption.(5) However, water and wastewater treatment plants are usually not well optimized to save electricity since the treatment plants have duties and priorities to meet for the public services. For example, the effluent should comply with the regulatory requirements; the reliability of their treatment needs to stay high; operational and maintenance costs and revenue are required to be balanced and under control to ensure the longevity of assets. An analysis was conducted on a small-scale wastewater treatment plant showing the total energy intensity was 1.046 kWh/m³ of wastewater treated, among which electricity accounted for half of the total energy including manual energy, diesel, and chemical energy.(6) In addition, growing water scarcity has led to a requirement for a better and more effective treatment of water. Although conventional treatment processes in municipal wastewater treatment plants can deliver good wastewater treatment with high stability, a life cycle analysis showed that a conventional aerobic activated sludge treatment process was no longer cost effective due to high energy costs, low automation, and low food to microorganism conditions.(7) Therefore, wastewater treatment technologies with lower energy costs and higher efficiencies need to be developed to mitigate the energy crisis and the water supply burden.

1.3 Bioelectrochemical and membrane systems for wastewater treatment and energy recovery

Conventionally, domestic wastewater is treated by aerobic biological processes, such as the activated sludge (AS) process. However, the AS process has several disadvantages, such as high energy demands, high sludge production, and insufficient nutrient removal. For example, the energy needed for aeration alone can be ~500 Wh m⁻³ for 1 kg organic removal during operation.(8) Large amounts of solids will be produced daily, ranging from 15-100 L/kg BOD₅ removed, due to high yield coefficients from aerobic microorganisms.(9) Recently, anaerobic

treatment technique has drawn much attention due to its high energetic efficiency and low sludge production. Bioelectrochemical systems (BESs), such as microbial electrolysis cells (MECs) and microbial fuel cells (MFCs), and membrane bioreactors, such as anaerobic fluidized bed membrane bioreactor (AFMBR), are among the most promising anaerobic treatment techniques to aerobic processes.

BESs, such as MFCs and MECs, accomplish direct extraction of electrons from organics in wastewater, and the extracted electrons can be donated to the electron acceptor (usually oxygen or water) to obtain energy as electricity or hydrogen gas. Compared with other anaerobic treatment process, where methane is produced first and then converted into electricity, MFCs can accomplish direct biological conversion of chemical energy in organic matter into electricity. For an MEC, however, an additional energy supply is needed to drive the cathodic hydrogen evolution reaction, but the hydrogen produced in an MEC can have a higher efficiency than water electrolysis and a less emissions than industrial steam reforming.

Anaerobic membrane bioreactors can achieve both good wastewater treatment and have low energy demands compared with conventional AS processes, with a potential to accomplish a net energy gain while meeting strict discharge standards. In addition, the addition of membranes in anaerobic wastewater treatment systems can overcome barriers to effective treatment at low temperatures and low organic matter concentrations.

1.4 Objectives

My research focused on evaluating the effects of buffer charge and buffer retention on the performance of MFCs and MECs, and on optimizing membrane bioreactors as a post-treatment process for the effluent from MFCs in terms of COD concentrations and ammonia nitrogen removal. In addition, I examined methods that minimized dissolved methane concentrations and membrane fouling.

Objective 1: Evaluate the effect of buffer charge on cathode performance in MFC.

Objective 2: Develop a polymeric buffer with a large molecular weight (>10,000 Da) achieving buffer retention in the catholyte of two-chamber MECs to evaluate the effect of buffer retention compared to ion transport through membrane

Objective 3: Develop an aerobic fluidized bed membrane bioreactor (AOFMBR) using rising air bubbles to fluidize granular activated carbon (GAC) particles to avoid dissolved methane and lower membrane fouling.

Objective 4: Develop an aerated membrane fluidized bed membrane bioreactor (AeFMBR) by combining membrane aerators and an AFMBR to achieve simultaneous nitrogen and COD removal with low dissolved methane in the effluent.

1.5 Outline of Dissertation

This dissertation is organized in 7 chapters including this Chapter 1. Chapter 2 is a literature review of MFCs, MECs, membrane aerator bioreactors, and anaerobic fluidized bed membrane bioreactor. The following Chapters 3 to 6 report on the results that address each of the research objectives. An outlook and future works is presented in Chapter 7.

In Chapter 3, the effect of buffer charge on air cathode performance was evaluated using linear sweep voltammetry (LSV). This work was published as ‘Ye, Yaoli, Xiuping Zhu, and Bruce E. Logan. "Effect of buffer charge on performance of air-cathodes used in microbial fuel cells." *Electrochimica Acta* 194 (2016): 441-447.’ I conducted all experiments, and Dr. Zhu

provided profound suggestions on the experiment design. Dr. Logan contributed to improve the quality of data, figure and text presented in the paper.

In Chapter 4, I examined the use of a high molecular weight buffer in the catholyte in order to avoid buffer loss through the separator (membrane) between the chambers. A polymer buffer was first synthesized and tested as the catholyte for buffer capacity, buffer retention, LSVs and hydrogen production. The effect of ion transport through membrane with phosphate buffer was compared to that of buffer retention using polymer buffer. This study was concluded as a manuscript as: ‘Ye, Yaoli and B. E. Logan. "Simultaneous nitrogen and organics removal using membrane aeration and effluent ultrafiltration in an anaerobic fluidized membrane bioreactor."’, which was submitted to the International Journal of Hydrogen Energy. I conducted all the tests and prepared the manuscript. Dr. Logan contributed to the revision of the manuscript.

In Chapter 5, three membrane bioreactors, AFMBR, AOFMBR and aerobic membrane bioreactor were compared side by side for 102 days for treating diluted domestic wastewater in terms of COD removal, membrane fouling, and methane production. Membrane surface morphology was imaged by scanning electron microscopy. Microbial communities in each of the bioreactors were compared by DNA analysis. This work was published as ‘Ye, Yaoli, Nicole LaBarge, Hiroyuki Kashima, Kyoung-Yeol Kim, Pei-Ying Hong, Pascal E. Saikaly and Bruce E. Logan. "An aerated and fluidized bed membrane bioreactor for effective wastewater treatment with low membrane fouling." *Environmental Science: Water Research & Technology* 2.6 (2016): 994-1003.’ I performed all the tests and reactors operation in this study. Ms. LaBarge and Dr. Kim gave suggestions to enhance the bioreactor operation stability. Dr. Hong and Dr. Saikaly contributed to the microbial community analysis. Dr. Logan gave advices to enhance a better presentation of the data and figures. All the coauthors also contributed to the revision of the manuscript.

In Chapter 6, the concept of an AeMFMBR was presented based on integrating membrane aerators into an AFMBR. The performance of the AeMFMBR was evaluated in terms of ammonium, nitrite and nitrate removal along with COD and TSS removals in both batch and continuous flow modes for more than 200 days. Dissolved methane and dissolved oxygen were also tracked during continuous flow mode operation. Microbial communities on the membrane aerator, GAC and mixed liquor were analyzed to gain insight into the ammonia removal mechanism. This study was concluded as a manuscript, 'Ye, Yaoli, Pascal E. Saikaly, and B. E. Logan. "Simultaneous nitrogen and organics removal using membrane aeration and effluent ultrafiltration in an anaerobic fluidized membrane bioreactor." *Bioresource Technology* (2017).'

I performed all the experiments, tests and reactor operation in this study, and prepared the manuscript. Dr. Saikaly and Dr. Logan contributed to the revision of the manuscript to enhance the paper quality.

1.6 Literature cited

1. "Electricity data browser - Net generation for all sectors". Available from:
<https://www.eia.gov/electricity/data/browser/> (accessed by 06/2017)
2. "The World Factbook". Available from:
<https://www.cia.gov/library/publications/resources/the-world-factbook/docs/notesanddefs.html?fieldkey=2237&term=Electricity - from fossil fuels>
(accessed by 06/2017)
3. Siegenthaler U, Sarmiento JL. "Atmospheric carbon dioxide and the ocean". *Nature*. 1993;365(6442):119–25.
4. Le Quéré C, Raupach MR, Canadell JG, Marland G, Bopp L, Ciais P, et al. "Trends in the sources and sinks of carbon dioxide". *Nat Geosci*. 2009;2(12):831–6.

5. Sleutels THJA, ter Heijne A, Kuntke P, Buisman CJN, Hamelers HVM. "Membrane selectivity determines energetic losses for ion transport in bioelectrochemical systems". *ChemistrySelect*. 2017;2(12):3462–70.
6. Singh P, Carliell-Marquet C, Kansal A. "Energy pattern analysis of a wastewater treatment plant". *Appl Water Sci*. 2012;2(3):221–6.
7. Tsagarakis KP, Mara DD, Angelakis AN. "Application of cost criteria for selection of municipal wastewater treatment systems". *Water, Air, Soil Pollut*. 2003;142(1):187–210.
8. Ahn Y, Logan BE. "Effectiveness of domestic wastewater treatment using microbial fuel cells at ambient and mesophilic temperatures". *Bioresour Technol*. 2010;101:469–75.
9. Universiteit V. "Aerobic domestic waste water treatment in a pilot plant with complete sludge retention by cross-flow filtration". *Water Res*. 1995;29(4):1179–89.

Chapter 2

Literature Review

2.1 BES for energy recovery from wastewater

BESs are systems capable of converting the chemical energy in organic wastes, such as domestic wastewaters and industrial wastewaters, into electricity, hydrogen or other chemical products (Fig. 2-1). The most studied BESs are MFCs, where the electrons are extracted from the organic matter by bacteria on the anode, they flow through the external circuit, and then they are consumed at the cathode typically by the oxygen reduction reaction. The oxygen reduction reaction has a more positive potential than organic (acetate) oxidation reaction on the anode, so electrical power is produced when electrons flow from the negative to the positive terminal (1). The MEC is a device that shares a similar working principle to the MFC, except the cathode reaction changes to water electrolysis (hydrogen evolution). Because the hydrogen evolution reaction (HER) at the cathode has a more negative potential than the anode reaction, additional power needs to be input to trigger the MEC electrode reactions (2). Other BESs are capable of generating valuable products by applying electrical power. For example, methane can be recovered using a biocathode catalyzed by methanogenic communities, which can directly accept electrons or hydrogen gas from the cathode (3). Cathodic production of alkali as high as ~1 mol/L, such as sodium hydroxide, can be achieved by introducing a ion exchange membrane as a separator into an MFC (4). Hydrogen peroxide was found to be collected in an MFC when an efficient catalyst (Platinum) was absent (5). Other organic chemicals, such as acetate (6), ethanol (7) and butyrate (8), have been generated by biocathodes when both electrical power and carbon sources (usually CO₂) were input. These reactors that produced organic molecules are often referred as microbial electrosynthesis (MES) systems.

Numerous studies have been done on BESs, especially MFCs and MECs, to enhance the performance of energy recovery by applying new materials or combining BESs with other renewable energy technologies. The performance of wastewater treatment performance has also been evaluated with many different designs of BESs or by integrating BESs with other treatment processes.

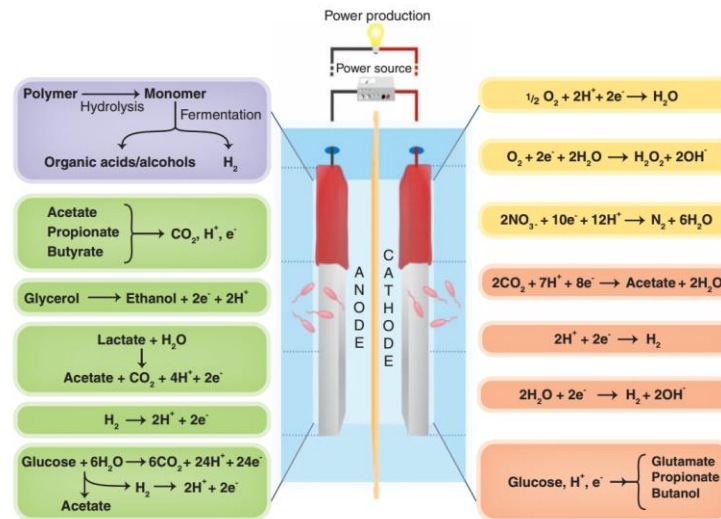


Fig. 2-1 Possible anode and cathode reactions in BESs (9)

2.1.1 MFC, electricity production and wastewater treatment

An MFC consists of an anode, cathode, electrolyte, separator (optional) and an external circuit (10). Many studies were conducted on each of the components to improve MFC performance. In MFCs, performance is usually evaluated based on maximum power generation (P_{\max}), internal resistance, and coulombic efficiency (CE). Power generation is assessed in terms of a power density, normalized either to an area (2-1) or liquid volume (2-2) using polarization tests (1), as:

$$P_{\text{area}} = \frac{E_{\text{cell}}^2}{A_e R_{\text{ext}}} \quad (2-1)$$

$$P_v = \frac{E_{cell}^2}{V_r R_{ext}} \quad (2-2)$$

where the E_{cell} is the voltage across the external load, A_e is the targeted electrode area, either anode or cathode, or the cross sectional area between the electrodes, R_{ext} is the resistance of the load, V_r is the volume of the reactor, P_{area} is the power density normalized to area and P_v is the power normalized to volume.

The internal resistance is the sum of activation resistance, concentration resistance, and ohmic resistance (11). The activation resistance is caused by the activation loss of the anode and cathode electrochemical reactions to initiate the oxidation or reduction reactions (11). The ohmic resistance consists of the contact resistance of the electrodes, solution resistance (dependent on conductivity), and the membrane resistance (if a membrane is used) (12). The concentration resistance is due to the difference between the bulk and local concentration. The internal resistance can be obtained using electrochemical techniques, such as polarization test, Tafel curves, electrochemical impedance spectroscopy (EIS), potential sweep and chronoamperometry.

The CE is the fraction of Coulombs actually extracted from the substrate in the total electrons available in substrate which can be calculated as (1)

$$\epsilon_{CE} = \frac{M \int_0^{t_b} I dt}{F b v_{an} \Delta COD} \quad (2-3)$$

where M is the molecular weight of the oxygen, F Faraday's constant, b the ratio of electron exchanges with the moles of oxygen, V_{An} the volume of anolyte and ΔCOD is the change in COD over the time period 0 to t_b .

2.1.1.1 MFC Anode

The selection of anode material is crucial for the effective attachment of exoelectrogenic bacteria. Anode materials used in MFCs need to have high electronic conductivity, biocompatibility, chemical stability, and high specific surface area (10). The mostly commonly

used material for the anode is a carbon based material, such as carbon fiber, carbon cloth, graphite, and carbon felt. A P_{\max} ranging from 893 to 1015 mW/m^2 was obtained in cubic MFCs with pre-treated carbon mesh anode, with a CE of 22% to 76% (13). MFCs with a carbon brush anode, made from carbon fibers, achieved a higher P_{\max} of 2400 mW/m^2 than the carbon mesh, with a CE of 60% (14). The ammonia treated carbon cloth anode achieved a P_{\max} of 1970 mW/m^2 , and the startup time was reduced by 50% compared to untreated carbon cloth (15). Non-porous graphite plates were also tested to be suitable for MFC anodes, and roughened graphite plates showed better biomass activity than Pt-coated titanium anodes (16).

In order to further increase anode performance, modification of the anode has been widely researched. For example, a RuO_2 film was deposited on a carbon felt anode, achieving a power density (3.08 W/m^2) 17 times as high as untreated carbon cloth, which was believed to be due to the enhanced electron transfer of the anode (17). A P_{\max} of 42 mW/m^2 was obtained using a carbon nanotube (CNT, 20%)/polyaniline (PANI) composite anode with *Escherichia coli* as anode bio-catalyst, which was higher than *E. coli* MFCs ($0.47\text{--}2.6 \text{ mW/m}^2$) (18). Rolling Fe_3O_4 into activated carbon anode loaded by stainless steel (SS) mesh increased the P_{\max} by 22% from 664 to 809 mW/m^2 , which was attributed to the improved capacitance (19). Another study also showed that enhanced anode capacitance can increase both stationary and transient power production (20). Other modifiers, such as polyaniline (21), PANI/poly(aniline-co-o-aminophenol) (PAOA) (22) and graphene (23), were tested on carbon-based anodes in MFCs, and improved anode performance were obtained as well. Other than carbon-based anodes, metals are also good candidates for the MFC anode material due to their superior electron conductivity. Gold (24), titanium oxide (16) and SS plate (25) have been used in MFCs, and some reported the metal anodes could produce current as effectively as carbon-based anodes (26).

The anode material has an effect on the attachment of microorganisms, which can then influence electron transfer. Three electron transfer mechanisms are proposed (Fig. 2-2), direct

electron transfer (DET), mediated electron transfer (MET), and microbial nanowires. DET only takes place when the exoelectrogenic bacteria are in contact with the anode (27). Electrons from inside the bacteria are transferred to external electron acceptor via outer membrane cytochromes. However, based on this mechanism, the current generated can be limited to only several $\mu\text{A}/\text{cm}^2$ based on a cell density of a single monolayer of bacteria (28). The other two electron transfer mechanisms allow microorganisms to utilize electron acceptors other than anode, leading to a thicker electroactive biofilms grown on the anode. Molecular pili (conductive nanowires) are evolved by some microorganisms, such as *Shewanella* strains (29), through which the electrons can be transferred from cytochromes to external electron acceptors. The conductive nanowires enable remote electron transport (28) and the formation of conductive biofilm matrix (30). It is believed that 100% of electron harvesting can be achieved with the electron transfer mechanism of DET and nanowires (28). However, exoelectrogenic microorganisms are typically not capable of using complex substrates, resulting in limited current generation unless complex substrates are broken down to simple molecules that can be used by the exoelectrogenic microorganisms. The MFCs involving MET, on the contrary, can produce orders of magnitude higher current than that produced with DET (28). Mediators are usually added as electron shuttles in the early stage of MFC studies to produce appreciable power (31). The mediator is a reversible electron acceptor/donor that can receive electrons from microorganisms and to donate electrons to the anode. The presence of a mediator can significantly increase the rate of electron release by the microorganisms. The use of mediators, such as neutral red (32), humic acid (33) and anthraquinon-2, 6-disulphonic disodium salt (AQDS) (34), have been studied showing the addition of mediators can contribute to a higher power generation.

The review here on anodes suggests that modified carbon based materials may be the most promising ones since they are cheap, stable and well-studied. Although mediators can enhance the anode performance, mediated MFCs are not likely to be used in commercial

applications due to the environmental and cost concerns. The mediators are usually, phenolic compounds, which may be toxic and have adverse effect to the environment in long term (35). In addition, the use of mediator also adds an extra cost for MFC operation since the mediators are likely to be washed out with the effluent.

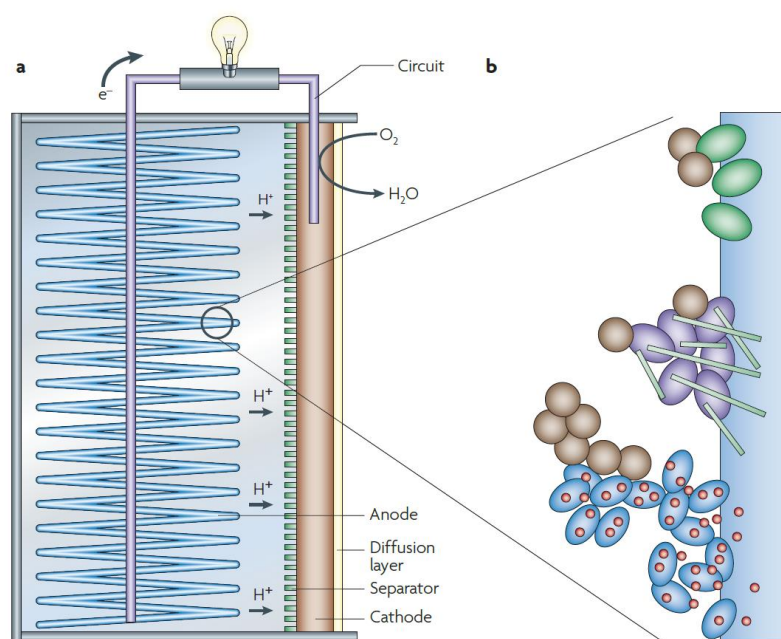
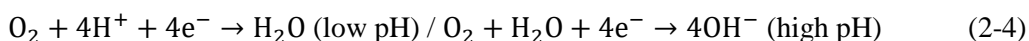


Fig. 2-2 Extracellular electron transfer mechanisms. From top to bottom, direct electron transfer, nanowire and mediator (31)

2.1.1.2 MFC cathode

In MFCs, many oxidants can be the candidates as the electron acceptors for cathode reduction reaction, such as ferricyanide (36), persulfate (37) and oxygen (14). Among all the candidates, the most commonly used oxidant is oxygen due to its low cost and non-toxic properties (10). The oxygen reduction reaction (ORR) in an air-cathode MFC is a tri-phase reaction as electrons, protons and oxygen meet and react at the catalyst layer on the cathode.

Complete and incomplete ORR pathways are proposed based on proton consumption and either a 4-electron (2-4) or 2-electron transfer (2-5):



The 4-electron pathway is believed to be predominant on a noble metal catalyst, while the 2-electron pathway is likely predominant on many carbon based materials, gold, and oxide-covered metals (38). The pH in MFC is usually around neutral, which makes ORR in MFC fundamentally different from that in fuel cell, which occurs under an acidic pH. The proton, as a reactant, has a low concentration at neutral pH, resulting in slow ORR kinetics. Therefore, many studies have indicated that the cathode performance is the limiting factor in power generation. For example, volumetric power density was shown to have a linear function with the cathode specific surface area, indicating that the MFC configuration was less important than cathode specific surface area in terms of scaling up MFC (39). In addition, doubling the cathode size can increase P_{\max} by 62%, while doubling anode size only contributed to an increase of 12%. Another study supported a cathode limitation in power by reporting that the polarization resistance of the anode obtained by EIS was one or two orders of magnitude smaller than the cathode resistance (40). The cathode limitation for power is further confirmed by analyzing internal resistance (41). The cathode had 780% higher resistance (285 Ω) than that of anode (33 Ω). The limitation by the cathode is caused by the high cathodic activation losses, ohmic losses, and mass transport losses. Numerous of catalysts are developed to reduce activation losses.

The most widely used air cathode in MFC is still the Pt/C carbon cloth cathode (42), which is manufactured by loading a catalyst layer (Pt/C) on one side of carbon cloth, and carbon based layer and diffusion layer (polytetrafluoroethylene, PTFE) onto the other. The use of this Pt/C carbon cloth cathode can contribute to an increase in P_{\max} by 42% compared with a commercialized fuel cell cathode (43). Cathodes with other catalyst are developed based on this

general structure of catalyst layer, current collector, and diffusion layer (Fig. 2-3), but with other catalysts since the platinum is costly. When the Pt/C catalyst was replaced with cobalt tetramethylphenylporphyrin (CoTMPP), for example, the cathode performance only decreased slightly compared with a Pt/C cathode (43). In another study, pyrolyzed CoTMPP and Pt catalyzed cathodes were compared with a pyrolyzed iron (II) phthalocyanine (pyr-FePc) catalyzed cathode, and there was only a small difference in the cathode performance using the different catalyst (44). Ferric iron reduced on graphite electrode as the catalyst was applied as MFC cathode, achieving a P_{\max} of 0.86 W/m^2 with a current density of 4.5 A/m^2 (45). The catalyst of metal oxides and metal complexes, though less expensive than platinum, still can cost several hundred dollars per square meter (46).

In order to further reduce the cathode cost without lose in power generation, activated carbon (AC) powders have become more widely used as the cathode catalyst because AC is inexpensive and it has a large specific surface area. For example, MFC with cathode made by pressing a mixture of AC and PTFE onto nickel mesh current collector produced P_{\max} as high as $1220 \pm 46 \text{ mW/m}^2$, 16% higher than the Pt/C carbon cloth cathode (46). In another study, cathodes were made by applying a mixture of AC and PTFE paste as the catalyst layer with four PTFE layers as the diffusion layer, onto a nickel foam current collector, producing a P_{\max} of $1190 \pm 50 \text{ mW/m}^2$, which was comparable to 1320 mW/m^2 by the Pt/C carbon cloth control (47). Another AC catalyzed cathode was fabricated by rolling method using a conductive gas diffusion layer consisting of carbon black and PTFE on one side of SS mesh, and rolling catalyst layer consisting of AC and PTFE on the other side, which produced a P_{\max} of 802 mW/m^2 at 3.44 A/m^2 (48).

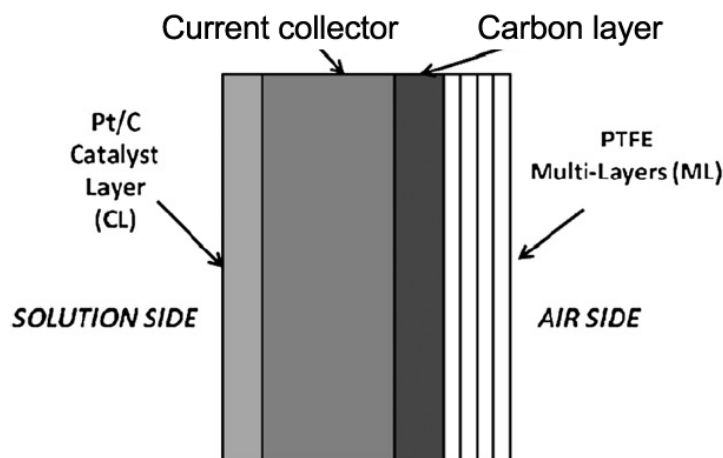


Fig. 2-3 The air cathode structure with a catalyst layer facing the solution side, and a carbon layer and diffusion layer facing the air side (49)

Another difference between the cathode in an MFC and a conventional fuel cell is the cathode fouling caused by biological fouling, organic and inorganic matter deposition in the MFC because the anode is biologically catalyzed. Therefore, the long term performance of an MFC is a concern due to deterioration of the cathode performance caused by fouling. Some attempts have been reported for fouling control by cathode modification. Applying the biocide vanillin on an air cathode catalyzed by AC showed the greatest reductions in fouling and power after 5 weeks of operation compared with the cathode without an anti-fouling coating (50). Cathodes made from nitrogen doped carbon powder sprayed with amino-trimethylene-phosphate was found to effectively reduce chemical fouling, resulting in a decrease of 13% in power after 40 days of operation, which was lower than the 56% reduction in power for MFCs with a carbon powder cathode (51). Enrofloxacin, a fluoroquinolone antibiotic, was also incorporated in the catalyst layer of an air cathode catalyzed by AC, resulting in a decrease in biomass content on the cathode

by 60.2% compared with an untreated cathode, after 92 days of operation (52). No substantial decrease in P_{\max} s were shown for the cathode with enrofloxacin.

The studies in this section suggest that AC or modified AC as the catalyst other than Pt or a metal based catalyst are the most promising catalysts for MFC air cathodes. In addition, inhibitors for biofilm growth on the cathode or methods to reduce or reverse fouling are needed for maintaining stable, long-term cathode performance.

2.1.1.3 MFC separator

MFCs can be classified as single-chamber or double-chamber configurations based on whether or not a separator is used to physically separate the solution into anolyte and catholyte chambers. Without a separator, single-chamber MFCs have achieved higher power densities than two chamber MFCs due to the reduction in internal resistance in the absence of a separator. However, the lack of a separator or membrane can result in high oxygen intrusion from air cathode, and a decrease in CE and cathode fouling due to contact with microorganisms, compared to two-chamber MFCs (53). The use of separator can also result in problems. For example, a pH gradient will be created between anolyte and catholyte due to limited transport of ions such as protons compared with the proton consumption rate at cathode (4). The anolyte will become more acidic, while the catholyte more alkaline. The difference in electrolyte pH can cause a potential loss and an increase in internal resistance (54). With an initial high anolyte pH and low catholyte pH, a tubular MFC achieved 3.8 times higher P_{\max} than an MFC starting with a neutral pH (55). In addition, the drop in anolyte pH may not only lead to decrease in microbial activity on anode (56). The use of separator may also cause fouling of the separator (57) and increasing the maintenance costs for MFCs.

Up to now, cation exchange membrane (CEM), anion exchange membrane (AEM), ultrafiltration membrane (UFM), microfiltration membrane (MEM), bipolar membrane (BPM)

and porous fabrics have been used in MFCs as separators. A CEM was used in an MFC treating diluted starch processing wastewater, showing the proton transport became limited when the resistance was below 200 Ω (56). The use of UFM, AEM, CEM, proton exchange membrane (PEM) were compared in MFCs treating synthetic wastewater, with that AEM producing the highest P_{\max} (610 mW/m²) with comparable internal resistance to the CEM, PEM and UFM (~90 Ω) (58). The suitability of using an AEM, CEM or BPM as the separator was evaluated in MFCs, showing that the BPM was the least suitable for MFC due to its high resistance (59). J-cloth, glass fiber mesh, and CEM were compared in MFCs with various configurations, with the higher P_{\max} obtained using J-cloth and glass fiber compared with a CEM due to their low ohmic resistances (60). In addition, a higher CE was achieved with glass fiber due to its lower oxygen transport. MFCs with MFM as the separator showed a comparable P_{\max} with a membrane-less configuration, double that of obtained with a CEM, without negative effect on internal resistance (61).

The use of separator is a trade-off between oxygen intrusion and internal resistance. The use of J-cloth or glass fiber separators are more promising than others, such as CEMs, AEMs, and BPMs, due to their lower ohmic resistances.

2.1.1.4 MFC configurations

Various MFC configurations have been developed to enhance power generation and improve wastewater treatment. The configurations include upflow, downflow, tubular reactors, cassette-electrode setups, separator electrode assemblies (SEA), and fluidized beds. A P_{\max} of 170 mW/m² was obtained in a two-chamber MFC (CEM) with an upflow configuration in continuous flow mode with a reticulated vitreous carbon cathode (62). Another upflow MFC with porous sponges as separator achieved a P_{\max} of 315 mW/m² using an activated carbon fiber cathode. A downflow configuration was compared with an upflow configuration in a single-chamber MFC,

with the down-flow configuration producing a higher P_{\max} due to better cathode performance, and the simpler design of the down-flow configuration was claimed to contribute to an easier design for scaling up (63). In a tubular reactor, the graphite granule anode was wrapped around a Pt/C cathode, producing a P_{\max} as high as 50 W/m^3 (64). A innovative cassette-electrode setup was developed, with a detachable cassette of two flat cathodes sandwiched between a PEM and anodes, resulting in a P_{\max} of 899 mW/m^2 (65). The cassette-electrode MFC was tested for treating organic wastes like cattle manure (66). The cassette-electrode MFC was believed to be scalable. SEA MFCs, which can increase power generation by reducing electrode spacing with a separator to avoid short circuiting between the electrodes, have the disadvantage of oxygen transport from cathode inhibiting anode bacterial activity. A P_{\max} of 975 mW/m^2 was obtained from an SEA MFC with a graphite fiber brush and single air cathode using a textile separator (67). An improved power generation was achieved as high as 4.30 W/m^2 in a SEA MFC by using a non-woven fabric layer separator and a U-shaped Ti wire as the current collector (68). In another study, several different reactor configurations were compared along with two different separators, glass fiber and J-cloth, with the highest P_{\max} of 696 W/m^3 produced by a double SEA with electrode spacing of 0.3 cm and glass fiber separator (60). An innovative fluidized bed MFC was introduced by using a graphite rod as the anode surrounded by fluidized carbon particles, producing a higher output voltage and shortening the start-up time (69). The configuration will be crucial for MFC scaling up, so the simple structure, such as cassette-electrode, which can be easily expanded by hydraulic connection of single unit, is preferable.

2.1.1.5 Scaling up MFCs

A number of methods have been proposed and tested for scaling up MFCs. One way is to electrically connect unit MFCs in series or parallel to increase the total voltage or current generation. For example, 6 MFC units were connected in series to reach a voltage of 2.02 V (228

W/m³) and in parallel to reach a current of 225 mA (248 W/m³) (70). Three fluidized bed MFCs were connected in series achieving a P_{\max} of 11.7 mW/m² with 14.7 mW/m² for each single MFC, with 99% of COD removal with series flow of the fluid through the MFCs (71). Although the total power generation of a stacked MFCs is close to the sum of unit MFCs, there is a risk of voltage reversal when the MFCs are connected in series (72). Voltage reversal happens when some MFCs in the series are charged (consuming energy) by others instead of discharging (73). The voltage reversal is believed to be due to poor working conditions of some MFCs, such as substrate starvation. This problem can be avoided by using continuous flow operation mode to make sure sufficient substrate is supported. In addition, eliminating the MFCs with voltage reversal out from the circuit by short circuiting is also an effective solution. Urine powered stack of 24 MFCs was capable of charging a mobile phone, achieving a 25 min of mobile phone use with ~24 hours of charging by a stack of MFCs (74).

The second way for MFC scaling up is to increase the surface area of anode, cathode and reactor volume. If the power density stays constant, scale-up of MFCs with the same structure as those at small-scale would be expected to produce power proportionally. However, a review paper concluded that this trend was not true due to the factors such as the mechanism of mass transport and the electron transport across the anode biofilm (75). Another study reported the anode lead-out terminals were very important for large-scale MFCs, which could result in 47% of power loss in large-scale MFC compared with small-scale MFC (76). In addition, unknown factors or factors that have not been understood well may also account for the power loss of the larger-scale MFCs.

Numerous scaled-up MFCs with large electrode areas have been developed with different configurations, and the power densities produced have not been consistent among studies. Some claimed that power generation could be maintained during scale-up, while other studies reported substantial power losses. A 10-L serpentine type MFC was constructed by combining 40 tubular

air cathode MFC units with graphite felt anodes and carbon cloth felt cathodes with nickel and MnO_2 powder for treating brewery wastewater, achieving a power generation of 4.1 W/m^3 (77). The comparison between this serpentine MFC and a small-scale MFC suggested the power was effectively maintained during scale-up. Ammonia was found to be removed along with COD with an efficiency higher than 85% due to ammonia volatilization. Long-term tests showed a decrease in power generation as wastewater was treated, but the loss in power was mostly recovered by a cathode rinse with deionized (DI) water. A 20-L bipolar plate MFC stack of four cells produced a high P_{max} of 144 W/m^3 by decreasing pH, purging with pure oxygen, and increasing flow rate, resulting in a small volumetric resistivity of $1.2 \text{ m}\Omega/\text{m}^2$, comparable to or lower than small-scale MFC of 0.5 L (78). However, some other studies showed a decrease in power generation during scale-up. For example, a multi anode/cathode MFC was constructed by integrating a GAC bed with multiple anodes and cathodes into a single-chamber MFC (20 L) (79). As the number of anodes and cathodes increased to 12, a power generation of 3.4 mW was obtained, which was 3 times as high as the 4-anodes/cathodes configuration (1.25 mW). Compared with the small-scale MFC, the large-scale MFC achieved a lower power density due to the large internal resistance caused by large electrode spacing. Good treatment of both COD and TKN was achieved at an HRT of 20 h with efficiencies of 80% for COD, and 30% for TKN. A 12 L-MFC treating synthetic wastewater (sodium acetate) achieved a P_{max} of 431 mW/m^2 resulting in a low anode polarization resistance of 0.44Ω (76). The comparison between the small-scale and the large scale MFC with the same configuration showed a power generation decrease of 38% from 696 mW/m^2 during scale-up. A 47% loss in power was identified as due to ohmic losses as a result of poor lead-out of the terminals, while reasons for the remainder of power loss remained unknown.

2.1.2 MEC, hydrogen production

The anode of an MEC works similarly to the anode in an MFC, as both are based on oxidation of organics catalyzed by microbes. The produced electrons travel through an external circuit, but in the MEC they are consumed at the cathode by the hydrogen evolution reaction (HER) (Fig. 2-1), which dissociate water to form hydrogen gas. However, this process cannot happen spontaneously, since the equilibrium cathode potential for HER of -0.414 V (vs. NHE) is more negative than anode potential under standard biological condition (-0.296 V vs. NHE, with 5 mM acetate under pH of 7). An additional power supply of at least ~ 0.114 V is needed to be added on MEC electrodes to initiate HER, but in practice this voltage is even larger (>0.130 V) (80). Although electrical energy is input into the MEC, this voltage is much lower than the theoretical voltage at neutral pH (1.21 V) to split water, or the voltage input in practice for water electrolysis (1.8 - 2.0 V) (81). Compared with biological hydrogen production process, such as photo- and dark-fermentation, the MEC has a higher energy conversion efficiency, higher hydrogen production rate, and higher hydrogen quality (82).

The performance of MEC can be evaluated in terms of many different factors, including current densities, CE, hydrogen production rate (HPR), cathodic efficiency, hydrogen recovery efficiency, and energy efficiency based on energy input or energy input and substrate energy. Current and CE can be obtained using the same approach as that in MFC. Since a product of hydrogen instead of current is collected in a MEC, cathodic efficiency is adopted to evaluate the fraction of current converted into hydrogen, which can be calculated as:

$$r_{cat} = \frac{n_{H_2}}{n_{CE}} = \frac{2Fn_{H_2}}{\int_{t=0}^t I dt} \quad (2-6)$$

where n_{H_2} is the moles of hydrogen collected, n_{CE} the theoretical hydrogen production calculated based on moles of coulomb transferred assuming a 2:1 hydrogen conversion ratio. The HPR can be calculated by normalizing the produced hydrogen gas in volume to time and reactor volume.

The term hydrogen recovery efficiency is defined as the fraction of electrons in substrate converted into hydrogen, which can be calculated by multiply CE with cathodic efficiency as:

$$\epsilon_{hre} = \epsilon_{CE} r_{cat} \quad (2-7)$$

Three energy efficiencies are used to assess energy conversion. The energy yield relative to electrical input, the ratio of energy content in the collected hydrogen relative to the electrical energy required, is:

$$\eta_E = \frac{W_{H_2}}{W_E} = \frac{n_{H_2} \Delta H_{H_2}}{IEt} \quad (2-8)$$

where W_{H_2} is the energy generated as hydrogen gas, W_E the energy input as electricity and ΔH_{H_2} the enthalpy contained in hydrogen. Another energy efficiency describing the energy yield relative to the added substrate, η_S , as:

$$\eta_S = \frac{W_{H_2}}{W_S} = \frac{n_{H_2} \Delta H_{H_2}}{n_s \Delta H_S} \quad (2-9)$$

where W_S is the energy content in the consumed substrate, which is calculated by multiplying the enthalpy, ΔH_S , and the moles of substrate, n_s . The last energy efficiency, overall energy recovery, is calculated as:

$$\eta_{E+S} = \frac{W_{H_2}}{W_E + W_S} \quad (2-10)$$

2.1.2.1 MEC cathode

Many factors have been shown to affect MEC performance, such as the cathode material, separator, electrolyte buffer, electrode spacing, and electrical power sources, among which cathode material has a primary impact on MEC performance. Because the HER on plain carbon material is slow, a metal based catalyst usually is used to reduce the activation overpotential.

The most commonly used metal catalyst for HER is platinum due to its good performance for the HER. A low overpotential can be obtained by using a platinum based catalyst. For example, the overpotential of Pt cathode was evaluated using various buffers, such as phosphate

buffer, ammonium chloride, ammonium bicarbonate and Good's buffer, showing that the minimum overpotential of 0.05 V at pH of pH 6.2 with phosphate buffer, and 0.09 V at pH 9.0 with ammonium chloride, and 0.09 V at pH 9.3 with ammonium bicarbonate and 0.07 V at pH 7.3 with Tris (one of Good's buffer) (83). Low HER overpotential substantially reduced the electrical energy input needed for MECs to produce comparable H₂ production rates, resulting in higher energy efficiencies. For example, a maximum HPR of $3.12 \pm 0.02 \text{ m}^3\text{-H}_2/\text{m}^3\text{-d}$ with a high CE of 98% and cathodic efficiency of 96% under 0.8 V was achieved in a membrane-less MEC with platinum catalyzed cathode (84). However, platinum is expensive, scarce, and its mining can cause adverse environmental problems (85).

To overcome this dilemma with the use of Pt, other metal-based catalyzed and bio-catalyzed cathodes have been developed and tested in MECs. Stainless steel (SS) is a cheap alternative proposed to replace Pt in many studies. SS mesh cathodes with different sizes were compared with carbon cloth loaded with Pt/C, showing that #60 SS mesh produced a HPR as high as $3 \text{ m}^3\text{-H}_2/\text{m}^3\text{-d}$ with a high CE of $98 \pm 4\%$ and overall energy efficiency of $74 \pm 4\%$ with 0.9 V applied (86). Another study reported on using a SS brush with high specific surface area of $810 \text{ m}^2/\text{m}^3$ as the MEC cathode (0.6 V), which produced hydrogen at a rate of $1.7 \text{ m}^3\text{-H}_2/\text{m}^3\text{-d}$ with overall energy efficiency of $78 \pm 5\%$. The control cathode, a graphite bush, had a larger specific surface area, but resulted in a much slower HPR due to its poor catalyst properties (87). Other than SS, nickel is also a good candidate for an MEC cathode catalyst. Different metal cathodes, including SS, nickel and Pt, were assessed together in MECs at 0.9 V applied, showing that nickel and SS cathodes had a similar performance, surpassing Pt sheet in terms of overall energy efficiency and HPR (88). An electrodeposited nickel oxide layer, produced an overall energy efficiency of 48% for both SS and nickel cathodes at 0.6 V applied, which was 10 times higher than a Pt sheet (4%). In another MEC study, nickel powder (0.5-1 μm) was applied onto carbon cloth with or without carbon black as the cathode, and compared with Pt/C cathode and

electrodeposited nickel cathode (89). The HPR of nickel powder catalyzed cathodes were comparable with that of Pt/C cathodes, as well as having similar cathodic efficiencies, CEs, and hydrogen recovery efficiencies. However, the use of both nickel and SS might lead to corrosion and loss of metal. A list of metal cathodes, including platinum, nickel alloy, SS, were compared using cyclic voltammetry (CV) in terms of overpotential and anti-corrosion property (90). The results showed that the material with the best catalyst performance might not be the best choice due to lack of anti-corrosion. SS EN 1.4401 was shown to have highest resistance to corrosion at a pH of 9. Therefore, the choice of catalyst should depend on the operation conditions, especially the pH.

Other than chemically catalyzed cathodes, bio-cathodes are another alternative to noble-metal catalysts. The first biocathode was proposed in 2008 by reversing the polarity of a bioanode inoculated with acetate and hydrogen oxidizing bacteria in a half cell (91). A current density of 1.2 A/m^2 was achieved under cathode potential of -0.7 V without the addition of mediators. A subsequent study identified the feasibility of combining the bioanode and biocathode in one MEC (92). However, a low hydrogen recovery efficiency was obtained of $\sim 20\%$. In addition, deterioration of biocathode was shown, which was believed to be caused by precipitation of calcium phosphate and the production of methane. Another approach for enriching autotrophic electrotrophy on electrodes as a biocathode was proposed by inoculating the anode as a sediment-type MFC, followed by setting potential below -0.4 V (93). The experiment and clone library analysis indicated that the microorganisms grown on the biocathode were hydrogenotrophic methanogens and autotrophic electrotrophy.

Unlike MFC cathodes where the AC catalyst is the promising, carbon based catalysts have a large overpotential for HER. Non-noble metal catalyzed cathodes, such as nickel and stainless steel, therefore appear to be more promising for MECs since the use of Pt is costly and a biocathode does not provide stable performance.

2.1.2.2 MEC separator

Separators, usually membranes, are needed in water electrolysis to avoid mixing of hydrogen and oxygen gas produced. In an MEC, a separator, such as ionic exchange membrane, is also commonly used to separate the anode and cathode chambers. This separation of electrodes can increase hydrogen yield relative to electrical energy by reducing hydrogen cycling (hydrogen utilized by anode bacteria) and ensure high purity of hydrogen in the gas by avoiding methanogenesis (80). However, the addition of a separator in an MEC introduces an additional internal resistance. In addition, the pH differences that develop between the catholyte and anolyte result from the limited transport of protons or hydroxide ions through the membrane can cause a drop in electrochemical potential (54). When an MEC was operated without separator, the maximum HPR was $3.12 \text{ m}^3\text{-H}_2/\text{m}^3\text{-d}$ at applied voltage of 0.8 V. However, the methane concentration could be as high as 28% with low applied voltage of 0.2 V due to the long cycle time (80). In another membrane-less study a MEC with a non-ion selective J-cloth as the separator and gas-phase cathode, compared to an MEC with Nafion 117 as the separator (84). A smaller internal resistance of 19Ω was shown for membrane-less MEC, with HPR as high as $6.3 \text{ m}^3\text{-H}_2/\text{m}^3\text{-d}$.

Ion exchange membranes have been widely used and compared in MECs as the separator. CEM, charge mosaic membrane (CMM) and BPM were compared in a continuous mode MEC with potassium phosphate buffer treating synthetic wastewater, showing that AEM produced the highest hydrogen and the BPM mitigated the pH increase the best (94). A forward osmosis membrane was utilized as the separator in an MEC, and a comparable HPR of $0.3 \text{ m}^3 \text{ H}_2/\text{m}^3 \text{ d}$ was obtained for both the AEM and CEM at 1.0 V, with a larger pH gradient for the CEM but higher cathode overpotential for the AEM (95). However, another comparison of an AEM and a CEM showed a large difference in performance, in which 5 times higher HPR was obtained in the

MEC with an AEM at 1 V, due to the low internal resistance of $192 \text{ m}\Omega/\text{m}^2$ for AEM (96).

Another explanation for better performance using AEM was believed to be because some pH gradient potential loss could be recovered by anion transport in the AEM, while the cation transport in CEM could cause an additional potential loss (97).

2.1.2.3 MEC buffer

In two-chamber MEC studies, buffers are usually added to stabilize pH and increase solution conductivity resulting in better current and hydrogen production, because the catholyte tends to become more alkaline and the anolyte more acidic. Even in single-chamber MECs, the local pH near the electrodes can vary (98), leading to a concentration overpotential (99). The same problems are present in MFCs as well. Therefore, inorganic buffers, such phosphate buffer (PBS), bicarbonate buffer (BBS), and ammonium buffer solutions have been used to buffer both the anolyte and catholyte in MFCs and MECs.

The extent of the effect of the buffer on cathode performance remains unclear, with some studies supporting the concept that the addition of buffer can enhance the cathode performance, while with others concluding the addition of buffer had no effect. Some studies reported that a reduced cathode overpotential could be obtained when the catholyte was buffered. The minimum overpotential of HER was reported to be reached at a pH close to the pKa for all buffers (PBS, BBS, ammonium chloride, ammonium bicarbonate, and Tris) at a constant current density of 15 A m^{-2} (50 mM), but the minimum overpotential ranged from 0.05 V to 0.09 V for the different buffers (83). Furthermore, increasing buffer concentration also led to lower cathodic overpotentials. Another study showed that the overpotential caused by pH differences could reach as much as 0.3 V, but the overpotential was nearly removed by sparging using CO_2 as the buffer (100). Other studies suggested that the use of buffer can improve cathode performance by facilitating the transport of protons and hydroxide ions as carriers. For example, in one study,

carbon dioxide was added to the influent of the air used to aerate the catholyte, and the dissolved carbon dioxide (bicarbonate) was used as a buffer to provide hydroxide ions (101). A 45% of power increase was found when carbon dioxide was mixed in the air influent. However, some studies reported that the use of buffer did not contribute to improved performance. For example, the addition of 50 mM PBS to the catholyte in an MEC did not improve hydrogen production compared to a non-buffered saline catholyte (similar conductivity) (102). Another study compared the effect of different buffers on MFC performance, showing that the conductivity instead of buffer has more significant impact on the power generation (103).

2.1.3 MxC

BESs with functions other than electricity production and hydrogen generation have also been developed, which are collectively referred to as MxCs. This innovative functions include enhanced energy production, reverse osmosis membranes are used for water purification. These two types of membrane processes need high pressure as the driving force for water transport. On the contrary, microfiltration and ultrafiltration membranes, due to the large pore size than nanofiltration membrane, have a higher permeability, thus are more economical when used in wastewater treatment for solids removal.

In addition to solid-liquid separation, gas-permeable membranes can also serve as the gas diffusor or membrane aerator in a biological treatment process. The membrane can also act as the substrate for microorganisms to be immobilized on. The counter-diffusion configuration, where oxygen diffuses out from the lumen to bulk in one direction, while the nutrient diffuses in from bulk to membrane in the other direction, allows the simultaneous removal of organics and nutrient. A third use of membrane in wastewater treatment is as an extractive membrane. In an extractive membrane, the biomedium and wastewater stream are separated by membrane (104).

The biodegradable organics in the wastewater are first diffused through the membrane into biomedium side, and removed subsequently by biological process.

In the following sections, membrane applications in wastewater treatment are reviewed with a focus on the use of membrane incorporated in MBRs for solids removal, and the use of membrane bioreactors in MABRs for nutrient removal.

2.2 Membrane bioreactor

Strict legislation on wastewater effluent discharges has led to requirements for enhanced treatment processes with high removal rates and efficiencies for COD, nutrients, and suspended solids. One of the most promising new technologies that has received much attention is the membrane bioreactor (MBR). By integrating a membrane module into the bioreactor, the wastewater effluent is pulled through the membrane so that most of the suspended solids are removed by filtration. In addition, membranes can help to separate the hydraulic retention time (HRT) from the solids retention time (SRT), which can produce a low HRT but high a SRT. Compared with conventional AS processes, the MBR uses less land area, which contributes to a savings in construction costs. MBRs can be further categorized into anaerobic MBRs (AnMBR) and aerobic MBRs (AeMBRs), depending on whether wastewater aeration is used or not.

2.2.1 Membrane fouling

Although MBRs can achieve high organics removal, high solids removal and low sludge production, a major obstacle for using membranes for wastewater treatment is membrane fouling. Membrane fouling refers to a decrease in flux and an increase transmembrane pressure (TMP) to pull the effluent through the membrane, which can increase the cost for operation and maintenance. Membrane fouling is a complex process that includes interactions between microbes and membrane, and therefore the design and operation of MBRs for biological and

membrane treatment is quite empirical (105). For a membrane, the driving force of pulling permeate is due to a pressure gradient or a concentration gradient (106). In MBRs, the biological process and membrane filtration cannot be separated, so the potential foulants along are attracted by the gradients to the membrane surface. The foulants have a great diversity. Inorganic chemicals, such as clays, salts, and organic matter in the wastewater or those produced by microbial metabolism, and grease, oil, surfactants, proteins, and the biofilm formation on the membrane, all can contribute to membrane fouling (107). As shown in Fig.2-3, membrane fouling could be caused by pore blocking with colloids and solutes, and formation of cake layer on the surface of membrane.

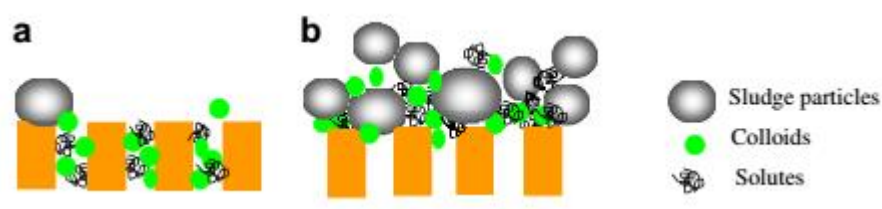


Fig. 2-4 Membrane fouling mechanism (a) pore blocking and (b) cake layer (107)

Much research has been conducted to identify and characterize foulants to better understand the nature of membrane fouling, but the major contributors to the membrane fouling remain unclear. Extracellular polymeric substances (EPS) formation was studied in a pilot-scale submerged MBR, showing that loosely bound EPS in solution rather than tightly bound EPS contributed to membrane fouling, the release of which was enhanced under shear stress and low temperature (108). A linear relationship was obtained between the fouling rate of the membranes and the concentration of polysaccharides in the sludge during operation with an SRT of 8 days, in two MBRs operated in parallel (109). The effect of particle size distribution on membrane resistance was studied in a MBR, showing that the hydraulic resistance of the membrane filtering recirculated activated sludge suspension was greater than that without recirculation (110). Further

analysis showed that the soluble particles generated from the microorganisms imposed under shear stress accounted for half of the total membrane resistance. A review paper summarized the contribution of sludge composition (flocs, colloids and solutes) on membrane fouling (Table 2-1) (107). Although flocs seemed to be the main contributor to membrane fouling (Table 2-1), the difference between each case indicated that the membrane fouling also depends on operational conditions. Many other operational factors, such as membrane material, aeration and reactor dimension, are all reported to have an effect on membrane fouling (105). Another study reported that the operational configuration, such as membrane type and membrane module configuration, can have a larger impact on membrane fouling and permeate flux decline than mixed liquor over the range of solids from 3600 to 8400 mg/L (111).

Table 2-1 Contribution of each sludge fraction to membrane fouling during membrane filtration of sludge suspension (reconstructed) (107)

	Flocs (%)	Colloids (%)	Solutes (%)	Remarks	Reference
CA-1	83	4	13	This study was performed in a cross-flow membrane filtration cell for 5 h with a constant TMP of 100 kPa	Membrane composition (112)
CA-2	76	10	14		
CA-3	74	13	13		
CA-4	72	14	14		
Bulking sludge	76	11	13	This study was performed in a batch filtration unit for 4 h with a constant TMP of 4.0 kPa	Sludge characteristic (113)
Normal sludge	52	22	26		
Deflocculated sludge	22	47	13		
20 days	63	37		The sludge samples from lab scale MBRs were filtered in a batch test with a constant TMP of 27 kPa	SRT (114)
40 days	72	28			
60 days	71	29			
	52	24	24	This study was tested in a cross-flow MBR TMP=100 kPa, u=3 m/s, T=15 °C, SRT=60 d	(115)
	65	30	5		(116)
	24	50	26		(117)

Three stages, conditioning fouling, steady fouling, and transmembrane pressure jump, have been identified to describe membrane fouling in MBRs (106,118). Membrane fouling starts with the irreversible adsorption of soluble biological products, such as EPS, soluble microbial

products (SMP), other related organics and colloids, to produce pore blocking, called conditioning fouling (107). In this period, the TMP rapidly increases. Following conditioning fouling is steady fouling, with the attachment of biomass on the membrane which is enhanced by adsorption of organics in the first stage of fouling, resulting in a formation of cake layer of biofilm and flocs on the surface (Fig. 2-3). In the final stage, due to the uneven distribution of fouling conditions on the membrane, caused by previous two fouling stages, less available surface area due to clogging will result in an exponential increase and a jump in the TMP.

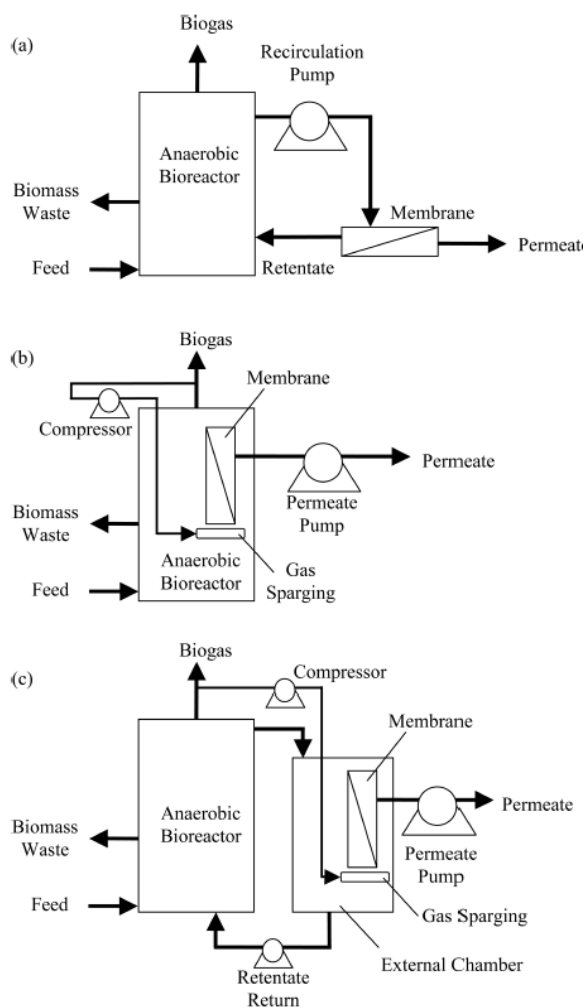


Fig. 2-5 Three common membrane configurations: (a) external flow membrane; (b) submerged membrane; (c) external submerged membrane (119).

2.2.2 Membrane configuration

Generally, two membrane configurations, external cross-flow membrane and submerged membranes, are used for membrane bioreactors based on the different placement of the membranes (119). When the membrane is placed in a recirculation line and operated under pressure (Fig. 2-4A), this configuration is referred as external-flow membrane. When the membrane is placed in the mixed liquor in the bioreactor and operated under suction (Fig. 2-4B), this configuration is called a submerged membrane. In external-flow membranes, the fast cross-flow velocity is applied to the membrane surface as a way to disrupt the formation of cake layer. In submerged MBRs, rising gas bubbles are used to scouring media to inhibit cake layer formation. Less commonly, a third configuration has been developed by combining the first two configurations. The membrane is placed in the circulation line, but a vacuum pump is used as the driving force to pull effluent through membrane in the recirculation line (Fig. 2-4C).

An analysis of the membrane flux of the two configurations showed that external-flow membranes (4 to 250 L/m²/h) had a higher flux than the submerged configuration (3 to 80 L/m²/h) (119). Another study concluded that the energy cost for submerged membranes to treat wastewater (0.25–1.0 kWh/m³) was lower than that of the external-flow setup (3–7.3 kWh/m³) (120). Due to the lower energy costs and pressure applied, the commercialization of submerged MBRs has been accelerated due to the production of cheap polymeric membranes (121). The review of submerged MBRs is therefore the focus of the following sections.

2.2.3 Aerobic membrane bioreactor

Ultrafiltration and microfiltration membranes are placed in submerged AeMBRs to replace the clarifier in the AS process for solids removal, leading to some advantages, such as fast start-up, small footprint, and low sludge production compared to AS (122). In addition, the

removal of bacteria and virus by membrane filtration can decrease the disinfection by-products produced in subsequent treatment. The use of the submerged configuration has reduced the energy consumption to be competitive with AS process, which makes AeMBRs effective for wastewater treatment (123). AeMBRs have been successfully incorporated into municipal and industrial wastewater treatment process, due to the separation of HRT and SRT, and complete solids retention by the use of filtration membrane.

Municipal wastewater treatment with AeMBRs has been extensively evaluated, with good treatment obtained in both pilot and full scales. For example, pilot-scale AeMBRs were studied to treat municipal wastewater in two different places, both achieving good COD removal (>95%) and ammonia removal (>97%) with HRTs of 2-9 h. Low TMP was maintained (20 kPa) during the operation with air bubbling, periodic backwashing, and chlorine washing (124). Another study on municipal wastewater treatment showed that a 95% of COD removal was obtained using a pilot-scale AeMBR (3.9 m³) for 535 days. With air bubbling and periodic cleaning of the membrane, the average TMP was maintained around 0.3 bar with an HRT of 10-15 h (123). A full-scale AeMBR was integrated with an anoxic basin to evaluate COD, nitrogen, and phosphorus removals. A COD removal of 95% and an effluent phosphorus concentration below 0.05 mg/L was obtained by dosing either ferric chloride or sodium aluminate to the anoxic basin (125).

Other wastewaters with that require a high organic loading for treatment, such as non-food processing industrial wastewaters, landfill leachate, sludge digestates, and human excrement, were also successfully treated with AeMBRs (121). Food processing industrial wastewater, for example, from food ingredients (126), were also treated with high COD removals, nitrogen removals, and low effluent TSS using AeMBRs. Combined sanitary and industrial wastewaters were treated using an external cross-flow AeMBRs, resulting in an effluent with COD of 400 mg/L and BOD of 10 mg/L (127). Compared with other treatment processes,

the MBR allows the retention of biomass even if an inhibitor in the industrial wastewater impairs biological treatment (119).

Due to the good and stable performance, AeMBRs are being commercialized world-wide, and the volume of wastewater being treated using AeMBRs is estimated to continue to grow in the future (128). However, there are some challenges, such as high maintenance costs, the membrane lifespan, membrane fouling control, and further scaling up AeMBRs to obtain higher capacities.

2.2.4 Anaerobic membrane bioreactor

AnMBRs were developed by not using aeration in MBRs, resulting in advantages, such as low energy costs due to the absence of aeration, volatile compounds removal, methane production for energy recovery, and less sludge production. Compared with AeMBRs, there are several differences in operation for AnMBRs. Since methane can be generated in AnMBRs, dissolved methane is in the effluent, which needs to be removed by using, for example, an air-stripping unit (129). Operating AnMBRs under low temperature was regarded as obstacle for anaerobic treatment technologies due to the slow microbial growth, but two review papers independently concluded that no barriers for microbial activity were found in AnMBRs (130). Methane solubility increases with lower temperatures, which complicates effective methane removal (131). The membrane fouling mechanisms in AeMBRs and AnMBRs are believed to be different, as reported in a previous study that the molecular weight distribution fingerprint of the foulants, such as EPS (on membrane) and SMP (in the effluent and retentate), were different for aerobic and anaerobic MBRs. The majority of SMP in AnMBRs was retained by the membrane, while all SMP fragments passed through, indicating the retention of these SMP fractions contributed to membrane fouling (132).

A review paper concluded that the extensive opportunities for AnMBRs lies in treating highly particulate and high-strength wastewaters, while AeMBRs are more suitable for low-strength wastewater treatment (119). AnMBRs have also been tested for treating various wastewaters, including synthetic wastewaters, food processing wastewaters, industrial wastewaters, and municipal wastewaters, and good effluent quality has been obtained by AnMBRs with different configurations. For example, synthetic sewage wastewater with high salinity was successfully treated in AnMBRs with a 99% of DOC removal. The membrane was shown to be responsible for a large portion of DOC removal (133). An AnMBR treating simulated domestic wastewater was evaluated under various temperatures, showing a 95% of COD removal at temperatures as low as 6 °C. Analysis of the microbial communities illustrated that the microbial diversity increased with low temperature (134). Municipal wastewater was treated by an AnMBR (12.9 L, HRT of 2.6 h) with non-woven fabric membrane, achieving an effluent COD of 78 mg/L with TMP controlled under 30 kPa by periodic chemical cleaning (135). The foulants characterized using various techniques showed that they were mostly proteins and EPS, with a broader molecular weight distribution than the influent. Food processing wastewater treatment by AnMBRs showed COD removals above 90% at organic loading rates ranging from 2-15 kg-COD/m³/d (136). Other industrial wastewaters, such as pulp and paper industrial wastewater, was treated in AnMBRs at both mesophilic and thermophilic conditions, achieving a COD removal above 93% with a high concentrated influent (>10,000 mg-COD/L) (137). In addition, agricultural waste, such as animal wastes, was treated by an anaerobic digester and a pilot AnMBR, showing a TKN removal of 32% and total phosphorus and COD removal above 90% (138). The removal of *E. coli* and *Enterococci* were found to be similar with or without anaerobic digester. Overall, bench-scale and pilot-scale AnMBRs have shown similar treatment performance with AeMBRs, even at low temperature and short HRTs (130), but extra post-treatment is needed to handle dissolved methane in the effluent of AnMBRs.

Membrane fouling is still a concern in AnMBRs, which is reported to be more severe compared with AeMBRs due to the lack of surface shear from air bubbling. Many different strategies have been adopted for membrane fouling control, among which the conventional approaches, such as membrane relaxation, backwashing, chemical clean, are most widely used. A previous study compared these fouling control strategies, indicating that the cake layer was well removed by all of these approaches, while the irreversible fouling due to pore clogging was removed only by chemical cleaning and enhanced backwashing (139). Biogas sparging, similar to that of air bubbling in AeMBRs, is also commonly used in AnMBRs, reducing the membrane resistance by inducing a shear at the surface of the membrane (140). Other anti-fouling strategies have been developed and tested recently as well. The addition of absorbent media, such as powdered activated carbon (PAC) (133,141) and GAC (142), reduced membrane fouling effectively by absorbing fine colloids and soluble biodegradable organics. Applying an electric field in MBRs to drive the migration of charged EPS, solids, and other foulants away from the membrane module reduced irreversible membrane fouling (143). Employing ultra-sound treatment in an on/off mode reduced membrane resistance by 70% compared with a control membrane without ultra-sound irradiation (144).

2.2.5 Anaerobic fluidized bed membrane bioreactor

Recently, another anti-fouling strategy was developed by introducing a high concentration of fluidized GAC particles into an AnMBR, producing an AFMBR where the GAC are used to mechanically scour the membrane surface. The AFMBR was first developed as a post-treatment method for an anaerobic fluidized bed bioreactor (AFBR), achieving a COD removal of AFBR effluent of 87% with no detectable TSS (120). The TMP during operation increased from 0.075 to 0.1 bar without chemical cleaning in the 40 days after a chemical cleaning. Although membrane fouling is well controlled, the effect of the GAC on scouring is still unclear. In a

previous study, the use of fluidized GAC effectively removed the cake layer and absorbed the potential foulants before interaction with the membrane, but had a potential to induce loss of membrane integrity and introduce fine carbon particles as foulants (145). The GAC size was shown to have little effect on membrane scouring and membrane damage. However, a later study reported that the smaller the GAC particles were, the greater membrane fouling was reduced by GAC scouring (146). This trend reversed if the GAC was pre-adsorbed with organic matter. A recent study using wavelet decomposition to analyze the vibration signal during GAC scouring, showing that the smallest GAC particles (1.2 mm) needed the greatest energy input to achieve the same scouring effect as the larger GAC particles (1.85 and 2.18 mm) (147). Also, the solid phase dynamics correlated well with membrane fouling mitigation rather than liquid phase dynamics.

The AFMBR has primarily been used as the post-treatment reactor to follow several different types of reactors. For example, an AFMBR as a secondary treatment process to treat effluent from a MFC treating domestic wastewater achieved 85% of COD removal and 99.6% of TSS removal, with an estimated energy demand of 0.0186 kWh/m³ (148). Another study further evaluated the post-treatment of the effluent from MFC using AFMBR under different OLRs (149). A stable COD removal of 89% was obtained by the AFMBR with HRTs of 1.2 to 3.8 h. An AFMBR treating the effluent from an anaerobic baffled reactor (ABR) was evaluated, showing 87% of COD removal using a complex synthetic wastewater at an HRT of ~1 h, with an energy demand of 0.0087 kWh/m³ (150). In addition, another study reported that an AFMBR following an AFBR was capable of treating pharmaceutical chemicals (78-100% of removal) simultaneously with COD degradation (151). A long-term test of pilot staged AFBR-AFMBR treating domestic wastewater under temperature 8 to 30 °C showed high removal efficiency of COD (90%) and BOD (90%) was maintained even in the winter after full acclimation (152).

Other studies focused on the AFMBR itself, concluded that good effluent quality can also be obtained by an AFMBR alone treating low concentration wastewaters. The acclimation of

AMFBRs was tested with GAC inoculated by wastewater, anaerobic digestion sludge, or anaerobic bog sediment, showing that the AFMBR with GAC inoculated by anaerobic digestion sludge and acclimated with acetate had the highest COD removals (153). A single AFMBR was compared to a staged anaerobic fluidized membrane bioreactors (SAF-MBR) for treating synthetic wastewater (~200 mg COD/L), with no significant differences found between the processes in terms of COD removal efficiency, TMP, bulk liquid suspended solids, EPS production, and SMP (154).

2.3 Membrane aerators

Another application of membranes in wastewater treatment is to immobilize biofilms on the surface of membranes, so that the contaminants are removed by the immobilized biofilm. Two different configurations have been developed, called a membrane aerator and a membrane biofilter (155). The membrane aerator uses tubes pressurized with gas, where the gas diffuses out through membrane with a bubbleless form. The membrane biofilter works in the opposite way, where the liquid wastes flow inside the lumen, and the wastes diffused out is degraded by biofilm immobilized at the membrane surface. In the following sections, the membrane aerator will be focus of the literature review as this is the more commonly used membrane-based aeration approach.

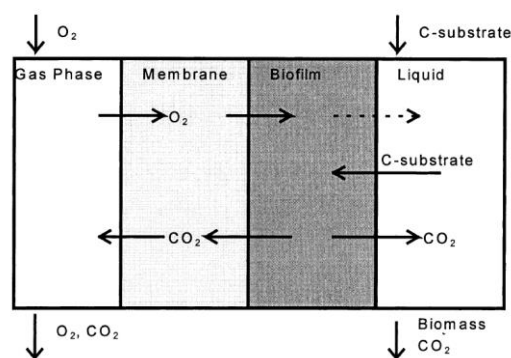


Fig. 2-6 The schematic diagram of the MABR (155)

2.3.1 Oxygenation

If air or oxygen is pressurized in the lumen, it diffuses out in a bubbleless form and is available as an electron acceptor for microorganisms in the biofilm. The difference between membrane-aerated bioreactor (MABR) and conventional treatment process is the counter diffusion of lumen gas from the membrane and organics to the biofilm on the membrane (Fig. 2-5). Oxygen from the lumen diffuses out into the biofilm, while the substrate diffuses into the biofilm from the bulk. This counter diffusion on the membrane allows the growth of stratified biofilm (156), where nitrifying bacteria can grow in the inner layer of biofilm near the membrane, with denitrifying and heterotrophic bacteria growing on the outer layer of the biofilm (157). The MABR has several advantages, such as the separation of the depth of the reactor and oxygen transfer efficiency by controlling lumen pressure, prevention of volatile fatty acid stripping during treatment due to bubbleless aeration, high oxygen transfer efficiency, and no need for adjusting pH by integrating nitrification and denitrification.

MABRs have successfully been applied for nitrogen nutrient removal. The MABR was first tested for treating synthetic wastewater (total organic carbon, TOC, 1000 mg/L and total nitrogen, TN, 58.5 mg-N/L) in batch mode (24 h), achieving a removal efficiency of 97.9% for TOC and 98.3% for TN with lumen pressure of 245 kPa (pure oxygen) (158). Another study investigated a MABR treating synthetic COD-free wastewater in continuous flow mode with HRT of 1-4 h, resulting in an ammonia removal flux as high as 5.4 mg-N/m²-d (159).

Good nitrogen removal was also obtained in an MABR supplied with air instead of pure oxygen, although longer HRTs were needed. A total nitrogen removal flux (NRF) of 1.7 g-N/m²-d was achieved by an MABR to treat COD-free wastewater (47.1 mM NH₃-N), resulting in a 75% removal of influent N (156). Both COD and ammonia in synthetic wastewater were simultaneously removed by a MABR (HRT of 6 h), with 90% of COD removal and 2 g-N/m²-d

of ammonia removal flux. However, stable treatment was only sustained for 3 months, due to excessive biofilm growth (160). Nitrogen and carbonaceous compounds in synthetic wastewater (total organic carbon of 100 mg/L and 25 g-N/m³) were simultaneously removed using an MABR with a carbon removal flux (CRF) of 7.4 g-C/m²-d and NRF of 2.8 g-N/m²-d, and a large difference in nitrogen and carbon removal rate was discovered at various membrane locations (161). A higher nitrogen removal flux of 4.48 g-N/m²-d were obtained in a MABR (HRT of 16 d) supplied with air treating artificial swine wastewater, with a 96% of TOC removal (157).

2.3.2 Hydrogen pressurized in the lumen

Hydrogen supplied by an MABR has also been used to achieve autotrophic nitrification. For example, separate arrays of juxtaposed hollow fiber membranes were used to supply pure bubbleless hydrogen and oxygen in a redox control bioreactor treating organic-free synthetic wastewater (217 mg-N/L of ammonium), with an ammonia removal flux of 5.8 g-N/m² membrane-d and a nitrate and nitrite removal flux of 4.4 g-N/m²-d (162). Another study applied MABR to remediate contaminated groundwater, achieving a 92% to 96% of nitrate removal with a nitrate removal flux ranging from 2.7 to 5.3 g-N/m²-d (163). The membrane aerator prevented the microbial contamination of the product water. The main disadvantage of the hydrogen gas MABR is the cost of the hydrogen gas.

2.4 Literature cited

1. Logan BE, Hamelers B, Rozendal R, Schröder U, Keller J, Freguia S, et al. Microbial fuel cells: Methodology and technology. *Environ Sci Technol.* 2006;40(17):5181–92.
2. Cheng S, Hamelers HVM, Logan BE, Call D, Cheng S, Hamelers HVM, et al. Microbial electrolysis cells for high yield hydrogen gas production from organic matter. *Environ Sci Technol.* 2008;42(23):8630–40.

3. Cheng S, Xing D, Call DF, Logan BE. Direct biological conversion of electrical current into methane by electromethanogenesis. *Environ Sci Technol.* 2009;43(10):3953–8.
4. Rozendal R a, Hamelers HVM, Buisman CJN. Effects of membrane cation transport on pH and microbial fuel cell performance. *Environ Sci Technol.* 2006;40(17):5206–11.
5. Rozendal RA, Leone E, Keller J, Rabaey K. Electrochemistry Communications Efficient hydrogen peroxide generation from organic matter in a bioelectrochemical system. *Electrochem commun.* 2009;11(9):1752–5.
6. Nevin KP, Woodard TL, Franks AE, Summers ZM, Lovley DR. Microbial electrosynthesis: feeding microbes electricity to convert carbon dioxide and water to multicarbon extracellular organic compounds. *MBio.* 2010;1(2):e00103-10.
7. Steinbusch KJJ, Hamelers HVM, Schaap JD, Kampman C, Buisman CJN. Bioelectrochemical ethanol production through mediated acetate reduction by mixed cultures. *Environ Sci Technol.* 2009;44(1):513–7.
8. Ganigu éR, Puig S, Batlle-Vilanova P, Balaguer MD, Colprim J. Microbial electrosynthesis of butyrate from carbon dioxide. *Chem Commun.* 2015;51(15):3235–8.
9. Logan BE., Rabaey K. Conversion of wastes into bioelectricity and chemicals by using microbial electrochemical technologies. *Science (80-).* 2012;337(6095):686–690.
10. Khera J, Chandra A. Microbial fuel cells: Recent trends. *Proc Natl Acad Sci India Sect A - Phys Sci.* 2012;82(1):31–41.
11. Zhang P-Y, Liu Z-L. Experimental study of the microbial fuel cell internal resistance. *J Power Sources.* 2010;195(24):8013–8.
12. Manohar AK, Mansfeld F. The internal resistance of a microbial fuel cell and its dependence on cell design and operating conditions. *Electrochim Acta.* 2009;54(6):1664–70.
13. Wang X, Cheng S, Feng Y, Merrill MD, Saito T, Logan BE. Use of carbon mesh anodes

- and the effect of different pretreatment methods on power production in microbial fuel cells. *Environ Sci Technol*. 2009;43(17):6870–4.
14. Logan B, Cheng S, Watson V, Estadt G. Graphite fiber brush anodes for increased power production in air-cathode microbial fuel cells. *Environ Sci Technol*. 2007;41(9):3341–6.
 15. Cheng S, Logan BE. Ammonia treatment of carbon cloth anodes to enhance power generation of microbial fuel cells. *Electrochem Commun*. 2007;9(3):492–6.
 16. Ter Heijne A, Hamelers HVM, Saakes M, Buisman CJN. Performance of non-porous graphite and titanium-based anodes in microbial fuel cells. *Electrochim Acta*. 2008;53(18):5697–703.
 17. Lv Z, Xie D, Yue X, Feng C, Wei C. Ruthenium oxide-coated carbon felt electrode: a highly active anode for microbial fuel cell applications. *J Power Sources*. 2012;210:26–31.
 18. Sun J-J, Zhao H-Z, Yang Q-Z, Song J, Xue A. A novel layer-by-layer self-assembled carbon nanotube-based anode: preparation, characterization, and application in microbial fuel cell. *Electrochim Acta*. 2010;55(9):3041–7.
 19. Peng X, Yu H, Wang X, Zhou Q, Zhang S, Geng L, et al. Enhanced performance and capacitance behavior of anode by rolling Fe₃O₄ into activated carbon in microbial fuel cells. *Bioresour Technol*. 2012;121:450–3.
 20. Feng C, Lv Z, Yang X, Wei C. Anode modification with capacitive materials for a microbial fuel cell: an increase in transient power or stationary power. *Phys Chem Chem Phys*. 2014;16(22):10464–72.
 21. Lai B, Tang X, Li H, Du Z, Liu X, Zhang Q. Power production enhancement with a polyaniline modified anode in microbial fuel cells. *Biosens Bioelectron*. 2011;28(1):373–7.
 22. Li C, Zhang L, Ding L, Ren H, Cui H. Effect of conductive polymers coated anode on the performance of microbial fuel cells (MFCs) and its biodiversity analysis. *Biosens*

- Bioelectron. 2011;26(10):4169–76.
23. Zhang Y, Mo G, Li X, Zhang W, Zhang J, Ye J, et al. A graphene modified anode to improve the performance of microbial fuel cells. *J Power Sources*. 2011;196(13):5402–7.
 24. Crittenden SR, Sund CJ, Sumner JJ. Mediating electron transfer from bacteria to a gold electrode via a self-assembled monolayer. *Langmuir*. 2006;22(23):9473–6.
 25. Erable B, Bergel A. First air-tolerant effective stainless steel microbial anode obtained from a natural marine biofilm. *Bioresour Technol*. 2009;100(13):3302–7.
 26. Richter H, McCarthy K, Nevin KP, Johnson JP, Rotello VM, Lovley DR. Electricity generation by *Geobacter sulfurreducens* attached to gold electrodes. *Langmuir*. 2008;24(8):4376–9.
 27. Schröder U. Anodic electron transfer mechanisms in microbial fuel cells and their energy efficiency. *Phys Chem Chem Phys*. 2007;9(21):2619–29.
 28. Kim HJ, Park HS, Hyun MS, Chang IS, Kim M, Kim BH. A mediator-less microbial fuel cell using a metal reducing bacterium, *Shewanella putrefaciens*. *Enzyme Microb Technol*. 2002;30(2):145–52.
 29. Gorby YA, Yanina S, McLean JS, Rosso KM, Moyles D, Dohnalkova A, et al. Electrically conductive bacterial nanowires produced by *Shewanella oneidensis* strain MR-1 and other microorganisms. *Proc Natl Acad Sci*. 2006;103(30):11358–63.
 30. Lovley DR. The microbe electric: conversion of organic matter to electricity. *Curr Opin Biotechnol*. 2008;19(6):564–71.
 31. Logan BE. Exoelectrogenic bacteria that power microbial fuel cells. *Nat Rev Microbiol*. 2009;7(5):375–81.
 32. Park DH, Zeikus JG. Electricity generation in microbial fuel cells using neutral red as an electronophore. *Appl Environ Microbiol*. 2000;66(4):1292–7.
 33. Thygesen A, Poulsen FW, Min B, Angelidaki I, Thomsen AB. The effect of different

- substrates and humic acid on power generation in microbial fuel cell operation. *Bioresour Technol.* 2009;100(3):1186–91.
34. Bond DR, Holmes DE, Tender LM, Lovley DR. Electrode-reducing microorganisms that harvest energy from marine sediments. *Science* (80-). 2002;295(5554):483–5.
 35. Jang JK, Pham TH, Chang IS, Kang KH, Moon H, Cho KS, et al. Construction and operation of a novel mediator-and membrane-less microbial fuel cell. *Process Biochem.* 2004;39(8):1007–12.
 36. Raghavulu SV, Mohan SV, Goud RK, Sarma PN. Effect of anodic pH microenvironment on microbial fuel cell (MFC) performance in concurrence with aerated and ferricyanide catholytes. *Electrochem commun.* 2009;11(2):371–5.
 37. Li J, Fu Q, Liao Q, Zhu X, Ye D, Tian X. Persulfate: A self-activated cathodic electron acceptor for microbial fuel cells. *J Power Sources.* 2009;194(1):269–74.
 38. Erable B, Féron D, Bergel A. Microbial catalysis of the oxygen reduction reaction for microbial fuel cells: a review. *ChemSusChem.* 2012;5(6):975–87.
 39. Cheng S, Logan BE. Increasing power generation for scaling up single-chamber air cathode microbial fuel cells. *Bioresour Technol.* 2011;102(6):4468–73.
 40. He Z, Huang Y, Manohar AK, Mansfeld F. Effect of electrolyte pH on the rate of the anodic and cathodic reactions in an air-cathode microbial fuel cell. *Bioelectrochemistry.* 2008;74(1):78–82.
 41. Fan Y, Sharbrough E, Liu H. Quantification of the internal resistance distribution of microbial fuel cells. *Environ Sci Technol.* 2008;42(21):8101–7.
 42. Cheng S, Liu H, Logan BE. Increased performance of single-chamber microbial fuel cells using an improved cathode structure. *Electrochem commun.* 2006;8(3):489–94.
 43. Cheng S, Liu H, Logan BE. Power densities using different cathode catalysts (Pt and CoTMPP) and polymer binders (Nafion and PTFE) in single chamber microbial fuel cells.

- Environ Sci Technol. 2006;40(1):364–9.
44. Zhao F, Harnisch F, Schröder U, Scholz F, Bogdanoff P, Herrmann I. Challenges and constraints of using oxygen cathodes in microbial fuel cells. *Environ Sci Technol.* 2006;40(17):5193–9.
 45. Ter Heijne A, Hamelers HVM, De Wilde V, Rozendal RA, Buisman CJN. A bipolar membrane combined with ferric iron reduction as an efficient cathode system in microbial fuel cells. *Environ Sci Technol.* 2006;40(17):5200–5.
 46. Zhang F, Cheng S, Pant D, Van Bogaert G, Logan BE. Power generation using an activated carbon and metal mesh cathode in a microbial fuel cell. *Electrochem Commun.* 2009;11(11):2177–9.
 47. Cheng S, Wu J. Air-cathode preparation with activated carbon as catalyst, PTFE as binder and nickel foam as current collector for microbial fuel cells. *Bioelectrochemistry.* 2013;92:22–6.
 48. Dong H, Yu H, Wang X, Zhou Q, Feng J. A novel structure of scalable air-cathode without Nafion and Pt by rolling activated carbon and PTFE as catalyst layer in microbial fuel cells. *Water Res.* 2012;46(17):5777–87.
 49. Santoro C, Agrios A, Pasaogullari U, Li B. Effects of gas diffusion layer (GDL) and micro porous layer (MPL) on cathode performance in microbial fuel cells (MFCs). *Int J Hydrogen Energy.* 2011;36(20):13096–104.
 50. Chatterjee P, Ghangrekar MM. Preparation of a fouling-resistant sustainable cathode for a single-chambered microbial fuel cell. *Water Sci Technol.* 2014;69(3):634–9.
 51. Kumar P, Chatterjee P, Ghangrekar MM. Fouling resistant nitrogen doped carbon powder with amino-tri-methylene-phosphate cathode for microbial fuel cell. *Mater Renew Sustain Energy.* 2017;6(2):9.
 52. Liu W, Cheng S, Sun D, Huang H, Chen J, Cen K. Inhibition of microbial growth on air

- cathodes of single chamber microbial fuel cells by incorporating enrofloxacin into the catalyst layer. *Biosens Bioelectron.* 2015;72:44–50.
53. Li W-W, Sheng G-P, Liu X-W, Yu H-Q. Recent advances in the separators for microbial fuel cells. *Bioresour Technol.* 2011;102(1):244–52.
 54. Sleutels THJA, Hamelers HVM, Rozendal RA, Buisman CJN. Ion transport resistance in Microbial Electrolysis Cells with anion and cation exchange membranes. *Int J Hydrogen Energy.* 2009;34(9):3612–20.
 55. Zhuang L, Zhou S, Li Y, Yuan Y. Enhanced performance of air-cathode two-chamber microbial fuel cells with high-pH anode and low-pH cathode. *Bioresour Technol.* 2010;101(10):3514–9.
 56. Gil GC, Chang IS, Kim BH, Kim M, Jang JK, Park HS, et al. Operational parameters affecting the performance of a mediator-less microbial fuel cell. *Biosens Bioelectron.* 2003;18(4):327–34.
 57. Xu J, Sheng G-P, Luo H-W, Li W-W, Wang L-F, Yu H-Q. Fouling of proton exchange membrane (PEM) deteriorates the performance of microbial fuel cell. *Water Res.* 2012;46(6):1817–24.
 58. Kim JR, Cheng S, Oh S-E, Logan BE. Power generation using different cation, anion, and ultrafiltration membranes in microbial fuel cells. *Environ Sci Technol.* 2007;41(3):1004–9.
 59. Harnisch F, Schröder U, Scholz F. The suitability of monopolar and bipolar ion exchange membranes as separators for biological fuel cells. *Environ Sci Technol.* 2008;42(5):1740–6.
 60. Zhang X, Cheng S, Wang X, Huang X, Logan BE. Separator characteristics for increasing performance of microbial fuel cells. *Environ Sci Technol.* 2009;43(21):8456–61.
 61. Sun J, Hu Y, Bi Z, Cao Y. Improved performance of air-cathode single-chamber microbial

- fuel cell for wastewater treatment using microfiltration membranes and multiple sludge inoculation. *J Power Sources*. 2009;187(2):471–9.
62. He Z, Minteer SD, Angenent LT. Electricity generation from artificial wastewater using an upflow microbial fuel cell. *Environ Sci Technol*. 2005;39(14):5262–7.
63. Zhu F, Wang W, Zhang X, Tao G. Electricity generation in a membrane-less microbial fuel cell with down-flow feeding onto the cathode. *Bioresour Technol*. 2011;102(15):7324–8.
64. You S, Zhao Q, Zhang J, Jiang J, Wan C, Du M, et al. A graphite-granule membrane-less tubular air-cathode microbial fuel cell for power generation under continuously operational conditions. *J Power Sources*. 2007;173(1):172–7.
65. Shimoyama T, Komukai S, Yamazawa A, Ueno Y, Logan BE, Watanabe K. Electricity generation from model organic wastewater in a cassette-electrode microbial fuel cell. *Appl Microbiol Biotechnol*. 2008;80(2):325.
66. Inoue K, Ito T, Kawano Y, Iguchi A, Miyahara M, Suzuki Y, et al. Electricity generation from cattle manure slurry by cassette-electrode microbial fuel cells. *J Biosci Bioeng*. 2013;116(5):610–5.
67. Rader GK, Logan BE. Multi-electrode continuous flow microbial electrolysis cell for biogas production from acetate. *Int J Hydrogen Energy*. 2010;35(17):8848–54.
68. Fan Y, Han S-K, Liu H. Improved performance of CEA microbial fuel cells with increased reactor size. *Energy Environ Sci*. 2012;5(8):8273–80.
69. Kong W, Guo Q, Wang X, Yue X. Electricity generation from wastewater using an anaerobic fluidized bed microbial fuel cell. *Ind Eng Chem Res*. 2011;50(21):12225–32.
70. Aelterman P, Rabaey K, Pham HT, Boon N, Verstraete W. Continuous electricity generation at high voltages and currents using stacked microbial fuel cells. *Environ Sci Technol*. 2006;40(10):3388–94.

71. Liu Xinmin Gong Benyue WJ. Series and parallel connection of anaerobic fluidized bed microbial fuel cells (MFCs). *Int J Appl Microbiol Biotechnol Res*. 2016;4(2):7–14.
72. Gurung A, Oh S-E. The performance of serially and parallelly connected microbial fuel cells. *Energy Sources, Part A Recover Util Environ Eff*. 2012;34(17):1591–8.
73. Oh S-E, Logan BE. Voltage reversal during microbial fuel cell stack operation. *J Power Sources*. 2007;167(1):11–7.
74. Ieropoulos IA, Ledezma P, Stinchcombe A, Papaharalabos G, Melhuish C, Greenman J. Waste to real energy: the first MFC powered mobile phone. *Phys Chem Chem Phys*. 2013;15(37):15312–6.
75. Dewan A, Beyenal H, Lewandowski Z. Scaling up microbial fuel cells. *Environ Sci Technol*. 2008;42(20):7643–8.
76. Cheng S, Ye Y, Ding W, Pan B. Enhancing power generation of scale-up microbial fuel cells by optimizing the leading-out terminal of anode. *J Power Sources*. 2014;248:931–8.
77. Zhuang L, Yuan Y, Wang Y, Zhou S. Long-term evaluation of a 10-liter serpentine-type microbial fuel cell stack treating brewery wastewater. *Bioresour Technol*. 2012;123:406–12.
78. Dekker A, Heijne A Ter, Saakes M, Hamelers HVM, Buisman CJN. Analysis and improvement of a scaled-up and stacked microbial fuel cell. *Environ Sci Technol*. 2009;43(23):9038–42.
79. Jiang D, Curtis M, Troop E, Scheible K, McGrath J, Hu B, et al. A pilot-scale study on utilizing multi-anode/cathode microbial fuel cells (MAC MFCs) to enhance the power production in wastewater treatment. *Int J Hydrogen Energy*. 2011;36(1):876–84.
80. Call D, Logan BE. Hydrogen production in a single chamber microbial electrolysis cell lacking a membrane. *Environ Sci Technol*. 2008;42(9):3401–6.
81. Kundu A, Sahu JN, Redzwan G, Hashim MA. An overview of cathode material and

- catalysts suitable for generating hydrogen in microbial electrolysis cell. *Int J Hydrogen Energy*. 2013;38(4):1745–57.
82. Azwar MY, Hussain MA, Abdul-Wahab AK. Development of biohydrogen production by photobiological, fermentation and electrochemical processes: A review. *Renew Sustain Energy Rev*. 2014;31:158–73.
 83. Jeremiasse AW, Hamelers HVM, Kleijn JM, Buisman CJN. Use of biocompatible buffers to reduce the concentration overpotential for hydrogen evolution. *Environ Sci Technol*. 2009;43(17):6882–7.
 84. Tartakovsky B, Manuel M-F, Wang H, Guiot SR. High rate membrane-less microbial electrolysis cell for continuous hydrogen production. *Int J Hydrogen Energy*. 2009;34(2):672–7.
 85. Cheng S, Hamelers HVM. Microbial electrolysis cells for high yield hydrogen gas production from organic matter. *Environ Sci Technol*. 2008;42(23).
 86. Zhang Y, Merrill MD, Logan BE. The use and optimization of stainless steel mesh cathodes in microbial electrolysis cells. *Int J Hydrogen Energy*. 2010;35(21):12020–8.
 87. Call DF, Merrill MD, Logan BE. High surface area stainless steel brushes as cathodes in microbial electrolysis cells. *Environ Sci Technol*. 2009;43(6):2179–83.
 88. Selembo PA, Merrill MD, Logan BE. The use of stainless steel and nickel alloys as low-cost cathodes in microbial electrolysis cells. *J Power Sources*. 2009;190(2):271–8.
 89. Selembo PA, Merrill MD, Logan BE. Hydrogen production with nickel powder cathode catalysts in microbial electrolysis cells. *Int J Hydrogen Energy*. 2010;35(2):428–37.
 90. Brown RK, Schmidt UC, Harnisch F, Schröder U. Combining hydrogen evolution and corrosion data-A case study on the economic viability of selected metal cathodes in microbial electrolysis cells. *J Power Sources*. 2017;356:473–83.
 91. Rozendal RA, Jeremiasse AW, Hamelers HVM, Buisman CJN. Hydrogen production with

- a microbial biocathode. *Environ Sci Technol.* 2007;42(2):629–34.
92. Jeremiasse AW, Hamelers HVM, Buisman CJN. Microbial electrolysis cell with a microbial biocathode. *Bioelectrochemistry.* 2010;78(1):39–43.
 93. Pisciotta JM, Zaybak Z, Call DF, Nam J-Y, Logan BE. Enrichment of microbial electrolysis cell biocathodes from sediment microbial fuel cell bioanodes. *Appl Environ Microbiol.* 2012;78(15):5212–9.
 94. Rozendal RA, Sleutels THJA, Hamelers HVM, Buisman CJN. Effect of the type of ion exchange membrane on performance, ion transport, and pH in biocatalyzed electrolysis of wastewater. *Water Sci Technol.* 2008;57(11):1757–62.
 95. Rozendal RA, Hamelers HVM, Molenkamp RJ, Buisman CJN. Performance of single chamber biocatalyzed electrolysis with different types of ion exchange membranes. *Water Res.* 2007;41(9):1984–94.
 96. Sleutels THJA, Hamelers HVM, Rozendal RA, Buisman CJN. Ion transport resistance in microbial electrolysis cells with anion and cation exchange membranes. *Int J Hydrogen Energy.* 2009;34(9):3612–20.
 97. Sleutels THJA, ter Heijne A, Kuntke P, Buisman CJN, Hamelers HVM. Membrane selectivity determines energetic losses for ion transport in bioelectrochemical systems. *ChemistrySelect.* 2017;2(12):3462–70.
 98. Ye Y, Zhu X, Logan BE. Effect of buffer charge on performance of air-cathodes used in microbial fuel cells. *Electrochim Acta.* 2016;194:441–7.
 99. Popat SC, Ki D, Young MN, Rittmann BE, Torres CI. Buffer pKa and transport govern the concentration overpotential in electrochemical oxygen reduction at neutral pH. *ChemElectroChem.* 2014;1(11):1909–15.
 100. Ki D, Popat SC, Torres CI. Reduced overpotentials in microbial electrolysis cells through improved design, operation, and electrochemical characterization. *Chem Eng J.*

- 2016;287:181–8.
101. Torres CI, Lee HS, Rittmann BE. Carbonate species as OH⁻ carriers for decreasing the pH gradient between cathode and anode in biological fuel cells. *Environ Sci Technol*. 2008;42(23):8773–7.
 102. Nam JY, Logan BE. Enhanced hydrogen generation using a saline catholyte in a two chamber microbial electrolysis cell. *Int J Hydrogen Energy*. 2011;36(23):15105–10.
 103. Nam J-YY, Kim H-WW, Lim K-HH, Shin H-SS, Logan BE. Variation of power generation at different buffer types and conductivities in single chamber microbial fuel cells. *Biosens Bioelectron*. 2010;25(5):1155–9.
 104. Strachan LF, Livingston AG. The effect of membrane module configuration on extraction efficiency in an extractive membrane bioreactor. *J Memb Sci*. 1997;128(2):231–42.
 105. Drews A. Membrane fouling in membrane bioreactors—characterisation, contradictions, cause and cures. *J Memb Sci*. 2010;363(1):1–28.
 106. Gkotsis PK, Banti DC, Peleka EN, Zouboulis AI, Samaras PE. Fouling issues in membrane bioreactors (MBRs) for wastewater treatment: major mechanisms, prevention and control strategies. *Processes*. 2014;2(4):795–866.
 107. Meng F, Chae S-RR, Drews A, Kraume M, Shin H-SS, Yang F. Recent advances in membrane bioreactors (MBRs): membrane fouling and membrane material. *Water Res*. 2009;43(6):1489–512.
 108. Wang Z, Wu Z, Tang S. Extracellular polymeric substances (EPS) properties and their effects on membrane fouling in a submerged membrane bioreactor. *Water Res*. 2009;43(9):2504–12.
 109. Lesjean B, Rosenberger S, Laabs C, Jekel M, Gnirss R, Amy G. Correlation between membrane fouling and soluble/colloidal organic substances in membrane bioreactors for municipal wastewater treatment. *Water Sci Technol*. 2005;51(6–7):1–8.

110. Wisniewski C, Grasmick A. Floc size distribution in a membrane bioreactor and consequences for membrane fouling. *Colloids Surfaces A Physicochem Eng Asp.* 1998;138(2):403–11.
111. Hong SP, Bae TH, Tak TM, Hong SP, Randall A. Fouling control in activated sludge submerged hollow fiber membrane bioreactors. *Desalination.* 2002;143(3):219–28.
112. Bae T-H, Tak T-M. Interpretation of fouling characteristics of ultrafiltration membranes during the filtration of membrane bioreactor mixed liquor. *J Memb Sci.* 2005;264(1):151–60.
113. Meng F, Yang F. Fouling mechanisms of deflocculated sludge, normal sludge, and bulking sludge in membrane bioreactor. *J Memb Sci.* 2007;305(1):48–56.
114. Lee W, Kang S, Shin H. Sludge characteristics and their contribution to microfiltration in submerged membrane bioreactors. *J Memb Sci.* 2003;216(1):217–27.
115. Wisniewski C, Grasmick A. Floc size distribution in a membrane bioreactor and consequences for membrane fouling. *Colloids Surfaces A Physicochem Eng Asp.* 1998;138(2):403–11.
116. Defrance L, Jaffrin MY, Gupta B, Paullier P, Geaugey V. Contribution of various constituents of activated sludge to membrane bioreactor fouling. *Bioresour Technol.* 2000;73(2):105–12.
117. Bouhabila EH, Aïm R Ben, Buisson H. Fouling characterisation in membrane bioreactors. *Sep Purif Technol.* 2001;22:123–32.
118. Zhang J, Chua HC, Zhou J, Fane AG. Factors affecting the membrane performance in submerged membrane bioreactors. *J Memb Sci.* 2006;284(1):54–66.
119. Liao B-Q, Kraemer JT, Bagley DM. Anaerobic membrane bioreactors: applications and research directions. *Crit Rev Environ Sci Technol.* 2006;36(6):489–530.
120. Kim J, Kim K, Ye H, Lee E, Shin C, McCarty PL, et al. Anaerobic fluidized bed

- membrane bioreactor for wastewater treatment. *Environ Sci Technol*. 2011 Jan 15;45(2):576–81.
121. Cicek N. A review of membrane bioreactors and their potential application in the treatment of agricultural wastewater. *Can Biosyst Eng*. 2003;45:6–37.
122. Gander M, Je B, Judd S. Aerobic MBRs for domestic wastewater treatment: a review with cost considerations. *Sep Purif Technol*. 2000;18(2):119–30.
123. Rosenberger S, Krüger U, Witzig R, Manz W, Szewzyk U, Kraume M. Performance of a bioreactor with submerged membranes for aerobic treatment of municipal waste water. *Water Res*. 2002;36(2):413–20.
124. Côté P, Buisson H, Pound C, Arakaki G. Immersed membrane activated sludge for the reuse of municipal wastewater. *Desalination*. 1997;113(2):189–96.
125. Lorenz W, Cunningham T, Penny JP. Phosphorus removal in a membrane reactor system: a full-scale wastewater demonstration study. *Proc Water Environ Fed*. 2002;2002(15):406–14.
126. Cantor J, Sutton PM, Steinheber R, Novachis L. Industrial biotreatment plant capacity expansion and upgrading through application of membrane biomass-effluent separation. *Proc Water Environ Fed*. 2000;2000(12):794–808.
127. Roberts JA, Sutton PM, Mishra PN. Application of the membrane biological reactor system for combined sanitary and industrial wastewater treatment. *Int Biodeterior Biodegradation*. 2000;46(1):37–42.
128. Sutton PM. Membrane bioreactors for industrial wastewater treatment: Applicability and selection of optimal system configuration. *Proc Water Environ Fed*. 2006;2006(9):3233–48.
129. McCarty PL, Bae J, Kim J. Domestic Wastewater Treatment as a Net Energy Producer—Can This be Achieved? *Environ Sci Technol*. 2011;45(17):7100–6.

130. Smith AL, Stadler LB, Love NG, Skerlos SJ, Raskin L. Perspectives on anaerobic membrane bioreactor treatment of domestic wastewater: a critical review. *Bioresour Technol.* 2012;122:149–59.
131. Skouteris G, Hermosilla D, López P, Negro C, Blanco Á. Anaerobic membrane bioreactors for wastewater treatment: A review. *Chem Eng J.* 2012;198:138–48.
132. Xiong Y, Harb M, Hong PY. Characterization of biofoulants illustrates different membrane fouling mechanisms for aerobic and anaerobic membrane bioreactors. *Sep Purif Technol.* 2016;157:192–202.
133. Vyrides I, Stuckey DC. Saline sewage treatment using a submerged anaerobic membrane reactor (SAMBR): effects of activated carbon addition and biogas-sparging time. *Water Res.* 2009;43(4):933–42.
134. Smith AL, Skerlos SJ, Raskin L. Anaerobic membrane bioreactor treatment of domestic wastewater at psychrophilic temperatures ranging from 15 °C to 3 °C. *Environ Sci Water Res Technol.* 2015;1(1):56–64.
135. An Y, Wang Z, Wu Z, Yang D, Zhou Q. Characterization of membrane foulants in an anaerobic non-woven fabric membrane bioreactor for municipal wastewater treatment. *Chem Eng J.* 2009;155(3):709–15.
136. Lin H, Peng W, Zhang M, Chen J, Hong H, Zhang Y. A review on anaerobic membrane bioreactors: applications, membrane fouling and future perspectives. *Desalination.* 2013;314:169–88.
137. Lin HJ, Xie K, Mahendran B, Bagley DM, Leung KT, Liss SN, et al. Sludge properties and their effects on membrane fouling in submerged anaerobic membrane bioreactors (SAnMBRs). *Water Res.* 2009;43(15):3827–37.
138. Wong K, Xagorarakis I, Wallace J, Bickert W, Srinivasan S, Rose JB. Removal of viruses and indicators by anaerobic membrane bioreactor treating animal waste. *J Environ Qual.*

- 2009;38(4):1694–9.
139. Zsirai T, Buzatu P, Aerts P, Judd S. Efficacy of relaxation, backflushing, chemical cleaning and clogging removal for an immersed hollow fibre membrane bioreactor. *Water Res.* 2012;46(14):4499–507.
 140. Xie K, Lin HJ, Mahendran B, Bagley DM, Leung KT, Liss SN, et al. Performance and fouling characteristics of a submerged anaerobic membrane bioreactor for kraft evaporator condensate treatment. *Environ Technol.* 2010;31(5):511–21.
 141. Akram A, Stuckey DC. Flux and performance improvement in a submerged anaerobic membrane bioreactor (SAMBR) using powdered activated carbon (PAC). *Process Biochem.* 2008;43(1):93–102.
 142. Hu AY, Stuckey DC. Activated carbon addition to a submerged anaerobic membrane bioreactor: effect on performance, transmembrane pressure, and flux. *J Environ Eng.* 2007;133(1):73–80.
 143. Liu L, Liu J, Gao B, Yang F. Minute electric field reduced membrane fouling and improved performance of membrane bioreactor. *Sep Purif Technol.* 2012;86:106–12.
 144. Sui P, Wen X, Huang X. Feasibility of employing ultrasound for on-line membrane fouling control in an anaerobic membrane bioreactor. *Desalination.* 2008 Jan;219(1–3):203–13.
 145. Wu B, Wong PCY, Fane AG. The potential roles of granular activated carbon in anaerobic fluidized membrane bioreactors: effect on membrane fouling and membrane integrity. *Desalin Water Treat.* 2015;53(6):1450–9.
 146. Aslam M, McCarty PL, Bae J, Kim J. The effect of fluidized media characteristics on membrane fouling and energy consumption in anaerobic fluidized membrane bioreactors. *Sep Purif Technol.* 2014;132:10–5.
 147. Wang J, Wu B, Yang S, Liu Y, Fane AG, Chew JW. Characterizing the scouring

- efficiency of granular activated carbon (GAC) particles in membrane fouling mitigation via wavelet decomposition of accelerometer signals. *J Memb Sci*. 2016;498:105–15.
148. Ren L, Ahn Y, Logan BE. A two-stage microbial fuel cell and anaerobic fluidized bed membrane bioreactor (MFC-AFMBR) system for effective domestic wastewater treatment. *Environ Sci Technol*. 2014;48(7):4199–206.
149. Kim K-Y, Yang W, Ye Y, LaBarge N, Logan BE. Performance of anaerobic fluidized membrane bioreactors using effluents of microbial fuel cells treating domestic wastewater. *Bioresour Technol*. 2016;208:58–63.
150. Lee R, McCarty PL, Bae J, Kim J. Anaerobic fluidized membrane bioreactor polishing of baffled reactor effluent during treatment of dilute wastewater. *J Chem Technol Biotechnol*. 2015;90(3):391–7.
151. Dutta K, Lee M-YY, Lai WW-PP, Lee CH, Lin AY-CC, Lin C-FF, et al. Removal of pharmaceuticals and organic matter from municipal wastewater using two-stage anaerobic fluidized membrane bioreactor. *Bioresour Technol*. 2014;165(C):42–9.
152. Shin C, McCarty PL, Kim J, Bae J. Pilot-scale temperate-climate treatment of domestic wastewater with a staged anaerobic fluidized membrane bioreactor (SAF-MBR). *Bioresour Technol*. 2014;159:95–103.
153. LaBarge N, Ye Y, Kim K-Y, Yilmazel YD, Saikaly PE, Hong P-Y, et al. Impact of acclimation methods on microbial communities and performance of anaerobic fluidized bed membrane bioreactors. *Environ Sci Water Res Technol*. 2016;2(6):1041–8.
154. Bae J, Shin C, Lee E, Kim J, McCarty PL. Anaerobic treatment of low-strength wastewater: a comparison between single and staged anaerobic fluidized bed membrane bioreactors. *Bioresour Technol*. 2014;165(C):75–80.
155. Casey E, Glennon B, Hamer G. Review of membrane aerated biofilm reactors. *Resour Conserv Recycl*. 1999;27(1):203–15.

156. Gilmore KR, Terada A, Smets BF, Love NG, Garland JL. Autotrophic nitrogen removal in a membrane-aerated biofilm reactor under continuous aeration: a demonstration. *Environ Eng Sci.* 2013;30(1):38–45.
157. Terada A, HIBIYA KK, NAGAI J, Tsuneda S, Hirata AA. Nitrogen removal characteristics and biofilm analysis of a membrane-aerated biofilm reactor applicable to high-strength nitrogenous wastewater treatment. *J Biosci Bioeng.* 2003;95(2):170–8.
158. Hirasa O, Ichijo H, Yamauchi A. Preparation of new support for immobilization of activated sludges. *J Ferment Bioeng.* 1991;71(5):376–8.
159. Brindle K, Stephenson T, Semmens MJ. Nitrification and oxygen utilisation in a membrane aeration bioreactor. *J Memb Sci.* 1998;144(1):197–209.
160. Semmens MJ, Dahm K, Shanahan J, Christianson A. COD and nitrogen removal by biofilms growing on gas permeable membranes. *Water Res.* 2003;37(18):4343–50.
161. Hibiya K, Terada A, Tsuneda S, Hirata A. Simultaneous nitrification and denitrification by controlling vertical and horizontal microenvironment in a membrane-aerated biofilm reactor. *J Biotechnol.* 2003;100(1):23–32.
162. Smith DP, Rector T, Reid-Black K, Hummerick M, Strayer R, Birmele M, et al. Redox control bioreactor: A unique biological water processor. *Biotechnol Bioeng.* 2008;99(4):830–45.
163. Mansell BO, Schroeder ED. Hydrogenotrophic denitrification in a microporous membrane bioreactor. *Water Res.* 2002;36(19):4683–90.

Chapter 3

Effect of buffer charge on performance of air-cathodes used in microbial fuel cells

Abstract

In microbial fuel cells (MFCs), buffers are typically used to improve performance by stabilizing the electrode pH and increasing the electrolyte conductivity, but the importance of the buffer net charge at current densities typical of MFCs on cathode performance has received little attention. Current production results in an electric field that drives positive ions towards the cathode, and negative ions to the anode. A series of biological buffers were selected with positive, negative, and neutral charges that had pKas ranging from 5 to 10.8. Cathodic current production using these different buffers in solutions with different pHs and conductivities was compared using linear sweep voltammetry (LSV). At lower pHs, buffers with positive charge increased cathodic current by as much as 95% within certain ranges (potential windows) of cathode potentials. No difference in cathodic current was shown in current for buffers with neutral or negative charge. The reason for this increase with the net positive charge buffers was likely due to a more stable electrode pH produced by electric field driving the positively charged ions towards the cathode. The potential window for the positively charged buffers was positively correlated to the concentration of cationic buffer in the electrolyte. At a pH higher than 9, no improvement in cathodic current was shown for buffers with positive charge, indicating at these higher pHs diffusion dominated buffer transport.

3.1 Introduction

A microbial fuel cell (MFC) is a promising technology for wastewater treatment as it can be used to simultaneously extract electricity from organic compounds using bacteria as well as treat the wastewater (1). The power produced by a single-chamber MFC is usually limited by the cathode due to the poorly catalyzed oxygen reduction reaction under near-neutral pH conditions needed by the bacteria, with the optimal pH reported to range from 6.5 to 10 (2-4). In single-chamber MFCs there is no net change in pH due to current production, as protons released at the anode due to oxidation of organic matter are neutralized by OH^- ions produced at the cathode (4). The local pH around the electrodes can vary, with the anode becoming more acidic than the bulk solution, and the cathode more alkaline. In order to avoid deleterious impacts of pH on the bacteria or electrode reactions, phosphate (5, 6), bicarbonate (7), or Good's buffers (8) are usually added into the medium to avoid pH changes. For wastewaters, natural alkalinity can help avoid net pH changes (7).

The addition of a buffer to a medium not only enables control of the pH near the pK_a of the buffer, but it also increases solution conductivity which can improve performance. For example, an increase in the concentration of a phosphate buffer in a single-chamber MFC from 100 to 400 mM nearly doubled power production (9). In two-chamber MFCs, the use of a cation exchange membrane between the electrodes can result in large pH differences in the electrolytes unless high concentrations of buffer are used. In tests with a 10 mM phosphate buffer there was a 75% decrease in power (after 96 h) due to the increase in the catholyte pH, as this pH change increased the cathode overpotential (10). In a comparison of several different Good's buffers, that were either neutrally or negatively charged, it was shown that conductivity was more important than buffer type when buffers were all added at the same concentration (8).

The importance of the net charge of the buffer on cathode performance has received little attention in bioelectrochemical systems compared to the studies on effect of the buffer pKa. The solution in an MFC is not usually mixed, and so ion transport can be described by the extended Nernst-Planck Equation (11), in terms of concentration, chemical activities, and the electric field, as:

$$J_i = -D_i \nabla(c_i) - D_i \frac{z_i F}{RT} c_i \nabla(V) - D_i c_i \nabla(\ln \gamma_i) \quad (3-1)$$

where J is the chemical flux, i indicates the specific chemical species, c is the concentration, V the potential, γ the activity coefficient, T the temperature, D the diffusivity, R the gas constant, and z the charge of the species. In an MFC, the electrical field draws cations to the cathode, and anions towards the anode (Fig. 3-1). Most buffers examined to date in single-chamber MFCs have had a negative charge. A comparison of several different catholyte salts and buffers (NaCl, NaHCO₃, NH₄HCO₃, PBS, and NH₄Cl) in gas diffusion half cells, however, showed that positively charged NH₄⁺ worked better than the other chemicals examined (12). The predominant reaction at the cathode is the dissociation of water and release of OH⁻ ions (13). In MFCs and other bioelectrochemical systems, the pH near the cathode can become more alkaline with increased current. The improved performance using NH₄⁺ by Popat et al. (12) was therefore attributed to its pKa 9.2 and effective buffering of the hydroxide ion, consistent with other studies demonstrating the importance of the buffer pKa relative to the solution pH on cathode performance (14, 15). It was estimated, using the model PCBIOFILM, that an electrical field could impact current produced by the anode by as much as 15%, but the impact on the cathode was not examined (16). In other bioelectrochemical systems, such as microbial reverse electrolysis cells (MRECs), it has also been shown that cathode performance is improved in the presence of ammonium bicarbonate, compared to sodium bicarbonate buffer (17). The importance of the charge of the ion

on cathode performance in MFCs or MECs, however, has not been specifically examined in these studies.

The importance of the net charge of a buffer on cathode performance was examined here using linear sweep voltammetry (LSV) for buffers that varied in charge, pKa, and molecular diffusivities. It was hypothesized that the use of buffers with net positive charge would improve cathode performance as they are drawn to the cathode surface by the electrical field, while negatively charged ions would be repelled, but the magnitude of this difference in performance was not known. A total of 13 different buffers were selected categorized into three buffer groups with net positive, negative or neutral charge. Cathode performance was examined at several different pHs relative to the pKa of the buffers.

Table 3-1 Buffer selected from biologically compatible buffers. Abbreviations used for some buffers are defined in the text. The charged dissociation ligand (L) species is shown for each buffer. All the buffer pKa are given at 30 °C.

Neutrally Charged (0)		Negatively Charged (-)		Positively Charged (+)	
$HL^{\pm} = H^{+} + L^{-1}$		$HL^{-1} = H^{+} + L^{-2}$		$HL^{+} = H^{+} + L$	
Buffer	pKa	Buffer	pKa	Buffer	pKa
Pivalic acid	5.0	Succinic acid	5.3	Pyridine	5.2
MOPS	7.1	ADA	6.5	Imidazole	7.0
Tricine	8.0	POPSO	7.6	Tris	8.0
Ampso	9.0			Diethanolamine	8.9
Caps	10.3			Piperidine	11.0

3.2 Methods

3.2.1 Buffer selection and solution preparation

Buffers with a range of pKas and net charges were selected from commercially available biologically compatible buffers (Table 3-1). The buffers were categorized into three groups based on their net neutral, negative, or positive charged. The pKas of these buffers were 5, 7, 8, 9, and 10.8. The diffusivity (D_L) of each buffer in water was estimated calculated using the Wilke-Chang correlation (18) as:

$$D_L = \frac{1.173 \times 10^{-13} \times (\emptyset M)^{0.5} T}{\mu V_m^{0.6}} \quad (3-2)$$

where \emptyset is the association factor for the solvent (water, $\emptyset = 2.26$), M the molecular weight of the solvent, μ the viscosity of solvent (cp), T the temperature and V_m the molar volume of the solute at boiling point which was estimated from the structure (Table 3-2).

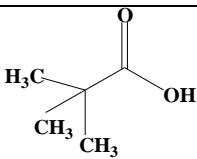
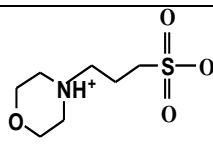
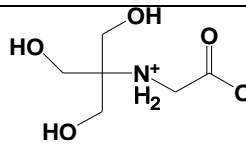
Each set of buffers, grouped based on their pKa, were prepared at both relatively high (HC) and low conductivity (LC) concentrations for LSV tests. For both LC and HC tests, each buffer was added at a concentration of 50 mM, followed by adjustment of the pH (using either sodium hydroxide or hydrochloric acid) to match that of the specific pKa of the buffer. Then, the conductivity of the solution was increased by adding sodium chloride. For LC tests, the conductivity of the solutions was increased to match the highest conductivity of the buffer prepared without NaCl addition within each pKa group. For HC buffers, conductivity was further increased to 7 mS/cm.

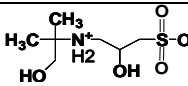
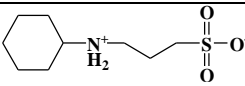
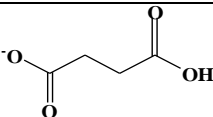
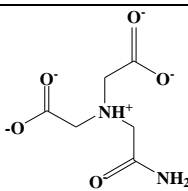
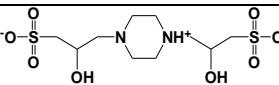
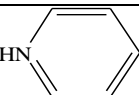
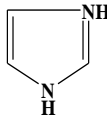
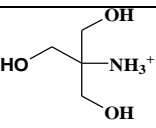
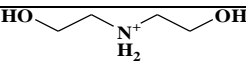
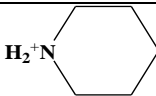
As indicated by Eq. 3-1, ion migration is influenced by the dominant ionic species, which can change with pH. To examine the impact of the net charge of the buffer on current generation in LSV tests, the pH of the solutions was shifted away from the buffer pKa. A change of one pH unit away from the buffer pKa not only can change net charge, but it greatly decreases the buffer

capacity compared to conditions with the pH at buffer pKa. Solution pH for buffers with pKa of 8 were adjusted to pHs of 7, 8, and 9, and the conductivity adjusted to the highest conductivity of these solutions (5.5 mS/cm) as described above. For example with the Tris buffer(positive charge, pKa of 8.1) at pH 7, the dominant species in the solution would have a net positive charge, while the dominant species would be with neutral charge at a pH of 9. The same procedure for adjusting the pH was repeated for the group of buffers with a pKa of 10.8, using final pHs of 9.8, 10.8, and 12, all at a solution conductivity of 4.9 mS/cm.

To clarify the charges on each of these different buffers under the various experimental pH conditions, a two-part notation was used for each buffer, indicated in parenthesis following each buffer name. The first symbol indicated that the buffer was selected to function as a positively (+), neutrally (0) or negatively (-) charged species, with the second pair of symbols indicating the predominant species at that pH. For Tris (pKa of 8.1) at a pH 8, for example, we indicated Tris (+, $\frac{+}{0}$). The first "+" shows that this chemical functions as a positively charged buffer, and the notation " $\frac{+}{0}$ " indicated that at this pH the chemical form of the buffer was approximately evenly distributed between neutral (0) and positive (+) ions. At a pH of 7, Tris ions are all predominantly positively charged, and thus it is indicated at this pH as Tris (+, $\frac{+}{+}$). Using this notation, the form of the buffer is easily clarified for the test conditions.

Table 3-2 Buffer common name, chemical structure and molecular weight.

Chemical Structure			
Chemical Name	Pivalic acid	MOPS	Tricine
Molecular Weight	102	209	179

Diffusivity(10^{-6} cm ² /s)	9.4	7.5	7.5
Chemical Structure			
Chemical Name	AMPSO	CAPS	Succinic acid
Molecular Weight	227	221	118
Diffusivity(10^{-6} cm ² /s)	6.6	6.5	9.8
Chemical Structure			
Chemical Name	ADA	POPSO	Pyridine
Molecular Weight	190	362	79
Diffusivity(10^{-6} cm ² /s)	7.5	5.2	10.8
Chemical Structure			
Chemical Name	Imidazole	Tris	Diethanolamine
Molecular Weight	68	121	105
Diffusivity(10^{-6} cm ² /s)	12.4	9.4	9.6
Chemical Structure			
Chemical Name	Piperidine		
Molecular Weight	85		
Diffusivity(10^{-6} cm ² /s)	9.6		

3.2.2 Electrochemical analyses

LSVs were conducted in a cubic reactor (19) containing a cylindrical chamber 3 cm in diameter, with a total volume of 26 mL. Anodes and cathodes with a projected surface area of 7 cm² each were located on the opposite ends (4 cm electrode spacing). A cation exchange membrane (CEM, Nafion 117, Boulder, CO, USA) was placed in the middle of the chamber. The anode (counter electrode) was a platinum plate in contact with a titanium wire as the current collector. The carbon cloth air cathode (working electrode) was manufactured as previously described (20). Four polytetrafluoroethylene (PTFE) layers were brushed onto one side of 30 wt % wet-proofed carbon cloth (type B-1B, E-TEK), followed by heating, to form a diffusion layer to prevent water leakage. Then, the catalyst layer consisting of platinum catalyst (0.5 mg/cm² Pt, 10 wt % Pt/C, E-TEK) and 5% Nafion solution was loaded onto the other side of carbon cloth, and dried for 24 h. A reference electrode (RE-5B, BASi, West Lafayette, IN; +0.209 V vs standard hydrogen electrode, SHE) was placed close to the cathode.

LSVs were done at a slow scan rate of 0.1 mV s⁻¹, from 0.2 V to -0.3 V vs Ag/AgCl using a potentiostat (VMP3 Multichannel Workstation, Biologic Science Instruments, U.S.A). The same buffer solution was placed into each chamber before conducting LSV tests. All potentials were reported versus a Ag/AgCl reference electrode, and all tests were conducted in a 30 °C constant temperature room.

3.3 Results

3.3.1 Impact of buffer charge for a pH similar to the buffer pKa

Buffers with a positive net charge reduced cathode overpotential, and therefore improved current production at pHs < 8, compared to neutrally or negatively charged buffers over a potential window of ~-0.15 V to 0.15 V (HC solution, 7 mS/cm). An example of LSVs for

buffers with three different net charges, all with a pKa of ~ 5 , is shown in Fig. 3-2A. Positively charged pyridine (+, $\overset{+}{0}$) at pH of 5 produced higher cathodic current densities than neutrally charged pivalic acid (0, $\overset{0}{0}$) or negatively charged succinic acid ($-$, $\overset{-}{2}$). Other LSVs are shown in the supporting information (Fig. A-S1).

In order to more directly compare the magnitude of the impact of the buffer on cathode overpotential, current densities were compared for each buffer at two specific potentials typical of an MFC air cathode during operation (0 V and -0.1 V). At pH 5, the current production buffering with pyridine (+, $\overset{+}{0}$) was 7.6 A m^{-2} , which was 69% greater than pivalic acid (0, $\overset{0}{0}$) (4.5 A m^{-2}), and 95% larger than succinic acid ($-$, $\overset{-}{2}$) (3.9 A m^{-2}) at 0 V. At a lower cathode potential of -0.1 V, differences in current differences between positively charged and other buffers were still significant, though the differences were smaller (Fig. 3-2C). Current production by positively charged pyridine (+, $\overset{+}{0}$) (7.6 A m^{-2}), for example, was 49% larger than pivalic acid (0, $\overset{0}{0}$), which was smaller than the 69% increase observed at 0 V. Compared to succinic acid ($-$, $\overset{-}{2}$) (5.3 A m^{-2}), current was improved using pyridine (+, $\overset{+}{0}$) by 59% at -0.1 V, compared to 95% at 0 V.

For buffers with a pKa > 8 , there were no appreciable differences in current among the buffers based on their net charge. For example, current with Diethanolamine (+, $\overset{+}{0}$) (pKa 8.9, 1.7 A m^{-2}) was only 6.3% greater than AMPSO (0, $\overset{0}{0}$) (pKa 9.1, 1.6 A m^{-2}) at pH 9.

The use of the LC solution reduced the cathodic current in all cases (Fig. 3-2D and 3-2E), which was expected due to the decrease in solution conductivity. (9). The use of the LC solution, however, did not change the observation that the use of a positively charged buffer improved cathode performance. At a pH of 5, cathodic current at 0 V with buffers with a pKa of ~ 5 was improved for pyridine (+, $\overset{+}{0}$) (4.1 A m^{-2}), as current was 37% larger than pavalic acid (0, $\overset{0}{0}$), and 41% higher succinic acid ($-$, $\overset{-}{2}$). Current production was also enhanced with buffers with pKas of 7 and 8, but not for buffers with a pKa > 8 .

No significant relationship was found between the cathode current production and the diffusion coefficient of the buffers (Fig. A-S2). This lack of a correlation shows that the current enhancement was not appreciably impacted by the chemical diffusivity.

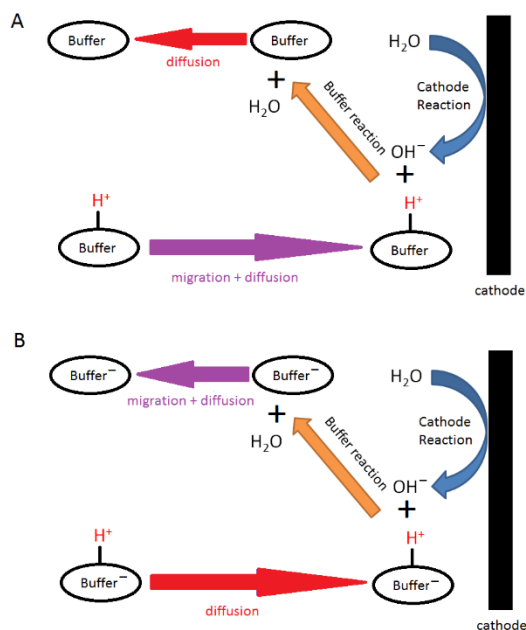


Fig. 3-1 Diagram of (A) a positively charged and (B) a neutrally charge buffer interfacing with cathode in an MFC

3.3.2 Buffer tests with the pH shifted away from the pKa

For the group of buffers with pKa of 8, lowering the pH below the pKa further improved performance of the positively charged buffer (Tris) compared to the other buffers. At a pH 7 the current (4.4 A m^{-2}) for Tris ($+$, \ddagger) at -0.1 V was 57% larger than that obtained using Tricine (0 , $\overset{0}{\underset{0}{\text{O}}}$), and 76% higher than with POPSO ($-$, $\ddot{\text{O}}$) (Fig. 3-3A). At a pH similar to the pKa, where there was a decreased net positive charge on the Tris ($+$, $\overset{\dagger}{\underset{0}{\text{O}}}$) buffer, current was 43% improved compared to Tricine (0 , $\overset{0}{\underset{0}{\text{O}}}$) and 36% improved compared to POPSO ($-$, $\ddot{\text{O}}_2$) at -0.1 V (Fig. 3-3B). When the pH was further increased to 9, where there was little net positive charge on the Tris ($+$, $\overset{0}{\underset{0}{\text{O}}}$), there was only a small increase ($< 21\%$) in current compared to Tricine (0 , $\ddot{\text{O}}$) or

POPSO ($-$, m^{-2}), which both carried net negative charges. In addition, the potential window for current improvement shrank from ~ 0.3 V to ~ 0.2 V as pH increased from 7 to 9 (Fig. A-S3), indicating the potential window for improved current was also pH dependent. While current production using with Tris (+) changed for the different pHs, the LSVs using POPSO ($-$) and Tricine (0) were quite similar for three pHs (Fig. A-S3), demonstrating that only the positively charged buffer was favorable affected by the electric field at the cathode.

For the buffers grouped with a pKa 10.8, there was no appreciable impact of pH on current. The LSVs were relatively unchanged for Piperidine (+) and CAPS (0) at pHs of 9.8, 10.8 and 12, at both 0 and -0.1 V (Fig. 3-4, Fig. A-S3B).

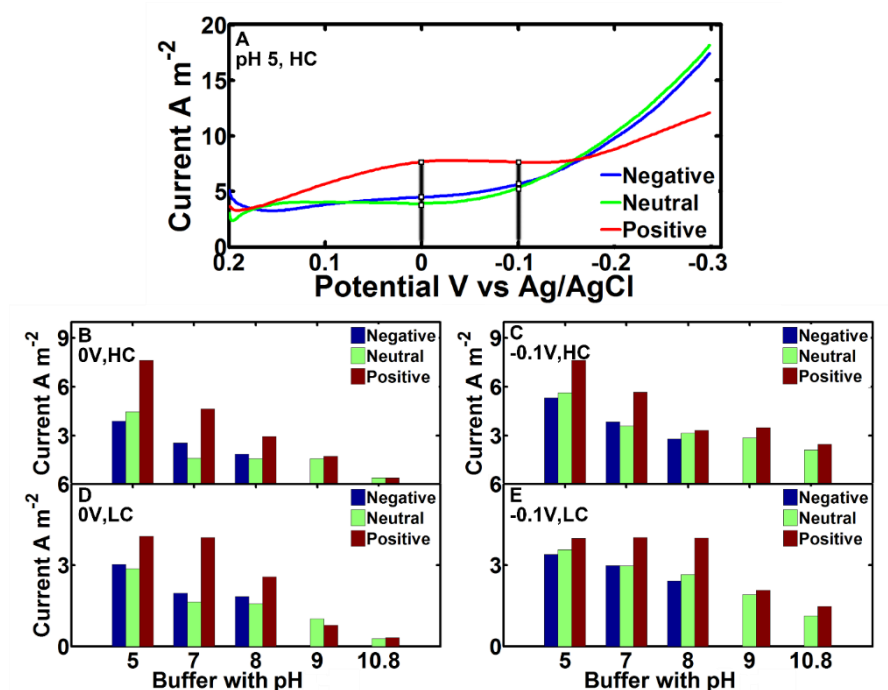


Fig. 3-2 A. Comparison of LSVs of three different buffers (with the charge of +, -, 0) with and without an electric field at pH 5 in a high concentration (HC) solution (7 mS/cm). For comparisons of different buffers at different pHs, the current is compared at two different potentials: current production corresponding to cathode potential and conductivity of B. 0 V and 7 mS/cm (HC), C. -0.1 V and

low conductivity (LC), D. 0 V and LC, E. -0.1 V and LC. The electrolyte conductivity for each low conductivity condition are at the top of bars.

3.3.3 Dominant buffer species and potential window

When a buffer is used in a solution with a pH that is more than one pH unit away from its pKa, the buffer capacity faded due to the predominance of only one form of the ionic species. Therefore, examination of the impact of the charge of the chemical can be studied separately from its importance as a buffer. At a pH 7, the dominant species in Tris (+, \ddagger) was completely positively charged, while for Imidazole (+, \ddagger) the portion of positively charged ion was only 50%. At a pH 7, in a solutions having the same conductivity (6.5 mS/cm), both positively charged Tris (+, \ddagger) and Imidazole (+, \ddagger) both showed higher current densities than the negatively or neutrally charged species (MOPS (0, \ddagger), ADA (-, \ddagger), Tricine (0, \ddagger) and POPSO (0, \ddagger)) (Fig. 3-5). While there was little difference in the maximum current produced by the two positively charged buffers, the width of the potential window (\sim -0.2 to \sim -0.2 V) was slightly larger for Tris (+, \ddagger) than Imidazole (+, \ddagger) (\sim -0.2 to \sim -0.1 V). Thus, the main impact of the higher concentration of positively charged species was to slightly increase the buffer window rather than the current densities over this range of potentials.

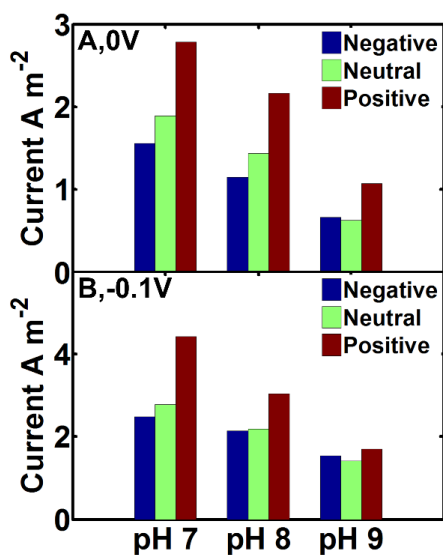


Fig. 3-3 Current production obtained from LSVs at the potential of A. 0 V and B. -0.1 V through adjusting buffers from pKa 8 to pH 7, 8, 9 with conductivity of 5.5 mS/cm (LC)

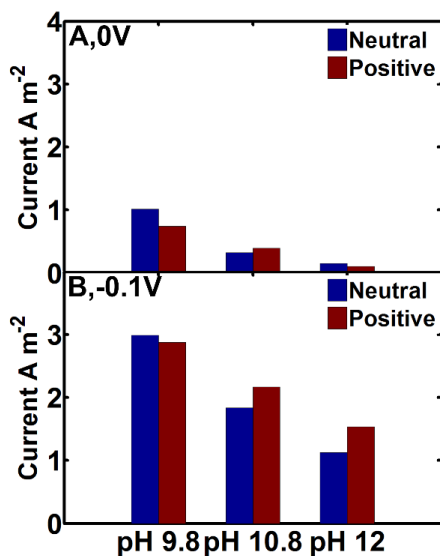


Fig. 3-4 Current obtained in LSVs at the potential of A.0 V and B. -0.1 V, using diethanolamine and CAPS (pKa 10.8) at pHs of 9.8, 10.8, and 12 in low conductivity electrolyte (LC, 4.9 mS/cm).

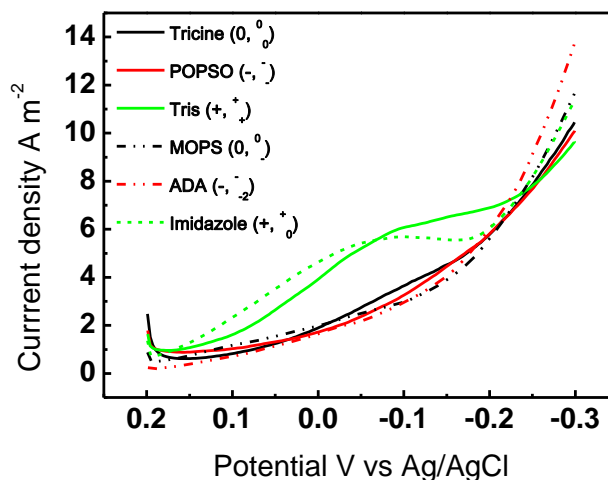


Fig. 3-5 Adjusting buffers with pKa 8 to pH 7 and comparing with buffers with pKa 7 (pH 7) under the same conductivity of 6.5 mS/cm

3.4 Discussion

3.4.1 Enhanced transport by migration

The current produced in LSVs was consistently improved by using buffers that had a net positive charge (pyridine (+), Imidazole (+), and Tris (+)) (Fig. 3-2B and 3-2C) when the pH was near neutral. This shows that the choice of the buffer would be quite important relative to the current densities produce in MFC tests, as most tests are done using solutions at a near neutral pH (9). The reason for the improved current is the impact of the electric field on the charged buffer. As shown by the Nernst-Planck model (Eq. 3-1), the electric field will drive the transport of positively charged ions towards the cathode. When the buffer is the predominant cation, this can help to improve current generation at near neutral pHs (Fig. 3-2). While Eq. 3-1 can be used to support this impact of an electrical field on a charged ion, it was not possible to predict the overall impact of the electrical field on current in this medium without conducting actual LSV tests.

When buffers carry a net negative charge, they will be driven away from the cathode towards the anode, while for neutrally charge buffers, the electric field should have no impact on buffer motion. We observed here that there was no difference in current production in LSVs for the neutral or negatively charged buffers. The predominant buffer in a wastewater at a neutral pH is the bicarbonate ion, which carries a net negative charge. Therefore, while there is a benefit to current generation using a buffer with a positive charge, there is no adverse impact on cathode performance using a buffer with a net negative charge compared to buffers with a neutral charge.

There was no improvement in current production for positively charged buffers with $pK_a > 9$, such as diethanolamine (pK_a 8.9) or piperidine (pK_a 11.1) (Fig. 3-2BC), in solutions at a $pH > 9$. The reason for this lack of impact of the positively charged buffer is unclear, but it is likely related to the high OH^- ion concentration at this pH. Oxygen reduction releases OH^- ions from the cathode and increase cathode local OH^- concentration. At a higher pH the change in the OH^- concentration relative to bulk solution conditions is reduced because of lower current and larger migration flux, which would result in smaller OH^- gradient in the diffusion layer near the cathode at a higher pH than that at lower pH. Thus, the impact of the buffer under these conditions may not be appreciable in the absence of such gradients.

All tests conducted here were performed using Nafion as the binder for the Pt/carbon catalyst. Catalyst binders with different ion exchange capacities have previously been shown to impact cathode performance, but only in tests using a negatively charged (phosphate) buffer (21, 22). The impact of the binder when using a positively charged buffer is therefore unknown. Nafion is a cation exchange polymer, which facilitates transport of protons in hydrogen fuel cells where other cations are absent. The ability of Nafion to improve proton transport is less clear when using well buffered solutions with high concentrations of other cations and anions. For example, it was shown that a neutrally-charged poly(phenylsulfone) Radel binder had improved cathode performance compared to negatively charged Nafion(21), but another-neutrally-charged

binder (poly(bisphenol A-co-epichlorohydrin, or BAEH) had poorer performance compared to Nafion (22). We observed here that using a buffer (+) improved current, but only when the cathode potential was in the range of around 0 V to -0.1 V. If the Nafion binder was a predominant factor for improved current, then we should have also observed improved performance at more negative potentials as well. Thus, the binder does not appear to be a critical factor in our results, but it is one that should receive further attention to better understand factors affecting cathode performance.

3.4.2 Comparison with other buffer studies

The impact of the charge of an ion on anodic current production was previously reported by others to increase by 15% when the impact of the electrical field was included in the model (16). Although that study only considered the impact of the buffer on anode performance, our results show a similar but more important impact of a positively charged buffer on the cathode performance. The impact of ion migration in the electrical field on current production was much higher in our study in part due to the higher buffer concentration used here (50 mM) compared to that of acetate (7 mM) in the previous study. The modeling result from another group showed that a high concentration of certain negatively charged ions would be maintained near the anode in electric field (11), which would account for the experimentally observed effects on the anode relative to current generation. It was also reported that there was little impact of buffer type (HEPES, phosphate, MES, and PIPES) was found on cathode performance (8), but there was a large impact of solution conductivity. However, the buffers they chose were all negatively or neutrally charged. Therefore, their results were consistent with ours, as we also found no impact on current generation for negatively or neutrally-charged buffers.

In a previous study, it was found that the presence of positively charged NH_4^+ (12) improved current production relative to the control (phosphate buffer), but only at current

densities $>10 \text{ A m}^{-2}$. In our LSV results, this current corresponds to a potentials more negative than $-0.2 \text{ V vs Ag/AgCl}$, which is a region where we did not observe any impact of the positively charge buffer on current production relative to a negatively charged buffer. One reason for the impact of the buffer at this high current density could be the different pH conditions examined for each chemical. While the pH for the PBS tests was 7.2, it was increased to 7.9 in tests with NH_4Cl . As a result, the buffer capacity of PBS at pH 7.2 ($\text{pK}_a=7.21$) would be higher than that of ammonia at a pH 7.9 ($\text{pK}_a= 9.25$). Thus, PBS could function better at stabilizing pH in their study as it was used at a pH near its pK_a . Second, as pointed out in their paper, when the current was as high as 10 A m^{-2} , the OH^- concentration at the cathode would be very high, and when NH_4^+ combined with OH^- and was deprotonated, it would form ammonia which could leak out through the air cathode (23). As a result, loss of ammonia would help to maintain the local pH. In both that study and our study, however, it is clear that the use of positively charge buffers could lead to improved current production under certain pH conditions and current densities.

3.5 Conclusions

Positively charged buffer enhanced cathodic current production at $\text{pH} < 8$, with the greatest improvement of 95% compared to neutral or negatively controlled buffers. This trend in current improvement was the same in high (7 mS/cm) or and low conductivity ($< 7 \text{ mS/cm}$) solutions. The improvement produced by using a positively charged buffer was greater at a cathodic potential of 0 V than -0.1 V (vs. Ag/AgCl), with the range of the improved potentials increased with buffer concentration. There was no adverse impact of using a negatively charged buffer compared to that of a neutrally charged buffer, and there was no difference in current for all buffers at a $\text{pH} > 9$. For MFC applications, while solution conductivity is more important than the choice of the buffer when using neutral or negatively charged buffers, the use of a positively

charged buffer can substantially impact performance depending on its pKa, charge, and the solution pH.

3.6 References

1. B.E. Logan, M.J. Wallack, K.-Y. Kim, W. He, Y. Feng, P.E. Saikaly. Assessment of microbial fuel cell configurations and power densities. *Environ. Sci. Technol. Lett.* 2015; 2(8): 206-14.
2. G.S. Jadhav, M.M. Ghangrekar. Performance of microbial fuel cell subjected to variation in pH, temperature, external load and substrate concentration. *Bioresour. Technol.* 2009; 100(2): 717-723.
3. Z. He, Y. Huang, A.K. Manohar, F. Mansfeld. Effect of electrolyte pH on the rate of the anodic and cathodic reactions in an air-cathode microbial fuel cell. *Bioelectrochemistry*, 2008; 74(1): 78-82.
4. G.-C. Gil, I.-S. Chang, B.H. Kim, M. Kim, J.-K. Jang, H.S. Park, H.J. Kim. Operational parameters affecting the performance of a mediator-less microbial fuel cell, *Biosensors and Bioelectronics*. 2003; 18(4): 327-334.
5. B. Logan, S. Cheng, V. Watson, G. Estadt. Graphite fiber brush anodes for increased power production in air-cathode microbial fuel cells. *Environ. Sci. Technol.* 2007; 41(9): 3341-3346.
6. Y. Fan, S.-K. Han, H. Liu. Improved performance of CEA microbial fuel cells with increased reactor size. *Energy Environ. Sci.* 2012; 5(8): 8273-8280.
7. Y. Fan, H. Hu, H. Liu. Sustainable power generation in Microbial Fuel Cells Using Bicarbonate Buffer and Proton Transfer Mechanisms, *Environ. Sci. Technol.* 2007; 41(23): 8154-8158.

8. J.-Y. Nam, H.-W. Kim, K.-H. Lim, H.-S. Shin, B.E. Logan. Variation of power generation at different buffer types and conductivities in single chamber microbial fuel cells. *Biosensors and Bioelectronics*. 2010; 25(5): 1155-1159.
9. H. Liu, S. Cheng, B.E. Logan. Power generation in fed-batch microbial fuel cells as a function of ionic strength, temperature, and reactor configuration. *Environ. Sci. Technol.* 2005; 39(14): 5488-5493.
10. R.A. Rozendal, H.V. Hamelers, C.J. Buisman. Effects of membrane cation transport on pH and microbial fuel cell performance. *Environ. Sci. Technol.* 2006; 40(17): 5206-5211.
11. E. Samson, J. Marchand. Numerical solution of the extended Nernst–Planck model. *J. Colloid Interface Sci.* 1999; 215(1): 1-8.
12. S.C. Popat, D. Ki, M.N. Young, B.E. Rittmann, C.I. Torres. Buffer pKa and transport govern the concentration overpotential in electrochemical oxygen reduction at neutral pH. *ChemElectroChem*. 2014; 1(11): 1909-1915.
13. S.C. Popat, D. Ki, B.E. Rittmann, C.I. Torres. Importance of OH⁻ transport from cathodes in microbial fuel cells. *ChemSusChem*. 2012; 5(6): 1071-1079.
14. A.W. Jeremiase, H.V. Hamelers, J.M. Kleijn, C.J. Buisman. Use of biocompatible buffers to reduce the concentration overpotential for hydrogen evolution. *Environ. Sci. & Technol.* 2009; 43(17): 6882-6887.
15. M.D. Merrill, B.E. Logan. Electrolyte effects on hydrogen evolution and solution resistance in microbial electrolysis cells. *J. Power Sources*. 2009; 19(2): 203-208.
16. A.K. Marcus, C.I. Torres, B.E. Rittmann. Evaluating the impacts of migration in the biofilm anode using the model PCBIOFILM. *Electrochim. Acta*. 2010; 55(23): 6964-6972.

17. R.D. Cusick, M. Hatzell, F. Zhang, B.E. Logan. Minimal RED cell pairs markedly improve electrode kinetics and power production in microbial reverse electro dialysis cells, *Environ. Sci. Technol.* 2013; 47(24): 14518-14524.
18. J.F.R. R K Sinnott, J.M. Coulson. *Chemical engineering: an introduction to chemical engineering design.* 2013; 255-256.
19. B.E. Logan, B. Hamelers, R. Rozendal, U. Schröder, J. Keller, S. Freguia, P. Aelterman, W. Verstraete, K. Rabaey. *Microbial fuel cells: methodology and technology.* *Environ. Sci. Technol.* 2006; 40(17): 5181-5192.
20. S. Cheng, H. Liu, B.E. Logan. Increased performance of single-chamber microbial fuel cells using an improved cathode structure. *Electrochem. Commun.* 2006; 8(3): 489-494.
21. T. Saito, M.D. Merrill, V.J. Watson, B.E. Logan, M.A. Hickner. Investigation of ionic polymer cathode binders for microbial fuel cells. *Electrochim. Acta.* 2010; 55(9): 3398-3403.
22. T. Saito, T.H. Roberts, T.E. Long, B.E. Logan, M.A. Hickner. Neutral hydrophilic cathode catalyst binders for microbial fuel cells. *Energy Environ. Sci.* 2011; 4(3): 928-934.
23. J.R. Kim, Y. Zuo, J.M. Regan, B.E. Logan. Analysis of ammonia loss mechanisms in microbial fuel cells treating animal wastewater. *Biotechnol. Bioeng.* 2008; 99(5): 1120-1127.

Chapter 4

The importance of OH⁻ transport through anion exchange membrane in microbial electrolysis cells

Abstract

In two-chamber microbial electrolysis cells (MECs) with anion exchange membranes (AEMs), a phosphate buffer solution (PBS) is typically used to avoid increases in catholyte pH as Nernst equation calculations indicate that high pHs adversely impact electrochemical performance. However, ion transport between the chambers will also impact performance, which is a factor not included in those calculations. To separate the impacts of pH and ion transport on MEC performance, a high molecular weight polymer buffer (PoB), which was retained in the catholyte due to its low AEM transport and cationic charge, was compared to PBS in MECs and abiotic electrochemical half cells (EHCs). In MECs, catholyte pH control was less important than ion transport. MEC tests using the PoB catholyte, which had a higher buffer capacity and thus maintained a lower catholyte pH (<8), resulted in a 50% lower hydrogen production rate (HPR) than that obtained using PBS (HPR=0.7 m³-H₂ m⁻³ d⁻¹) where the catholyte rapidly increased to pH=12. The main reason for the decreased performance using PoB was a lack of hydroxide ion transfer into the anolyte to balance pH. The anolyte pH in MECs rapidly decreased to 5.8 due to a lack of hydroxide ion transport, which inhibited current generation by the anode, whereas the pH was maintained at 6.8 using PBS. In abiotic tests in ECHs, where the cathode potential was set at -1.2 V, the HPR was 133% higher using PoB than PBS due to catholyte pH control, as the anolyte pH was not a factor in performance. These results show that hydroxide transport through AEM to control anolyte pH is more important than obtaining a more neutral pH catholyte.

4.1 Introduction

Microbial electrolysis cells (MECs) are devices which can achieve simultaneous degradation of organic matter in wastewater and conversion of the chemical energy into hydrogen gas.(1) A separator, such as an ion exchange membrane, is usually placed between the electrodes to reduce hydrogen consumption by microbes on the anode that results in hydrogen cycling (consumption of hydrogen produced on the cathode by microorganisms on the anode), and loss of hydrogen due to methanogenesis.(2) The use of an anion exchange membrane (AEM) is more common in MECs than a cation exchange membrane (CEM), as hydrogen gas production is higher with an AEM than a CEM.(3,4) However, the addition of a membrane increases internal resistance and creates pH differences between the electrolyte chambers, with the anolyte becoming more acidic and the catholyte more basic. The anolyte should be kept above a pH=6 so that pH does not inhibit current generation by the exoelectrogens. An increase in the catholyte pH is not desirable because it increases the voltage needed to evolve hydrogen gas at equilibrium,(5) which according to the Nernst equation is: .

$$E_{eq} = E_{cat}^0 - \frac{RT}{zF} \ln \frac{a_{red}}{a_{oxi}} - E_{an} = -0.414 V - \frac{RT}{2F} \ln p_{H_2} [OH^-]^2 - (-0.289 V) \quad (4-1)$$

assuming an equilibrium anode potential of $-0.289 V$ (acetate as substrate at pH 7,(6) where E_{cat}^0 is the cathode potential at equilibrium ($-0.414 V$), R the ideal gas law constant ($8.314 J K^{-1} mol^{-1}$), F the Faraday's constant ($96485 C mol^{-1}$), T the absolute temperature (K), z the electron transferred ($2 e^{-} mol^{-1}$) per mole of hydrogen gas, p_{H_2} the hydrogen partial pressure and $[OH^-]$ the concentration of hydroxide ions. Even in MECs lacking a membrane, the local pH near the electrodes can vary, with the anolyte becoming more acidic and the catholyte more alkaline,(7) leading to concentration overpotential.(8) To avoid large pH changes, buffers such as phosphate (9,10) or bicarbonate buffers(11) are usually used in MECs.

Buffers improve the performance of the MEC by reducing the overpotential of the hydrogen evolution reaction (HER) on the cathode, as predicted by the Nernst equation, as long as the pH is near the pKa of the buffer. The minimum overpotential for the hydrogen evolution reaction (HER) can range from 0.05 V to 0.09 V for a variety of buffers (PBS, BBS, ammonia, Tris, or Hepes; 50 mM, at 15 A m^{-2}) when the pH is near the buffer pKa.(12) Buffers in MEC catholytes also increase the solution conductivity (13) and serve an additional function of shuttling charge between the electrolyte chambers, primarily through the transport of negatively-charged buffer ions through the AEM.(3) The importance of ion transport in an MEC, relative to pH changes, cannot be assessed using the above Nernst calculation approach, and thus it is not clear whether pH control or charge balance by the buffer is more critical for hydrogen gas production. For example, it was shown that MECs with a highly conductive, but non-buffered saline solution (68 mM NaCl), had a higher hydrogen production rate (HPR) of $1.6 \text{ m}^3\text{-H}_2 \text{ m}^{-3}\text{-d}$ than MECs using a phosphate buffer solution (PBS, HPR= $1.0 \text{ m}^3\text{-H}_2 \text{ m}^{-3}\text{-d}$) in MECs with an AEM.(14) This finding suggested that solution conductivity was more important than pH for HER in MECs, which conflicts with the calculation based on the Nernst equation which shows the importance of pH.

To separate the impacts of pH and ion transport on MEC performance, we synthesized a polymer buffer (PoB) that produced a high solution conductivity and had a pKa similar to that of PBS, but was restricted from passage through the AEM due to its high molecular weight (MW, 30 kDa) and positive charge. The PoB are polycations that deprotonate at basic pHs or gain protons at acidic pHs.(15) It was reasoned based on past studies showing the importance of catholyte pH that the HPR would be improved by better pH control, by preventing the loss of the buffer, compared to low MW buffers such as PBS. However, the charge would not be balanced by buffer ion transport between the chambers as the transport of PoB is restricted by its large MW from transport through the AEM into the anolyte, and thus the importance of charge transfer could be separated from that of pH. The two buffers (PoB or PBS) were initially compared by

demonstrating their different transport through the AEM, and by measuring their solution conductivities and buffer capacities at the selected concentrations. The performance of MECs using PoB or PBS was compared in terms of current densities and hydrogen production, while monitoring electrolyte conductivity and pH. In addition, hydrogen production was examined using PoB and PBS in abiotic electrochemical half cells (EHCs), with a set cathode potential, to separate the impact of the catholyte pH on HER from the impacts of pH changes of the anodes observed in MECs. Hydrogen production in MECs was also evaluated over many cycles without catholyte replacement. The differences in the performance of the MECs and EHCs were used to support findings that the transport of OH^- through AEM was more important than buffer capacity, solution conductivity, and buffer transport through AEM in MECs.

4.2 Material and Methods

4.2.1 PoB synthesis and preparation

Poly-DMAEMA (PDMAEMA) was synthesized as reported by others.(16) Briefly, 1 g of DMAEMA, 19 mg 2,2'-bipyridine, and 9.14 mg of copper (I) bromide were mixed and degassed using pure N_2 gas. Then, 1 g of degassed deionized (DI) water was added, followed by the addition of methyl 2-bromopropionate as the initiator. The reaction was carried out at 20 °C. After PDMAEMA was collected and dissolved in 10 mL of DI water, the solution was purified by dialysis (Sigma-Aldrich, average flat width 35 mm, 12 kDa MW cut off) to remove copper ions and small-MW compounds. The dialysate was used as the PoB after adjusting pH to 7.0 by adding hydrochloric acid.

The MW distribution of PoB was measured using an ultrafiltration method.(17) Briefly, PoB was first diluted and then passed in parallel through several ultrafiltration membranes with different MW cutoffs of 2, 10, 30 and 100 kDa (Ultrafiltration membrane disc, 62 mm, Amicon,

US) in a stirred cell (200 mL, Amicon, US). The concentration of total organic carbon (TOC) was measured (Shimadzu TOC-V, Shimadzu Corp., Japan) of the original PoB and at several different times of the permeate solution. The MW distribution was obtained with the permeate concentration data using the permeate coefficient model (17) (detailed protocol given in the SI).

4.2.2 Buffer retention and buffer capacity tests

A side-by-side test of buffer retention using PBS (4.58 g Na₂HPO₄, 2.45 g NaH₂PO₄, 0.31 g NH₄Cl and 0.13 g KCl in 1 L, 50 mM) and PoB was compared using a diffusion test. The AEM (AMI-7001, Membrane International Inc.) was placed in the middle of an MEC reactor (without electrodes and anaerobic tube, Fig. B-S1A) which had a cylindrical chamber with 3 cm in diameter and 4 cm in length (a total volume of 26 mL), to separate it into two chambers. Buffer solution (PoB or PBS) was put in one of the chambers (buffer chamber), while DI water was added to the other one (water chamber). The water chamber was emptied and refilled with DI water every two days. The two chambers were sealed to prevent liquid evaporation. Samples (0.2 mL) were collected from the buffer chamber every four days. The concentration of PoB was monitored based on concentrations of TOC (Shimadzu TOC-V, Shimadzu Corp., Japan), while the concentration of PBS was obtained using a phosphate analysis kit (total phosphorus TNT reagent set, Hach, US). Buffer losses were monitored based on the change of the percentage of buffer in the chamber. A minimum buffer retention curve was calculated by assuming that half of the buffer in the buffer chamber was lost within two days before the water chamber is refilled, using

$$r = (0.5)^{0.5t} \times 100\% \quad (4-2)$$

where r is the percentage of buffer retained, and t is time in day.

Titration of the two buffer solutions, PoB and 50 mM PBS, were conducted to determine their buffer capacities. Concentrated NaOH (1.7 M) was added into the buffer solution (20 mL)

with constant mixing until a pH of 12 was reached, with the amount of NaOH used measured as a function of pH during titration.

4.2.3 MEC operation and hydrogen test

The A schematic of the MEC used in this study is shown in [Fig. B-S1A](#). The anode (carbon felt) and cathode (stainless steel mesh, #60, SS mesh) were placed in a cubic reactor 3 cm in diameter with two 2-cm long chambers separated using an AEM. The anode was pushed next to the endplate, while the cathode placed next to the membrane, resulting in an electrode spacing of 2 cm. An anaerobic tube was epoxied onto a hole on the top of the cathode chambers to collect hydrogen gases produced during the tests. A thick butyl rubber stopper (20 mm diameter, Chemglass Inc., Vineland, NJ) was used to seal the anaerobic tube on the cathode chamber, with the produced hydrogen gas collected using a gas bag (Calibrated Instruments, Inc, US), collected through a needle pierced through the rubber stopper. The reference electrode (Ag/AgCl, RE-5B, BASi, West Lafayette, IN; +0.209 V vs. standard hydrogen electrode, SHE) was placed in the anode chamber to measure the anode potential every 10 min.

The anodes of MECs were initially inoculated and acclimated in microbial fuel cells (MFCs) using the effluent from other MFCs operated for more than six months. After the current of the MFCs stabilized, the feed solution was switched to the synthetic wastewater, which consisted 10 mM sodium bicarbonate, 2 g L⁻¹ of sodium acetate, vitamin and mineral solution.⁽¹⁴⁾ The pH of the synthetic wastewater was adjusted to 7.5 using hydrochloric acid and the conductivity was increased to 7.0 mS cm⁻¹ by adding sodium chloride. The low anolyte buffer concentration (10 mM) used here was intended to mimic the low buffer capacity of municipal wastewater with alkalinity reported to be 100–300 mg-CaCO₃ L⁻¹.⁽¹⁸⁾ MFCs were then converted into MECs, which were then operated with same synthetic wastewater as anolyte and PBS or PoB as catholyte for two months at an applied voltage of 1.1 V to ensure a stable biofilm.

The pH for both PBS and PoB was 7.0, while the conductivity for PoB was 12.0 mS cm^{-1} compared to 7.0 mS cm^{-1} for PBS. A higher conductivity for PoB was chosen to compensate the conductivity decline when pH increases.

Hydrogen production in the MECs was evaluated daily in 3-cycle tests, by replacing the anolyte each cycle (daily) with fresh medium, but not replacing catholyte, in order to study changes of the catholyte over time. The anolyte and catholyte pH and conductivity were also monitored daily. The hydrogen produced was measured using a gas chromatograph (SRI 301c, SRI instruments) with the gas bag method.(11) Total phosphate concentrations in the catholyte were measured using the phosphate analysis kit (total phosphorus TNT reagent set, Hach, US) to calculate buffer losses. Long-term performance of MECs with a high catholyte pH was evaluated after 15 cycles (no catholyte replacement) for MECs with PoB.

4.2.4 Electrochemical tests

Hydrogen production using the PoB was compared to that obtained with PBS in electrochemical half cells (EHCs) with a Pt plate as counter electrode, and SS mesh as working electrode. The reactor structure of the EHCs was similar with those used as MECs, except that the electrode spacing was increased to 4 cm and a reference electrode (Ag/AgCl, +0.209 V vs SHE) was inserted close to the cathode and outside current path, as recommended in a previous study (Fig. B-S1B).(19) All potentials were reported versus the Ag/AgCl reference electrode. The same anolyte solution, 10 mM sodium bicarbonate solution with 2 g L^{-1} sodium acetate (pH, 7.0 and conductivity, 7.0 mS cm^{-1}) was added to the anode chamber, while one of the buffer solutions, PoB or PBS, was tested as the catholyte. The cathodic potential was set and fixed at -1.2 V (vs. Ag/AgCl). The hydrogen production test was carried out in a similar fashion with that in MECs in a 3-cycle test, with replacement of the anolyte every daily cycle but not the catholyte. The pH and conductivity of the anolytes and catholytes were monitored each day.

Solution resistance was compensated in EHCs using a current interrupt technique with a potentiostat (BioLogic model; software version = 10.23; 80% compensation based on the average of 10 measurements). Both MEC and EHC tests were conducted in duplicate, and all tests were conducted in a constant temperature room (30 °C).

4.2.5 Calculations

The overpotential due to the bulk solution pH increase, η , (3) was calculated as

$$\eta = \left| \frac{RT}{F} \ln \left(\frac{10^{-7}}{10^{-pH}} \right) \right| \quad (4-3)$$

The overpotential reported here only accounts for the bulk pH change, but the overpotential of HER can also be due to the specific response of the electrode material (SS mesh) to pH changes, as noted by others.(20) The cathodic coulombic efficiency (CCE) is used to evaluate the conversion of electrons to hydrogen gas, and it was calculated from current and hydrogen production using Simpson's rule as

$$e_{cathode} = \frac{n\rho FV_m}{m \int_{t=0}^{t_{end}} i dt} = \frac{n\rho FV_m}{m \left\{ \frac{\Delta t}{3} \left[i_0 + i_{end} + 2 \sum_{j=1}^{\frac{n}{2}-1} i_{2j} + 4 \sum_{j=1}^{\frac{n}{2}} i_{2j-1} \right] \right\}} \quad (4-4)$$

where V_m is the measured hydrogen production, n the number of electrons per mole of hydrogen ($2 e^- \text{ mol}^{-1}$), m the molar weight of hydrogen, ρ the density of hydrogen at 30 °C, i the current (A), t the time (s), Δt is the time interval between current sampling, i_0 the initial current (A), i_{end} the end current (A), n the total current sampling points, and i_j is the j^{th} current sampling point.

The average current was calculated based on the time for accumulation of 90% of charge ($I_{avg,90}$) to minimize the impact of low current at the end of the cycle on the calculation of the average.(21) It was calculated as:

$$I_{avg,90} = \frac{0.9 Q}{t_{90}} = \frac{0.9 \int_{t=0}^{t_{end}} i dt}{t_{90}} \quad (4-5)$$

where Q is the charge accumulated calculated by integral the current over time period, and t_{90} the time for accumulating 90% of charge.

4.3 Results and discussion

4.3.1 Characterization of PoB and buffer retention test

The MW distribution obtained from the ultrafiltration method showed that 60% of PDMAEMA had a MW between 30 kDa and 100 kDa. A small portion (6%) of PDMAEMA had a MW in the range of 2 kDa to 30 kDa, with the remaining material (34%) < 2 kDa. This < 2 kDa fraction likely consisted of monomers that were not polymerized or removed by dialysis. The MW distribution obtained in this study was consistent with a previous study using the same synthesis method.(16)

Based on titration results from a pH of 7 to 10, the buffer capacity of the PoB ($pK_a \sim 7.5$) was 2.2 times as high as that of 50 mM PBS (pK_a s of 7.2 and 12.3) commonly used in MECs (9,10) (Fig. B-S2). At the start of the titration for the PoB there was a slow increase in pH from 7 to 9, and then a rapid increase in pH from 9 to 10 indicating loss of buffer capacity. The polymer functioned differently than the small-MW PBS buffer in response to base addition due to the complexity of ionization of the polymer monomers and electric repulsion between adjacent charged monomers. This repulsion was reported to contribute to better deprotonation under high pHs.(22,23) The titration curve of PoB ($pK_a \sim 7.5$) obtained in this study was consistent with the titration of PDMAEMA in deionized water reported by a previous study.(24) The buffer capacity of PoB and PBS were similar when the pH increased from 7 to 12.

The PoB was effectively retained using an AEM (Fig. 4-1A), with $98 \pm 2\%$ of the buffer retained in the passive diffusion test (no current). The small loss of buffer was likely due to the diffusion of the < 2 kDa fraction of the PoB through the membrane. However, the PBS retention

of only $39 \pm 0.4\%$ was obtained with AEM after 16 days, indicating appreciable loss of buffer through AEM driven by concentration gradient. Compared with the minimum curve calculated (Fig. 4-1A), the PBS was better retained by AEM, indicating equilibrium was not reached before water replacement (2 days).

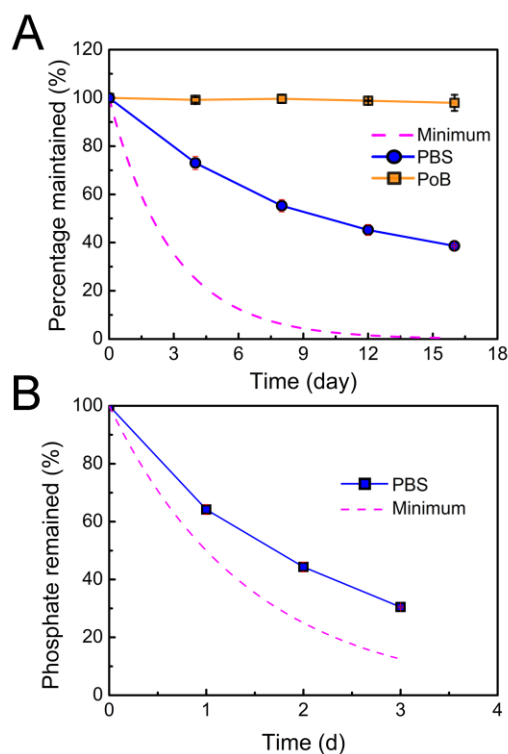


Fig. 4-1 The percentage of PoB or phosphate (PBS) buffers retained in (A) diffusion tests using an AEM (without current) and (B) in MECs. The dashed line (minimum) shows the result that would be based on equilibrium between the two chambers each time the counter electrolyte solution was changed (eq. 4-1). (B) The retention of PBS in MEC with AEM.

Linear sweep voltammetry (LSV) was conducted for SS mesh cathode buffered with PoB (data not shown). No extra peaks were found for PoB solutions indicating negligible electrochemical interactions between PoB and the cathode.

4.3.2 Hydrogen production in MECs with AEM after 1 cycle

Hydrogen production in the MECs with PBS were 25% higher ($HPR = 0.5 \pm 0.1 \text{ m}^3\text{-H}_2 \text{ m}^{-3} \text{ d}^{-1}$), and current was 26% higher ($I_{\text{avg},90} = 1.5 \text{ mA}$) than that with PoB ($HPR = 0.4 \pm 0.1 \text{ m}^3\text{-H}_2 \text{ m}^{-3} \text{ d}^{-1}$, $I_{\text{avg},90} = 1.2 \text{ mA}$) on day 1 (Fig. 4-2A). These higher rates were obtained with the PBS even though the buffer capacity (Fig. B-S2) and conductivity (Fig. 4-5A) of the PoB solutions were both higher than those of the PBS. Thus, having a better buffered catholyte with a higher conductivity was not sufficient to ensure better electrochemical performance.

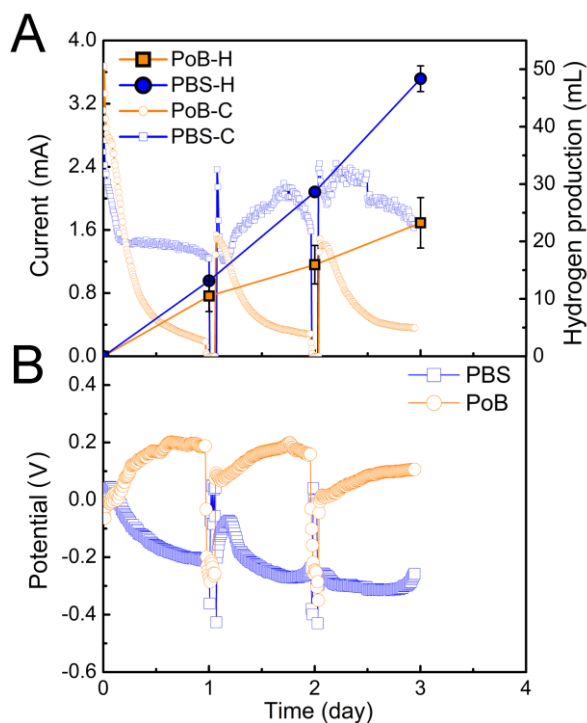


Fig. 4-2 (A) Current (C, open symbols) and hydrogen production (H, filled symbols) using PoB or phosphate (PBS) buffers in MECs with AEMs in three, one-day cycles. The anolyte was replaced daily, while the catholyte was not. (B) the anode potential of the MECs with PoB and PBS

The MECs with the PoB had less of a change in pH than those with PBS. The pH with PBS substantially increased ($\text{pH} = 11.4 \pm 0.1$) after the first cycle (day 1), consistent with pH changes reported in a previous study using this concentration of PBS.(25) There was much less of a rise in pH with PoB after the first day ($\text{pH} = 7.6 \pm 0.1$). The higher pH of PBS than PoB resulted in a higher overpotential of 0.2 V (eq. 2). The much more rapid rise in pH of the PBS was due to a combination of loss of phosphate ions (36%) due to transport through the membrane, and decreased buffer capacity with OH^- ion production at the cathode. In contrast, little PoB would be transported across the membrane due to its high MW, and it had twice the buffer capacity of PBS, so the pH change with the PoB was relatively smaller than that of PBS. Based on these changes in the pH, it was reasoned that on day 1, charge was balanced with the PoB primarily by transport of chloride ions through AEM, while for PBS the main ions transported were negatively charged phosphate ions (Fig. 4-3B). Therefore, though the calculated overpotential using the Nernst equation at the final pH conditions was calculated for the PBS to be 0.2 V higher than that of the PoB ($\text{pH} = 11.4$ for PBS vs $\text{pH} = 7.6$ for the PoB), the electrochemical charge balance by phosphate ions that could pass through the AEM was more important for improving current and hydrogen production than maintaining low catholyte pH. This indicated that the ion transport played a more important role than buffer capacity or conductivity in the MECs.

The differences in hydrogen production (day 1) with the two different buffers was consistent with the measured anode potentials (Fig. 4-2B). The anode potential with PBS became more negative, while the PoB anodes became more positive. Since the applied voltage was constant as 1.1 V, the more negative anode potential for PBS would result in a more negative cathode potential, and therefore a higher current according to the Butler-Volmer equation. The more positive anode potential in MECs with PoB was likely due to the low anolyte pH of 5.7 ± 0.1 , compared to the anode potential with PBS (pH of 6.3 ± 0.1) (day 1, Fig. 4-3A). A pH of ~ 6.0 or lower is known to inhibit current generation by exoelectrogenic bacteria.(26–28) The higher anolyte pH in MECs with

PBS was due to the transport of phosphate ions from the catholyte through the AEM (Fig. 4-3B), which contributed to a more stable anolyte pH.

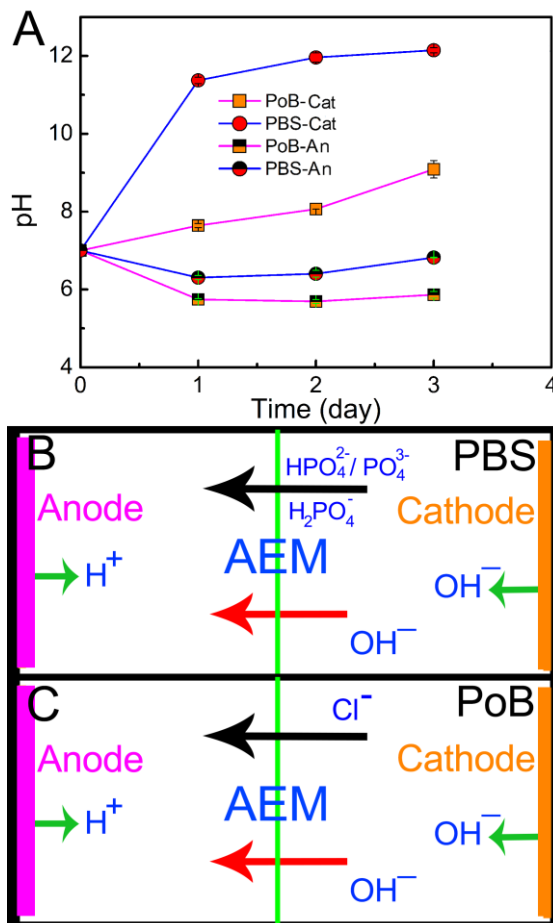


Fig. 4-3 (A) Changes in the pH of the anolytes (-An) and catholytes (-Cat) in MECs with AEMs. Schematic showing the main ions that are expected to be transported through the AEM with (B) PBS and (C) PoB.

4.3.3 Hydrogen production in MECs with AEM in 3 cycles

Hydrogen gas production was also evaluated over 3 cycles in order to study the impact on gas production when the catholyte was not replaced, and thus there was little buffering capacity

of both PoB or PBS. In addition, most of the PBS would have been transported out of the catholyte as well. The rates of hydrogen production with PBS increased over the second and third cycles (days 2 and 3), with a $0.6 \text{ m}^3\text{-H}_2 \text{ m}^{-3} \text{ d}^{-1}$ (day 2, $I_{\text{avg},90} = 1.7 \text{ mA}$) and $0.8 \text{ m}^3\text{-H}_2 \text{ m}^{-3} \text{ d}^{-1}$ (day 3, $I_{\text{avg},90} = 2.1 \text{ mA}$). In contrast, the rates of hydrogen production decreased for PoB to $0.2 \text{ m}^3\text{-H}_2 \text{ m}^{-3} \text{ d}^{-1}$ (day 2, $I_{\text{avg},90} = 0.6 \text{ mA}$) and $0.3 \text{ m}^3\text{-H}_2 \text{ m}^{-3} \text{ d}^{-1}$ (day 3, $I_{\text{avg},90} = 0.7 \text{ mA}$). The conversion of current into hydrogen gas was high for tests with both buffers, with CCEs of $98 \pm 2\%$ for PoB and $88 \pm 1\%$ for PBS, indicating that loss of hydrogen was not a decisive factor in the differences in the HPRs.

For PBS, the rapid rise in catholyte pH, combined with the loss of phosphate ions ($\sim 70\%$, Fig. 4-1B) meant that charge would have to be balanced by OH^- ion transport, as these ions were now present at a bulk concentration of 16 mM when the pH reached 12.2. The conclusion of dominant transport of OH^- ions through the AEM at high catholyte pH was consistent with that in another study proposing that the dominance of OH^- transport under steady conditions.(29) For the PoB solution, chloride ions likely dominated ion transport due to the lower pH of ~ 9 (0.01 mM of OH^-) (Fig. 4-3B). The different ions transported with the PBS and PoB therefore can explain why the pH of the anolyte was higher with PBS (pH=6.8, day 3) than with PoB (5.8), even though proton production would have been higher in the MECs with PBS than PoB due to the higher current.

The anolyte pH of the MECs with PBS continued to increase in days 2 and 3 (Fig. 4-3B), leading to more negative anode potentials (Fig. 4-2B), consistent with an increase in HPR and current. Even though the previous studies (12,13) suggested that lowest cathode overpotential of 0.05 V was achieved at pH 6.2 for PBS due to a weak acid catalysis effect, the increased HPR corresponded to increased anolyte pH indicating that OH^- ion transport that stabilized anolyte pH was more important than weak acid catalysis.

4.3.4 Hydrogen production tests in EHCs with AEM

In order to examine the impact of the buffer on HER in the absence of adverse conditions that impacted current generation by the biotic anode, hydrogen production was measured using the two buffers in abiotic EHCs at a fixed cathode potential (-1.2 V). Under these conditions, current and hydrogen generation are limited only by performance of the cathode and not ion transport or anode potentials. The average rate of hydrogen production with the PoB was 0.7 ± 0.1 $\text{m}^3\text{-H}_2 \text{ m}^{-3} \text{ d}^{-1}$ ($I_{\text{avg},90} = 2.6 \pm 0.2$ mA) in EHCs, which was 1.3 times higher than that for PBS (0.3 ± 0.1 $\text{m}^3\text{-H}_2 \text{ m}^{-3} \text{ d}^{-1}$, $I_{\text{avg},90} = 0.9 \pm 0.1$ mA) (Fig. 4-4A). This result was different with the hydrogen production obtained in MECs, where twice as high HPR was achieved by using PBS (0.7 ± 0.1 $\text{m}^3\text{-H}_2 \text{ m}^{-3} \text{ d}^{-1}$) compared to PoB. There was nearly complete recovery of hydrogen gases with both PoB (CCE= $96 \pm 4\%$) and PBS (CCE= $90 \pm 5\%$), consistent with the results from MECs, indicating that a large loss of hydrogen gas was not a factor in the HPR.

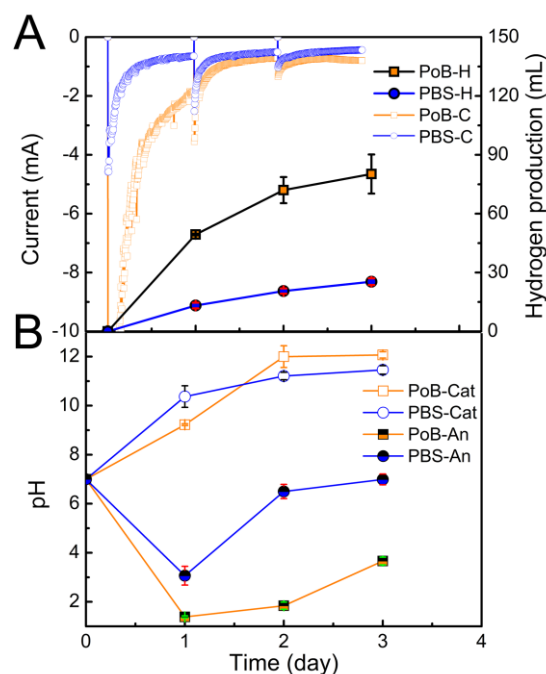


Fig. 4-4 (A) Hydrogen production (H, filled symbols) and current (C, open symbols) in an electrochemical cell separated using an AEM, with PoB and PBS as catholyte, at a fixed cathode

potential of -1.2 V. The negative current indicates a reduction reaction. (B) Changes in pH of the analytes (An) and catholytes (Cat) in electrochemical half cells with PoB or phosphate (PBS) buffers.

In EHCs, the higher buffer capacity of PoB than PBS accounted for the increased HPR, as the pH remained lower using PoB (9.2 ± 0.2) than using PBS (10.4 ± 0.2 , day 1) (Fig. 4-4B). The higher HPR for PoB is consistent with a weak acid catalysis effect.(12,13) The different results for the MECs and EHCs further supported the conclusion that the low analyte pH of <6 was the primary reason for the lower HPR ($0.3 \text{ m}^3\text{-H}_2 \text{ m}^{-3} \text{ d}^{-1}$) in the MECs with PoB, compared to that with PBS (HPR of $0.7 \text{ m}^3\text{-H}_2 \text{ m}^{-3} \text{ d}^{-1}$). The lower HPR in EHCs with PBS than that with the MECs with PBS was due to the more positive cathode potential in EHCs (-1.2 V) than -1.4 V (MECs, an anode potential of -0.3 V).

There was a decrease in the current and HPR for EHCs with both PoB and PBS in days 2 and 3, likely due to the increase in catholyte pH (PoB, 7 to 12.1 and PBS, 7 to 11.4). The increase in the bulk pH (Fig. 4-4B) resulted in an increase in overpotential, calculated using the Nernst equation, to be as high as 0.3 V with the pH increase from 7 to 12.

The conductivity of analyte of EHCs with PoB was four ($\sim 42 \text{ mS cm}^{-1}$, day 1) and two ($\sim 21 \text{ mS cm}^{-1}$, day 2) (Fig. 4-5B) times as high as the corresponding anode conductivity in MECs ($\sim 11 \text{ mS cm}^{-1}$) (Fig. 4-5A). With hydroxide and chloride ions as the anions in the cathode chamber, this increase in analyte conductivity indicated that chloride ions likely dominated the transport of ions through the AEM in EHCs with PoB (Fig. 4-3B), as there were no other ions at concentrations sufficient to balance charge with PoB. Hydroxide ions transported to the analyte could not increase conductivity because of the consumption by proton produced at the Pt electrode, although they would help to limit anode pH increases.

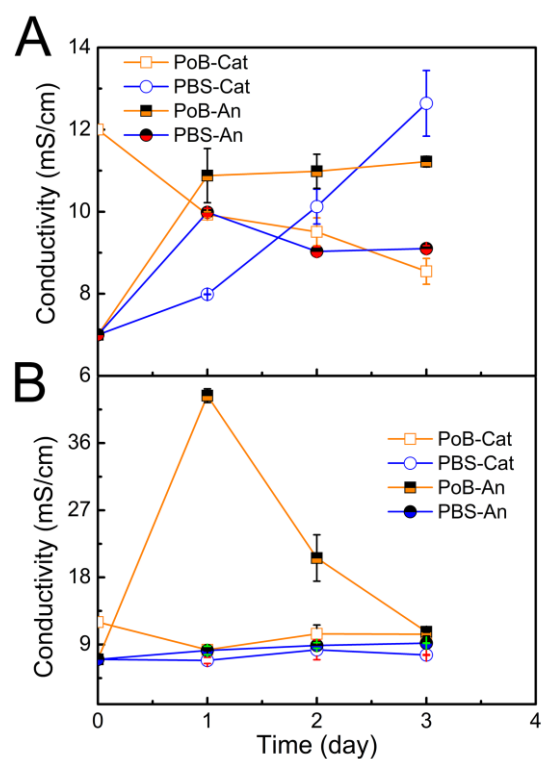


Fig. 4-5 Conductivities of the anolyte (An) and catholyte (Cat) over three days with one day cycles, with anolyte replaced daily in (A) MECs and (B) EHCs.

4.3.5 MECs with PoB without catholyte over 15 cycles

To examine the impact on hydrogen generation after loss of the buffering capacity of the PoB (due to the rise of the pH), hydrogen generation was studied in a daily batch cycle after a long period of time (15 cycles) without catholyte replacement. The HPR reached $0.7 \pm 0.1 \text{ m}^3\text{-H}_2 \text{ m}^{-3} \text{ d}^{-1}$ ($I_{\text{avg},90} = 1.4 \pm 0.3 \text{ mA}$, Fig. 4-6), which was similar to that produced in the MECs with PBS on day 3 ($0.8 \text{ m}^3\text{-H}_2 \text{ m}^{-3} \text{ d}^{-1}$) and 166% higher than the HPR of MECs with PoB at a lower pH (day 1-3, $0.3 \text{ m}^3\text{-H}_2 \text{ m}^{-3} \text{ d}^{-1}$). The high catholyte pH (12.2 ± 0.3) and conductivity ($17.4 \pm 0.4 \text{ mS cm}^{-1}$) measured at the start of this test were maintained over the batch cycle, with a final pH of 12.3 ± 0.2 and conductivity of $17.6 \pm 0.3 \text{ mS cm}^{-1}$, indicating a steady state was reached for MECs

catholyte. This final pH was five pH units above the measured pKa, so the buffer capacity of the PoB was negligible.

The anolyte pH was also higher here (6.9 ± 0.1) in the cycle than that with PoB in days 1-3 (~ 5.8), and this higher pH was comparable with that (~ 6.8) in MECs with PBS after 3 days. The high anolyte pH obtained after many cycles indicated that hydroxide ion transport from the catholyte was able to better maintain the pH in the anolyte pH, which is consistent with the more negative anode potentials (Fig. 4-6), which indicated better anode performance.

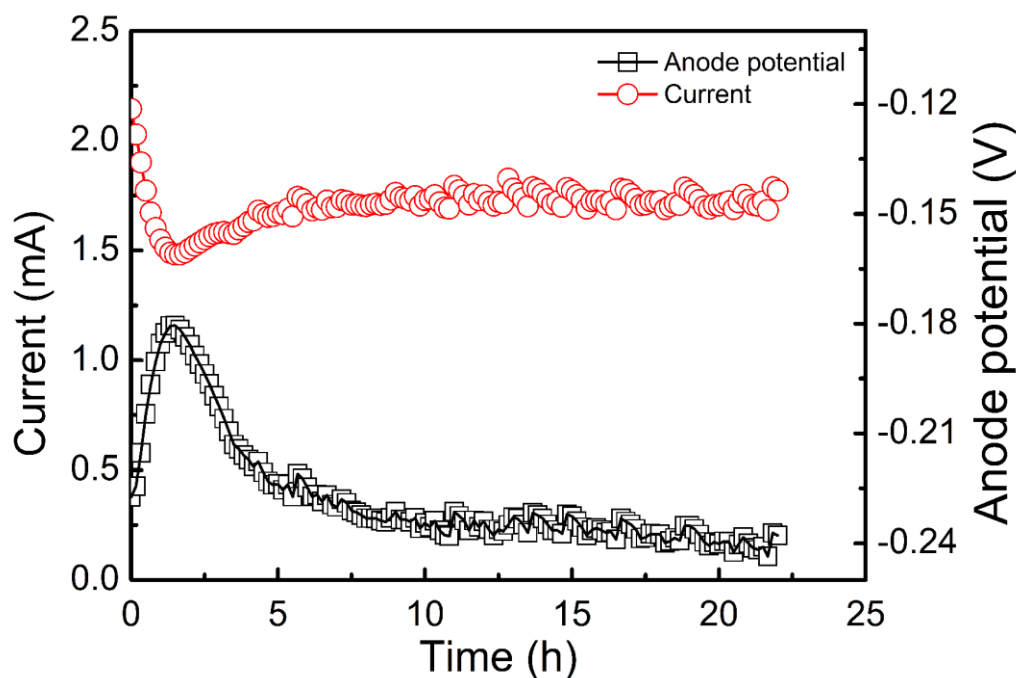


Fig. 4-6 Current and the anode potentials of MECs with PoB over a single, 24-h cycle after 15 cycles without catholyte replacement.

4.3.6 Outlook

The different effects of the PoB buffer in the EHCs, which had improved hydrogen generation with the PoB compared to PBS, and in the MECs where the anolyte pH was not well

maintained and hydrogen production was low compared to PBS, help to explain different observations among some previous MEC studies. For example, electrochemical tests, such as cyclic voltammetry(13,30), chronopotentionmetry(12) and resistance analysis(3) consistently show that addition of buffer can enhance cathode performance by reducing overpotential through weak acid catalysis, increasing conductivity and serving as charge carrier. However, these conclusions were different from those of an MEC study which showed a non-buffered saline solution had a higher hydrogen production than a buffered solution using PBS.(14) Although the mechanism for better performance with saline solution was not well understood in that study, our results suggest that the MEC result was likely due to a favorable anode pH due to hydroxide ion transport as a result of the high pH of the catholyte with NaCl. In another study, MECs were studied without catholyte (100 mM PBS) replacement over 10 cycles but using CEMs, which would not facilitate hydroxide ion transport.(25) They observed a reduction in HPR from 0.2 to $0.1 \text{ m}^3\text{-H}_2 \text{ m}^{-3} \text{ d}^{-1}$ over time, different from the result of increase in HPR in this study. Their result of reduction in HPR was likely due to a lack of OH^- or negatively charged buffer ions transport through the CEM to the AEM.

The importance of the hydroxide ion transport for buffering the anolyte pH suggests that a catholyte buffer is not needed. If PBS or other negatively charged buffers are used with AEMs, the loss of the buffer will occur unless it is constantly replenished. This loss of buffer capacity was clearly shown here. Moreover, buffering the catholyte can impair OH^- ion transport into the anolyte, as shown here by a 38% decrease in HPR with PBS (pH=7) at day 1 compared to 70% loss of PBS and a high catholyte pH at day 3 in MECs. When the buffering capacity was lost in the MECs with PoB (catholyte pH of 12.3) without catholyte replacement (after 15 cycles), the HPR of $0.7 \pm 0.1 \text{ m}^3\text{-H}_2 \text{ m}^{-3} \text{ d}^{-1}$ was comparable to that with PBS (pH=12.2) on day 3. These two observations support that operating MECs using high catholyte pH strategy would be more favorable than maintaining catholyte pH at a neutral pH when a poorly buffered solution, such as an actual

domestic wastewater, is treated in MECs. The cost of a PBS buffer in batch-mode MECs was estimated to be 3.39 \$ m⁻³-H₂ in a previous study, almost 8 times as high as the value of hydrogen gas (0.42 \$ m⁻³-H₂) produced. (25) In addition, using PBS in the catholyte would result in its undesirable loss into the wastewater, leading to potential environmental issues. Thus, operating MECs without PBS replacement is useful for many practical reasons.

4.4 Conclusions

The effect of buffer capacity and buffer capacity and ion transport was examined in this study by comparing MECs and EHCs with either a large-MW PoB, which was well retained by an AEM (98±2%), or PBS which readily passed through the AEM. A HPR of 0.7±0.1 m³-H₂ m⁻³ d⁻¹ was produced in MECs with PBS, which was twice as high as that with PoB, despite the higher buffer capacity of the PoB. It was concluded that the poorer performance of the PoB was due to the decrease in the anolyte pH with the PoB. In abiotic EHCs, however, where current was generated by setting the cathode potential, the HPR was 133% higher for PoB than PBS. The increased HPR for PoB in EHCs was due to the better buffer capacity and retention of the PoB. Hydroxide ion transport at high catholyte pH was needed to stabilize anolyte pH and avoid an adverse impact on the anode activity in MECs, while increasing buffer capacity and conductivity can enhance cathode performance by weak acid catalysis when the anode performance did not constrain current generation in EHCs. In addition, the catholyte pH (12.2±0.3) and conductivity (17.4±0.4 mS cm⁻¹) reached a steady state in MECs with PoB after long term without catholyte replacement (15 cycles), producing a high HPR of 0.7±0.1 m³-H₂ m⁻³ d⁻¹. This indicated that the use of buffer was unnecessary in MECs, which can lower the costs and simplify operational conditions.

4.5 References

1. Cheng S, Hamelers HVM, Logan BE, Call D, Cheng S, Hamelers HVM, et al. Microbial electrolysis cells for high yield hydrogen gas production from organic matter. *Environ Sci Technol*. 2008;42(23):8630–40.
2. Call D, Logan BE. Hydrogen production in a single chamber microbial electrolysis cell lacking a membrane. *Environ Sci Technol*. 2008;42(9):3401–6.
3. Sleutels THJA, Hamelers HVM, Rozendal RARA, Buisman CJN. Ion transport resistance in microbial electrolysis cells with anion and cation exchange membranes. *Int J Hydrogen Energy*. 2009;34(9):3612–20.
4. Cheng S, Logan BE. Evaluation of catalysts and membranes for high yield biohydrogen production via electrohydrogenesis in microbial electrolysis cells (MECs). *Water Sci Technol*. 2008;58(4):853–7.
5. Sleutels THJA, Hamelers HVM, Rozendal RA, Buisman CJN. Ion transport resistance in Microbial Electrolysis Cells with anion and cation exchange membranes. *Int J Hydrogen Energy*. 2009;34(9):3612–20.
6. Logan BE, Hamelers B, Rozendal R, Schröder U, Keller J, Freguia S, et al. Microbial fuel cells: Methodology and technology. *Environ Sci Technol*. 2006;40(17):5181–92.
7. Ye Y, Zhu X, Logan BE. Effect of buffer charge on performance of air-cathodes used in microbial fuel cells. *Electrochim Acta*. 2016;194:441–7.
8. Popat SC, Ki D, Young MN, Rittmann BE, Torres CI. Buffer pKa and transport govern the concentration overpotential in electrochemical oxygen reduction at neutral pH. *ChemElectroChem*. 2014;1(11):1909–15.
9. Cheng S, Logan BE. High hydrogen production rate of microbial electrolysis cell (MEC) with reduced electrode spacing. *Bioresour Technol*. 2011;102(3):3571–4.

10. Torres CI, Lee HS, Rittmann BE. Carbonate species as OH⁻ carriers for decreasing the pH gradient between cathode and anode in biological fuel cells. *Environ Sci Technol*. 2008;42(23):8773–7.
11. Ambler JR, Logan BE. Evaluation of stainless steel cathodes and a bicarbonate buffer for hydrogen production in microbial electrolysis cells using a new method for measuring gas production. *Int J Hydrogen Energy*. 2011;36(1):160–6.
12. Jeremiase AW, Hamelers HVM, Kleijn JM, Buisman CJN. Use of biocompatible buffers to reduce the concentration overpotential for hydrogen evolution. *Environ Sci Technol*. 2009;43(17):6882–7.
13. Merrill MD, Logan BE. Electrolyte effects on hydrogen evolution and solution resistance in microbial electrolysis cells. *J Power Sources*. 2009;191(2):203–8.
14. Nam JY, Logan BE. Enhanced hydrogen generation using a saline catholyte in a two chamber microbial electrolysis cell. *Int J Hydrogen Energy*. 2011;36(23):15105–10.
15. Almeida H, Amaral MH, Lobão P. Temperature and pH stimuli-responsive polymers and their applications in controlled and selfregulated drug delivery. *J Appl Pharm Sci*. 2012;2(6):01–10.
16. Zeng F, Shen Y, Zhu S, Pelton R. Atom transfer radical polymerization of 2-(dimethylamino)ethyl methacrylate in aqueous media. *J Polym Sci Part A Polym Chem*. 2000;38(20):3821–7.
17. Logan BE. *Environmental Transport Processes* [Internet]. John Wiley & Sons; 2012. 482 p. Available from: <http://www.wiley.com/WileyCDA/WileyTitle/productCd-0470619597.html>
18. Luo H, Xu P, Roane TM, Jenkins PE, Ren Z. Microbial desalination cells for improved performance in wastewater treatment, electricity production, and desalination. *Bioresour Technol*. 2012;105:60–6.

19. Zhang F, Liu J, Ivanov I, Hatzell MC, Yang W, Ahn Y, et al. Reference and counter electrode positions affect electrochemical characterization of bioanodes in different bioelectrochemical systems. *Biotechnol Bioeng*. 2014;111(10):1931–9.
20. Keith R, Christiane U, Harnisch F, Schr U. Combining hydrogen evolution and corrosion data - A case study on the economic viability of selected metal cathodes in microbial electrolysis cells. 2017;1–11.
21. Ivanov I, Ren L, Siegert M, Logan BE. A quantitative method to evaluate microbial electrolysis cell effectiveness for energy recovery and wastewater treatment. *Int J Hydrogen Energy*. 2013;38(30):13135–42.
22. Borukhov I, Andelman D, Borrega R, Cloitre M, Leibler L, Orland H. Polyelectrolyte titration: theory and experiment. *J Phys Chem B*. 2000;104(47):11027–34.
23. Lee H, Son SH, Sharma R, Won Y-Y. A Discussion of the pH-Dependent Protonation Behaviors of Poly (2-(dimethylamino) ethyl methacrylate)(PDMAEMA) and Poly (ethylenimine-ran-2-ethyl-2-oxazoline)(P (EI-r-EOz)). *J Phys Chem B*. 2011;115(5):844–60.
24. Ei-r-eoz PP, Lee H, Son SH, Sharma R, Won Y. A discussion of the pH-dependent protonation behaviors of poly (2- (dimethylamino) ethyl methacrylate) (PDMAEMA) and. *Synthesis (Stuttg)*. 2011;115(5):844–60.
25. Yossan S, Xiao L, Prasertsan P, He Z. Hydrogen production in microbial electrolysis cells: choice of catholyte. *Int J Hydrogen Energy*. 2013;38(23):9619–24.
26. Kim JR, Cheng S, Oh S-E, Logan BE. Power generation using different cation, anion, and ultrafiltration membranes in microbial fuel cells. *Environ Sci Technol*. 2007;41(3):1004–9.

27. Chae K-J, Choi M-J, Kim K-Y, Ajayi FF, Chang I-S, Kim IS. Selective inhibition of methanogens for the improvement of biohydrogen production in microbial electrolysis cells. *Int J Hydrogen Energy*. 2010;35(24):13379–86.
28. Torres CI, Kato Marcus A, Rittmann BE. Proton transport inside the biofilm limits electrical current generation by anode-respiring bacteria. *Biotechnol Bioeng*. 2008;100(5):872–81.
29. Sleutels THJA, ter Heijne A, Kuntke P, Buisman CJN, Hamelers HVM. Membrane selectivity determines energetic losses for ion transport in bioelectrochemical systems. *ChemistrySelect*. 2017;2(12):3462–70.
30. Brown RK, Schmidt UC, Harnisch F, Schröder U, Keith R, Christiane U, et al. Combining hydrogen evolution and corrosion data-A case study on the economic viability of selected metal cathodes in microbial electrolysis cells. *J Power Sources*. 2017;356:473–83.

Chapter 5

An aerated and fluidized bed membrane bioreactor for effective wastewater treatment with low membrane fouling

Abstract

Anaerobic fluidized bed membrane bioreactors (AFMBRs) use granular activated carbon (GAC) particles suspended by recirculation to effectively treat low strength wastewaters (~100-200 mg/L, chemical oxygen demand, COD), but the effluent can contain dissolved methane. An aerobic fluidized bed membrane bioreactor (AOFMBR) was developed to avoid methane production and the need for wastewater recirculation by using rising air bubbles to suspend GAC particles. The performance of the AOFMBR was compared to an AFMBR and a conventional aerobic membrane bioreactor (AeMBR) for domestic wastewater treatment over 130 d at ambient temperatures (fixed hydraulic retention time of 1.3 h). The effluent of the AOFMBR had a COD of 20 ± 8 mg/L, and a turbidity of <0.2 NTU, for low-COD influent (153 ± 19 and 214 ± 27 mg/L), similar to the AeMBR and AFMBR. For the high-COD influent (299 ± 24 mg/L), higher effluent CODs were obtained for the AeMBR (38 ± 9 mg/L) and AFMBR (51 ± 11 mg/L) than the AOFMBR (26 ± 6 mg/L). Transmembrane pressure of the AOFMBR increased at 0.04 kPa/d, which was 20% less than the AeMBR and 57% less than the AFMBR, at the low influent COD. Scanning electron microscopy (SEM) analysis indicated a more uniform biofilm on the membrane in AOFMBR than that from the AeMBR biofilm, and no evidence of membrane damage. High similarity was found between communities in the suspended sludge in the AOFMBR and AeMBR (square-root transformed Bray-Curtis similarity, SRBCS, 0.69). Communities on the GAC and suspended sludge were dissimilar in the AOFMBR (SRBCS, 0.52), but clustered in the AFMBR (SRBCS, 0.63).

5.1 Introduction

Aerated membrane bioreactors (AeMBRs) are effective alternatives to conventional processes for wastewater treatment because of the combination of good biochemical oxygen demand (BOD) removal and the lack of a need for a secondary clarifier. Other advantages of AeMBRs include the ability to obtain a high mixed liquor suspended solids (MLSS) concentration in the reactor (1), stability of performance during fluctuations in flow and organic loading, low excess sludge production, and relatively short hydraulic retention times (HRTs) (2,3). However, a major disadvantage of AeMBRs and other membrane bioreactors (MBRs) is the need for frequent membrane chemical cleaning to avoid excessive membrane fouling (4). The energy demands of all aeration systems, including AeMBRs and activated sludge, are also high compared to those needed for anaerobic treatment techniques (5).

Anaerobic membrane bioreactors (AnMBRs) are being developed as alternatives to activated sludge and aerated membrane bioreactors in order to reduce energy demands needed for wastewater treatment (6), because AnMBRs do not require aeration, and to reduce treatment plant operating costs as anaerobic processes can produce less sludge than aerobic systems. AnMBRs have been tested with many types of wastewaters, including municipal, synthetic, food processing, and industrial, at both laboratory and pilot scales, and have produced good effluent quality (6,7). However, membrane fouling is also challenging for AnMBR operation. Various strategies have been developed to reduce fouling, such as biogas recirculation and sparging (8), addition of granular or powdered activated carbon (PAC) as an absorbent (9) in a submerged membrane operation, ultrasonic irradiation (10), and high cross flow velocity (11) for the external cross-flow operation.

A new approach to reduce membrane fouling for low-strength wastewaters was recently developed based on using fluidized granular activated carbon (GAC), in a process called an

anaerobic fluidized bed membrane bioreactor (AFMBR). The AFMBR has primarily been used as the secondary treatment reactor to treat the effluent from several different types of reactors. In tests using effluent from an anaerobic fluidized bed bioreactor (AFBR) treating synthetic wastewater, the AFMBR achieved 87% removal of the chemical oxygen demand (COD) (influent of 59 mg COD/L) and nearly 100% solids removal, at an HRT of 2-3 h. Membrane fouling was well controlled as the reactor was operated for 120 days, and required only two chemical cleanings. The energy consumption of the AFMBR was estimated to be only 0.058 kWh/m³ (12). An AFMBR was also used as a secondary treatment process to treat effluent from a microbial fuel cell (MFC) treating domestic wastewater. At an HRT of only 1 h, the AFMBR removed 85% of the COD and 99.6% the TSS, with an estimated energy demand of 0.0186 kWh/m³ (13). An AFMBR treating the effluent from an anaerobic baffled reactor (ABR), showed 87% COD removal using a complex synthetic wastewater at an HRT of ~1 h, with an energy demand of 0.0087 kWh/m³ (14). A single AFMBR was compared to staged anaerobic fluidized membrane bioreactors (SAF-MBR) for treating synthetic wastewater (~200 mg COD/L), with no significant differences found between the processes in terms of COD removal efficiency, transmembrane pressure (TMP), bulk liquid suspended solids, extracellular polymer substances (EPS) production, and soluble microbial products (SMP) (15).

One of the main disadvantages of AnMBRs or AFMBRs is that the effluent can contain high concentrations of dissolved methane which must be removed prior to discharge to avoid the release of this greenhouse gas to the atmosphere (16,17). In this study, an aerobic fluidized bed membrane bioreactor (AOFMBR), containing 92 g/L fluidized GAC particles as scouring media, was examined to simultaneously avoid production of dissolved methane, as well as eliminate the need for water (AFMBR) or biogas recirculation (AnMBR) used in anaerobic membrane reactors. The performance of the AOFMBR was compared in side-by-side tests with two other processes as controls: an AFMBR and an AeMBR. Domestic wastewater was used at three different COD

concentrations (~150, 200, and 300 mg/L) to study the impact of organic loading on COD removal and membrane fouling. It was hypothesized that AOFMBR could achieve better organics removal and have less membrane fouling, as well as avoid generation of dissolved methane due to the aerobic conditions compared to the AFMBR. Treatment was evaluated in terms of COD and soluble COD (SCOD) removal and effluent turbidity, and TMP was monitored to assess membrane fouling. Scanning electron microscopy (SEM) was conducted to examine the morphology of biofilms on the membrane and membrane integrity. Analysis of microbial communities by 16S rRNA gene sequencing was done by sampling the solutions, and when present, the GAC, in the different reactors.

5.2 Materials and Methods

5.2.1 Reactor design

All three reactors (AFMBR, AOFMBR, and AeMBR) were constructed from polyvinyl chloride (PVC) tubes (30 cm long and 1.6 cm in diameter) with fittings and connectors as previously described (13). Each reactor had a volume of 65 mL, with slightly different configurations for aeration versus recirculation (Fig. C-S1). A thick butyl rubber stopper (20 mm diameter, Chemglass Inc., Vineland, NJ) was placed on the top of the AFMBR tube to keep it sealed. Biogas produced by the AFMBR was collected for analysis in a gas bag to the top of the reactor using a needle to pierce the rubber stopper. Each reactor contained a membrane module made by bundling eight polyvinylidene fluoride (PVDF) hollow fiber membranes (24 cm-long, 2.0 mm in outer diameter, 0.8 mm in inner diameter, 0.1 μm pore size, Kolon Inc., South Korea) together for a total exposed membrane area of 0.0048 m² per reactor. Epoxy was applied as the sealant. The module was placed in the middle of the reactor body, with the effluent pulled through the membrane by suction generated using a peristaltic pump (model no. 7523-90,

Masterflex, Vernon Hills, IL). GAC (DARCO MRX, 10 × 30 mesh, Norit Activated Carbon) was rinsed with deionized water several times, and added into the AFMBR (10 g wet weight, 153 g GAC/L) and AOFMBR (6 g wet weight, 92 g GAC/L). High concentrations of GAC were used to control membrane fouling by scouring in both the AFMBR and AOFMBR reactors, at concentrations similar to those used in previous AFMBR studies (13,18). Less GAC was added into AOFMBR in order to keep it better fluidized by rising air bubbles. AeMBR and AOFMBR had the same reactor configuration except no GAC was added into AeMBR. Mechanical scouring of GAC (AFMBR and AOFMBR) or shear generated by air bubbles (AeMBR) were the only strategies to control membrane fouling during the study. There was no chemical cleaning of the membrane.

5.2.2 Reactor operation

All three reactors were operated at an overall HRT of 1.3 h (11.6 L/m²-membrane-h), with pumps operating for 10 min on at 0.93 mL/min, and 1 min off for relaxation of the membranes. Fluid was recirculated by pumping (model no. 7523-90, Masterflex, Vernon Hills, IL) at a flowrate of 250 ± 30 mL/min (upflow velocity of 2.4 cm/s) to fluidize the GAC in the AFMBR. An air flow of 240 ± 20 mL/min (3.0 m³/m²-membrane surface-h) was used for both the AOFMBR and AeMBR, by placing a gas diffuser (Gas dispersion tubes, Medium Frit, Chemglass, US) at the bottom of the reactor (Fig. C-S1). The effluent tubing was cleaned with hydrochloric acid two times (day 41 and 89) in response to spikes in effluent turbidity, to remove accumulated biomass growing in the tubing.

In order to acclimate the microorganisms for growth on the GAC, the AFMBR and AOFMBR were inoculated using diluted municipal wastewater (primary clarifier of the Pennsylvania State University Wastewater Treatment Plant) with a COD of 150 mg/L, for one month, using the operation mode described above. The AeMBR was fed with the same diluted

wastewater for one month. To begin the experiments, the membrane modules were replaced by new ones (designated day 1).

In order to study the effect of wastewater strength on membrane fouling and effluent quality, the study conditions were separated into 4 Phases: Phase 1 (1-45 days), influent COD of 153 mg/L; Phase 2 (45-73 days), influent COD of 214 mg/L; Phase 3 (73-103 days), influent COD of 299 mg/L; Phase 4 (103-131 days), influent COD of 329 mg/L, and using a new membrane module. Operational details are summarized in [Table 5-1](#). The replacement of the membrane module for Phase 4 was needed due to the TMP drop in the AFMBR and AeMBR, which might have been caused by the failure of the membrane at some time in Phase 3. The wastewater strength was controlled by dilution of domestic wastewater using distilled water to obtain the targeted COD. Consistent pH and solution conductivity were obtained by adding sodium bicarbonate and sodium chloride as needed to each diluted wastewater sample (pH of ~7.6 and conductivity of 1.2 mS/cm). Effluent samples were taken from the effluent tubing every two days. All reactors were operated at ambient temperature (22 ± 10 °C).

Table 5-1 Wastewater characteristics (influent) and membrane condition.

Phase	1	2	3	4
COD (mg/L)	153 \pm 19	214 \pm 27	299 \pm 24	329 \pm 37
SCOD (mg/L)	87 \pm 18	115 \pm 19	185 \pm 26	179 \pm 28
pH	7.7 \pm 0.1	7.7 \pm 0.1	7.5 \pm 0.3	7.7 \pm 0.2
Conductivity (mS/cm)	1.2 \pm 0.1	1.2 \pm 0.1	1.3 \pm 0.1	1.2 \pm 0.1
Membrane	new	continued	continued	new

5.2.3 Measurement and analysis

COD was measured using a DR3900 Spectrophotometer (HACH, Company, Loveland, CO). Samples for SCOD analysis were filtered using 0.45 μ m pore size syringe filters (PVDF, 25

mm size, Restek Corporation). Differences in effluent CODs and SCODs between the reactors were assessed using the Student's *t*-test. The difference in results is considered to be significant here when the *P* value is less than 0.03. Conductivity and pH were measured using probes and meters (Seven-Multi, Mettler-Toledo International Inc.). Biogas production rates were calculated from the change in biogas composition (measured using gas chromatographs; SRI Instruments) and volume of gas in the collection bag. Turbidity was measured (2100P, HACH Company, Loveland, CO) as an indicator of solids removal. Pressure in the effluent tubing was monitored as the TMP of the membrane module using a pressure transducer (TDH 31, Transducer Direct, US). Suction pressure was reported as a positive value. TMP and turbidity data were collected starting on day 7.

Membranes from the reactors were examined with SEM at the end of Phase 3 to evaluate biofilm formation due to the three different reactor operational conditions. Small pieces of membrane were cut from the middle of the fiber, and prepared by: fixation in 2.5% glutaraldehyde in a 0.1 M phosphate buffer solution (PBS) at a pH of 7.2 for 30 minutes; rinsing with PBS for 3×5 min; successive dehydration using ethanol solutions of 5%, 50%, 70%, 85%, 95%, 3×100%, each for 5 min; critical point drying; sample mounting on aluminum stubs with conductive tabs; and coating with 10 nm Au/Pd. SEM images were viewed at 125 × and 10,000 × magnifications.

The microbial communities were analyzed using genomic DNA extracted from the suspended biomass and biomass on the GAC (0.25 g, if present) in the AOFMBR, AFMBR, and AeMBR at the end of Phase 4. For suspended biomass samples, liquid (13 mL) from the reactor was centrifuged at 4500 x g (Eppendorf 5804) for 1 h and the supernatant was decanted. For the AOFMBR and AeMBR suspended biomass analysis, 0.25 g of pellet was used for DNA extraction, but less was used for the AFMBR due to less solids collected. DNA was extracted from suspended biomass samples and GAC following the Power Soil DNA isolation Kit protocol

(Mo Bio Laboratories, Inc) with modifications: 0.1 μm diameter glass beads were used instead of garnet beads; samples were centrifuged for 1 min instead of 0.5 min; and the incubation time was increased for 10 min instead of 5 min. The 16S rRNA genes in the extracted DNA samples were amplified by polymerase chain reaction (PCR) according to a previous study (19). Briefly, thermal cycling was conducted with the barcoded forward primer of 515F (5'-Illumina overhang - GTGYCAGCMGCCGCGGTA-3') and reverse primer 805R (5'- Illumina overhang- GACTACHVGGGTATCTAATCC-3'), followed by the purification of amplicons. Equimolar 16S rRNA gene amplicons were mixed and submitted for high-throughput amplicon sequencing on an Illumina MiSeq platform (Illumina Inc, San Diego, CA, USA) in the KAUST Genomics Core Lab. The DNA sequences were processed for its quality and analyzed by the same approach as specified in previous study (20). Briefly, the relative abundances of various microbial genera and unclassified groups were square-root transformed and calculated for Bray-Curtis similarities (SRBCS) and metric multi-dimensional scaling (mMDS). Microbial groups that exhibited more than 0.95 Pearson's correlation to the spatial distribution of samples were overlaid onto the mMDS plot, and represented as vectors accounting for the spatial positions of samples. The microbial relative abundance was plotted in phylum level, with the predominant genus (>1%) shown separated. All high-throughput sequencing files were deposited in the Short Read Archive (SRA) of the European Nucleotide Archive (ENA) under study accession number PRJEB13756.

5.3 Results

5.3.1 Effluent quality and COD removal

The AOFMBR had the lowest effluent COD and SCOD among all three reactors on average, for tests with the influent COD of either 153 ± 19 mg/L (Phase 1) or 214 ± 27 mg/L (Phase 2). In Phase 1, the average effluent COD from the AOFMBR was 18 ± 7 mg/L, and the SCOD was

17 ± 8 mg/L (Fig. 5-1). These corresponded to removal efficiencies of $88 \pm 4\%$ for COD, and $80 \pm 9\%$ for SCOD. COD removal efficiencies averaged $84 \pm 6\%$ for the AFMBR, and $86 \pm 5\%$ for the AeMBR. Good treatment was therefore also obtained by AFMBR and AeMBR, as the effluent CODs and SCODs were all <30 mg/L.

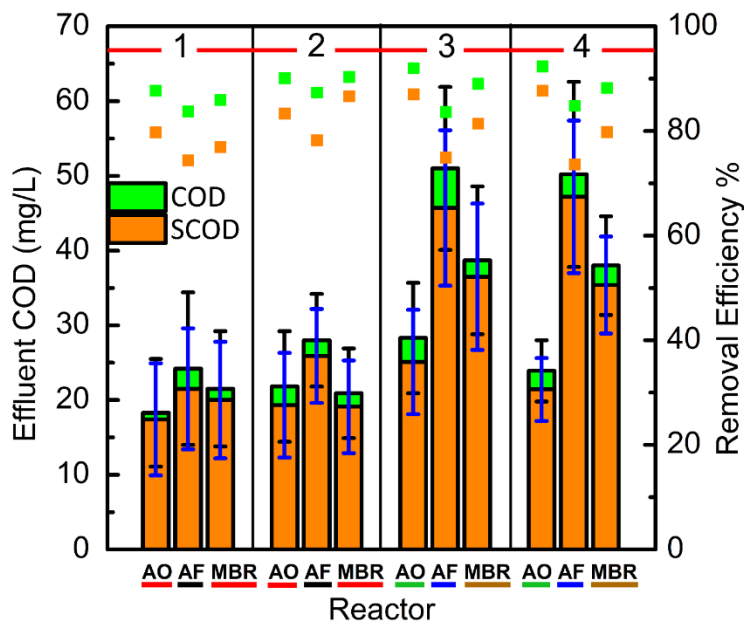


Fig. 5-1 Average CODs and SCODs in the effluents of the AFMBR (AF), AOFMBR (AO), and AeMBR (MBR) in four Phases of operation. The standard deviations for COD is in black and for SCOD is in blue. The corresponding removal efficiencies are shown above the bar chart. The thick lines below each designation indicate whether the effluent of one reactor has significantly different average COD compared with others. If the colors are the same, the average CODs are not significantly different, while if the colors are different, the average COD are different based on analysis using the Student's T-test.

When the organic loading rate was increased by 40% using an influent COD of 214 ± 27 mg/L (Phase 2), effluent COD concentrations from the AOFMBR (COD, 22 ± 7 mg/L; SCOD, 19 ± 7 mg/L) were not significantly different from those in Phase 1 (*t*-test, $P=0.13$), resulting in an

improved removal efficiency of $90\pm 3\%$ for COD and $82\pm 7\%$ for SCOD (Fig. 5-1). Increased COD removals were also obtained in for the AFMBR ($86\pm 4\%$) and AeMBR ($90\pm 3\%$). Thus, for Phase 1 and 2 tests, the effluent from all reactors had good effluent quality based on the effluent CODs.

When the influent COD was increased by another 40% to 299 ± 24 mg/L (Phase 3), the AOFMBR had better treatment performance than the other two reactors. The AOFMBR effluent COD increased slightly to 28 ± 7 mg/L (from 22 ± 7 mg/L) (Fig. 5-1) in Phase 3, resulting in average removal efficiencies of $91\pm 2\%$ for COD and $86\pm 3\%$ for SCOD. The effluent CODs were much higher for the other two reactors, with 39 ± 10 mg/L ($87\pm 3\%$ removal) for the AeMBR, and 51 ± 11 mg/L ($83\pm 3\%$ removal) for the AFMBR. The effluent CODs of the AOFMBR were significantly different from those of the AFMBR (*t*-test, $P<0.001$) and AeMBR (*t*-test, $P=0.002$). In addition, the effluent CODs of all three reactors in Phase 3 were significantly different from those in Phase 2 (*t*-test, AFMBR, $P<0.001$, and AOFMBR, $P=0.001$, and AeMBR, $P<0.001$). The AOFMBR had slightly improved COD and SCOD removals compared with Phase 1 and 2, while the percent COD removal decreased for the AFMBR and AeMBR.

Due to an unusual drop in TMP at the end of Phase 3, possibly due to a failure of the membrane or the epoxy seal, new membrane modules were installed in all reactors on day 103 (start of Phase 4). The influent COD of 329 ± 37 mg/L was not significantly different than that in Phase 3 (*t*-test, $P=0.04$). The effluent CODs from each reactor with the new membrane module were not significantly different from those obtained in the previous Phase 3 (*t*-test, AFMBR, $P=0.43$, and AOFMBR, $P=0.04$, and AeMBR, $P=0.42$) (Fig. 5-1), indicating that the membrane condition (after 103 d of operation for Phase 1-3 or a new membrane) had little impact on organics removal.

5.3.2 Effluent Turbidity

During the 131 d operation period, the AOFMBR effluent consistently had a very low turbidity of 0.2 ± 0.1 NTU (Fig. 5-2). The AeMBR had a comparable effluent turbidity (0.2 ± 0.1 NTU), but the AFMBR effluent turbidity was higher and more variable (0.9 ± 1.3 NTU). There were several spikes in the effluent turbidity of the AFMBR, with values as high as 6.0 NTU (day 23) and 8.2 NTU (day 27). However, these spikes in turbidity were likely a result of biomass growth and detachment from the effluent tubing. When the tubing of the AFMBR was cleaned, the turbidity immediately decreased, for example from 1.4 to 0.2 NTU (Day 41), and from 1.5 to 0.3 NTU (day 89). After about another half month of operation the effluent turbidity of AFMBR increased to 1.2 (day 59) and 1.1 (day 99) NTU, but no such effluent turbidity increases were measured for effluent samples from the AOFMBR and AeMBR. Even when the very high turbidity spikes (>2 NTU) were removed from the analysis, the average turbidity of AFMBR was 0.6 ± 0.4 NTU (Fig. 5-2), which was 300% as high as the other two aerobic reactors. This suggests that effluent quality in terms of turbidity was better in the aerated reactors (AOFMBR and AeMBR) than the anaerobic reactor (AFMBR).

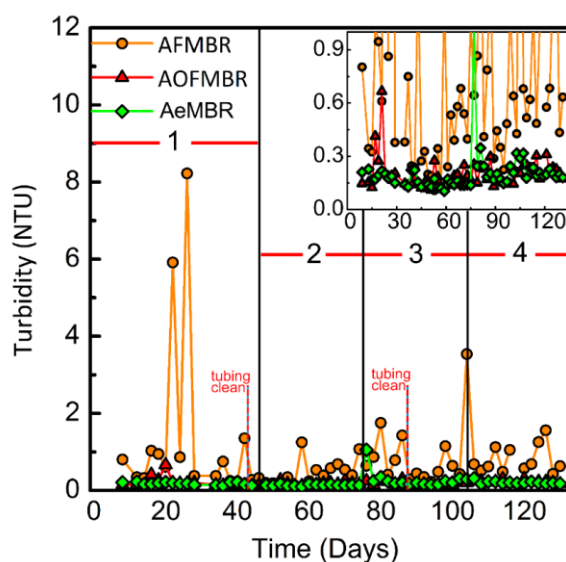


Fig. 5-2 Effluent turbidity over time measured for the three different types of membrane bioreactors. The inset shows the low turbidity range.

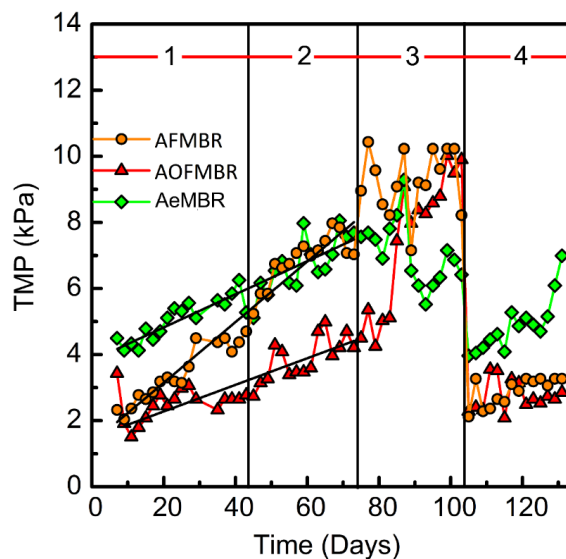


Fig. 5-3 Transmembrane pressure over time with the flux of $11.6 \text{ L/m}^2\text{-membrane-h}$. The lines were obtained by linear fitting of the TMP over the first two phases, where the slopes were 0.04 (AOFMBR), 0.05 (MBR), and 0.09 (AFMBR) kPa/d .

5.3.3 Transmembrane pressures

In the first two Phases (lower influent COD concentrations), the TMP of the three reactors all gradually increased over time, which indicated the membrane flux of $11.6 \text{ L/m}^2\text{/h}$ was below the critical flux, above which quick cake layer deposition occurs (6). The AOFMBR had the slowest increase rate in TMP (0.04 kPa/d , obtained by linear fitting) among the three reactors (Fig. 5-3), increasing from 1.9 kPa (day 7) to 4.2 kPa (day 73). The AFMBR had a starting TMP similar to that of the AOFMBR, but the TMP increased at a rate of 0.09 kPa/day , reaching 7.0 kPa at the end of Phase 2 (day 73), which was 67% larger than that of the AOFMBR. The AeMBR had a much higher initial TMP of 4.1 kPa , reaching 7.7 kPa by the end of Phase 2, which

was the highest of the three reactors. In general, the increase in TMP showed good agreement with a linear fit of the data in Phases 1 and 2 (Fig. 5-3), suggesting there was no appreciable change in membrane fouling due to the increased COD in these two Phases. The relative proportion of the increased TMP rate, based on the slopes of the three lines in Fig. 5-3, were 1.25 for the AeMBR and 2.3 for the AFMBR relative to the slope for the AOFMBR.

In Phase 3, there were large increases in TMP for both the AOFMBR and AFMBR but not the AeMBR. The AOFMBR had a particularly sudden increase in the TMP, reaching 9.9 kPa by the end of Phase 3, similar to that of the AFMBR (10.2 kPa). The AeMBR exhibited much different behavior, and the TMP decreased over Phase 3, which might be a result of membrane failure or failure of the membrane fittings. After replacing all membrane modules for continued testing Phase 4, the TMP showed a trend similar to that in Phase 1, with slow increases in the TMP. The AeMBR had a higher initial TMP in Phase 4 than the other two reactors, consistent with results from Phase 1.

5.3.4 SEM imaging

Biofilm growth was observed on the AOFMBR (Fig. 5-4B) and AeMBR membranes (Fig. 5-4C), based on comparisons with abiotic membranes (Fig. 5-4D). The AOFMBR biofilm was relatively uniform (Fig. 5-4F), but it appeared to have a coarser morphology (Fig. 5-4B) than those on the AFMBR (Fig. 5-4A), which had a relatively smooth and uniform morphology (Fig. 5-4A and 5-4E). However, no objects with sizes similar to those of bacteria were found on the AFMBR membrane surface (Fig. 5-4A). Without GAC addition, the biofilm on the AeMBR membrane surface was the most heterogeneous (Fig. 5-4C) and non-uniform (Fig. 5-4G) of the different membranes examined. No sign of membrane surface damage was observed on all the membrane imaged.

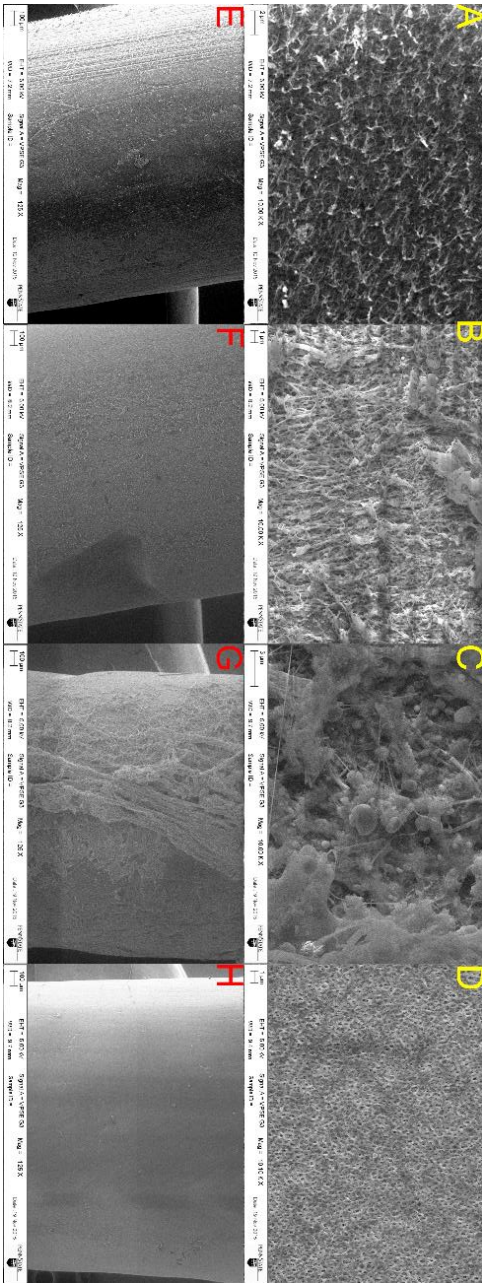


Fig. 5-4 SEM images with the magnitude of $10,000 \times$ (A–D) and $125 \times$ (E – H) for the surfaces of the membranes in the reactor of AFMBR (A and E), AOFMBR (B and F), AeMBR (C and G) and abiotic membrane (D and H).

5.3.5 Microbial community analysis

The microbial communities in the reactors formed three distinct groups based on clusters observed in mMDS plots (Fig. 5-5A). The microbial communities of the suspended solids in the two aerobic AOFMBR and AeMBR reactors were relatively more similar to each other (SRBCS, 0.69) than the other samples from the AFMBR or the GAC in the AOFMBR (Fig. 5-5A). The suspended solids microbial communities in the AFMBR were different from those in the two reactors, but were similar to communities on the GAC in that reactor (SRBCS, 0.63). The microbes on the GAC in the AOFMBR were distinct from all other samples.

The dominant phyla in all the samples were *Proteobacteria* (42% to 66%), *Bacteroidetes* (12% to 31%), *Firmicutes* (4% to 13%), while *Actinobacteria* was found to be abundant only in the suspended solids in the aerobic reactors (9% in AOFMBR and 5% in AeMBR) (Fig. 5-5B). *Fusobacteria* was found to be only abundant in the suspended solids in AFMBR (5%). At the genera level, there was no large predominance of any single genera in the suspended solids in AOFMBR and AeMBR. However, in the AOFMBR, *Arcobacter* (7%) and *Flavobacterium* (10%) were the predominant genus on the GAC (Fig. C-S3). There was also approximately five times higher relative abundance of *Nitrospira* (1.2%) on the GAC in the AOFMBR compared to the liquid samples in AOFMBR and AeMBR. Similarly, the GAC of AOFMBR had *Nitrosomonas* present at relative abundance of 0.03% while *Nitrosomonas* was present at a lower relative abundance in the suspended solids from the AOFMBR (0.006%) and AeMBR (0.003%). In contrast to the nitrifying populations, methane-oxidizing bacteria (e.g. *Methylomonas*, *Methylosarcina* and *Methylococcus*) were present at 145-fold higher relative abundance in the suspended solids of AOFMBR (average 0.03%) compared to that detected on the GAC in the AOFMBR. The abundance of methane-oxidizing bacteria in the suspended solids of AOFMBR

was higher than that detected in the AeMBR (0.002%) and much higher than that in the AFMBR (0.001%).

The same dominant genera, *Acrobacter*, was found in the suspended solids (31%) and GAC (13%) from the AFMBR, consistent with their close clustering in the mMDS plots. However, some other genera were present at different relative abundances on the GAC compared to those in the solution. For example, *Geobacter* was present at up to 7.8% relative abundance on GAC, but only <0.2% in the suspended solids, in the AFMBR. Methanogenic archaeal sequences were retrieved in higher relative abundance on the GAC from the AFMBR than the suspended solids. For example, *Methanothrix* was present in 0.2% on the GAC compared to 0.02% in the suspended solids in AFMBR, while *Methanospirillum* had a 4-fold higher relative abundance on the GAC (0.04%) than in the suspended solids (0.01%).

5.3.6 Energy production and consumption

The production of methane gas in Phases 3 and 4 averaged 6.2 ± 1.2 L/m³–wastewater treated. No methane gas was collected and analyzed in the first two phases of reactor operation. Dissolved methane was detected in the AFMBR effluent but not in the effluents of the aerated reactors (AOFMBR and AeMBR). The methane generated by the AFMBR could be used to produce 0.02 kWh/m³ of electricity [assuming a 33% conversion efficiency of methane to electricity (13)]. However, the amount of methane produced here would not be sufficient to provide the energy needed to strip the dissolved methane out of the effluent, which was estimated to be 0.05 kWh/m³ (21). On this basis of energy recovery versus that needed for methane gas stripping, avoiding methane generation could be more economically favorable than harvesting methane with potential energy cost for air stripping.

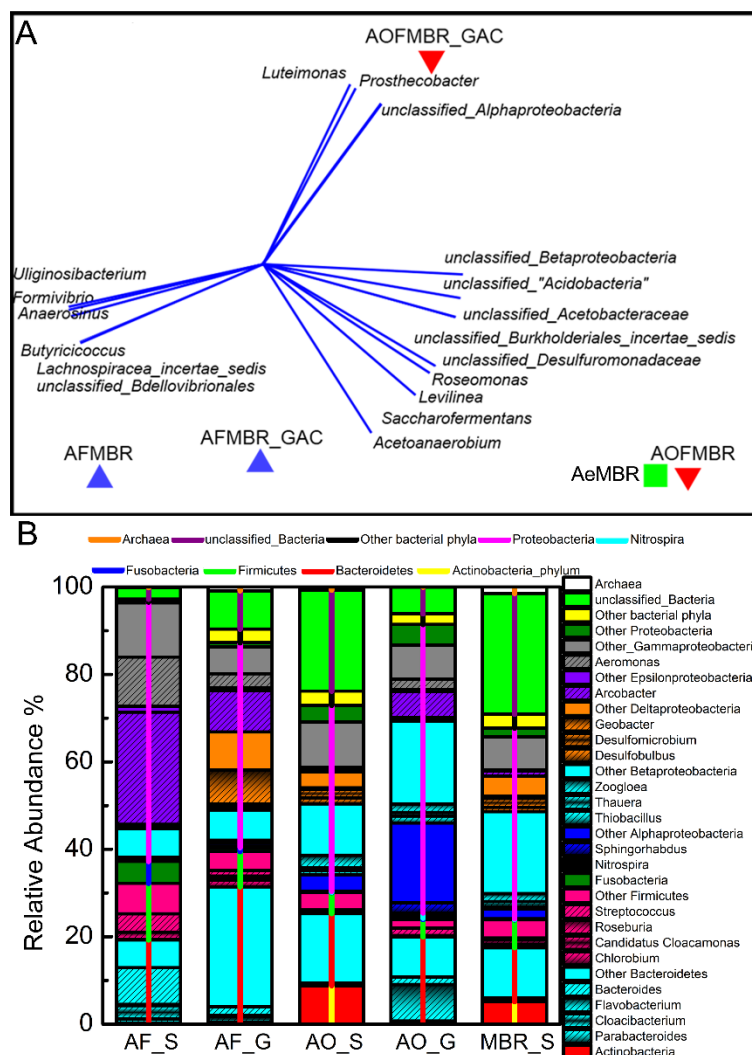


Fig. 5-5 (A) Similarity among the GAC or suspended biomass samples in the different reactors presented as an mMDS plot. (B) Analysis of the microbial communities in the solution (S) and on the GAC (G) in the AOFMBR (AO), AFMBR (AF) and AeMBR (MBR) reactors based on relative abundance at the genera level. Only genera with a relative abundance >1% were included, Unclassified sequences and minor genera (relative abundance <1%) were summarized at the phylum level. Vertical lines with different colors separate bacteria into 7 phyla. Archaea is shown as a kingdom.

The main advantage of using an AOFMBR compared to the AFMBR was avoiding the production of methane gas. However, it would also be desirable to reduce the energy for suspension of the GAC by aeration to be less than that needed for recirculation in the AFMBR. Based on the energy used here for aeration, however, using the air to replace recirculation did not provide a favorable energy balance (Table 5-2). The energy consumption in AOFMBR, as well as AeMBR (data not shown in Table 2), was still four times as high as that of AFMBR (energy calculation details are in SI). The main part of energy consumption in the AOFMBR was aeration, while the majority of energy needed for the AFMBR would be that used for methane gas stripping. The effluent pumping energy to drive the suction pressure of the membrane module was estimated to be only 0.6% of total energy in AOFMBR, and 4.3% in AFMBR. Even though the AOFMBR had an advantage compared to the AFMBR of less membrane fouling under low influent COD conditions, the reduced energy needed for the AOFMBR due to the lower TMP would not be sufficient to make it less costly to operate than the AFMBR. Although sludge production was not monitored in this study, and no sludge was removed from the reactor over the 131-day study, it will be necessary to consider the cost for sludge treatment in this aerobic system compared to the anaerobic AFMBR.

Table 5-2 Estimates of energy consumption for AOFMBR compared to the AFMBR.

Energy estimation	AFMBR (kWh/m ³)	AOFMBR (kWh/m ³)	AeMBR (kWh/m ³)
Recirculation pumping	0.019	NA	NA
Air blower	NA	0.24	0.24
Influent pumping	0.0014	0.0014	0.0014
Effluent pumping	0.0026	0.0013	0.0013
Methane stripping	0.05	NA	NA

Energy generation from methane	-0.02	NA	NA
Total	0.06	0.24	0.24

Stripping energy from (21)

NA: not applicable

5.4 Discussion

5.4.1 Enhanced effluent quality and membrane fouling control

The use of rising bubbles in the AOFMBR to suspend the GAC, rather than recirculation in the AFMBR, resulted in improved treatment, with a 49% lower effluent COD (average of 26 ± 6 mg/L) for the AOFMBR compared to the AFMBR (51 ± 11 mg/L). The use of GAC in the aerated AOFMBR also improved removal compared to the AeMBR, with a 32% lower effluent for the AOFMBR than the AeMBR (38 ± 9 mg/L), at the highest influent CODs of 299 mg/L (Phase 3) and 329 mg/L (Phase 4) at a HRT of 1.3 h. This improvement in performance for the AOFMBR compared to the AeMBR was due to the presence of the GAC, which make have reduced the COD levels by providing a high surfaced area for growth of microorganism and adsorption of the organic matter. The COD removals of the AFMBR (84-87%) in this study were within the large range of those previously reported of 63% (22) to 95% (15) using various wastewaters and HRTs. However, COD removals in most of these studies have ranged from 80% to 90% (12–14). AeMBRs treating domestic wastewater (low strength) generally are in the range of 80% to 95% COD removal (12,23), which is consistent with that observed here (86-89%) even though the AeMBR was not chemically cleaned during this study. The AOFMBR also consistently produced an effluent with a low turbidity (0.2 ± 0.1 NTU) that was on average 78% lower than that of the

more highly variable effluent turbidity of the AFMBR (0.9 ± 1.3 NTU). A low effluent turbidity was also obtained for the AeMBR (0.2 ± 0.1 NTU), consistent with a previous study (24).

Membrane fouling was better controlled for the AOFMBR compared to the AFMBR and AeMBR, when the influent COD was lower than 200 mg/L, as the TMP increase rate was only 45% of that in AFMBR and 80% of that in AeMBR. Biofilm was observed on the membrane of the AOFMBR, while no bacteria-size particle was found on the membrane of AFMBR, suggesting accumulated material was likely biomass debris, SMP or precipitated inorganics. The different surface morphologies suggest that the aerobic conditions or the way the GAC scoured the membranes when air bubbles were present was also important for achieving a reduction in the rate of membrane fouling. The effectiveness of GAC for scouring and minimizing membrane fouling was supported by SEM images, as the biofilm on the AOFMBR membrane appeared to be relatively uniform compared to the more heterogeneous biofilm on the AeMBR membrane. When a thick biofilm or mass of particulate organic matter forms on a membrane, it is referred to as the cake layer, and it usually is the major part of the membrane resistance (25). Therefore, the reduction of membrane fouling in the AOFMBR can be explained primarily by the effective reduction of the thickness of a cake layer by fluidizing GAC. One concern in using both air bubbles and high concentration of GAC (92 g/L) in the AOFMBR was the potential for damage of the membrane. However, there was no evidence of loss of membrane integrity in the system due to the high concentration of GAC and presence of air bubbles based on either visual observations or reactor performance.

While GAC has previously been used in other types of aerated membrane reactors, the concentration of GAC used here (92 g/L) was similar to that used in anaerobic reactor AFMBR studies (95-342 g/L) (12–14,18,26), but much higher than those used in aerated membrane reactors in many previous studies (up to 2 g/L). Thus, the use of a high concentration of GAC, which is a good adsorbent of organic matter, likely aided in reducing membrane fouling as

biopolymers and organics in the AOFMBR or AFMBR could be adsorbed by the GAC rather than deposited on the membrane surfaces. In a previous study, when only a relatively small amount (2 g/L) of powdered activated carbon (PAC) was added into an AeMBR, improved treatment was obtained for a distillery wastewater (27). Adding 0.75 g/L or 1.5 g/L of PAC into an AeMBR was also previously shown to reduce membrane fouling (24). GAC addition of 0.5 to 2 g/L was also found in another study to minimize sudden increases in membrane resistance, and organic removal was improved (28). It was concluded in all these other studies that the reduction in fouling was mainly due to adsorption of foulants onto the activated carbon, although scouring may have also been important. In the AOFMBR conditions examined here, the substantially higher GAC concentration compared to these previous studies made it possible that organic matter adsorption to the GAC was a factor, in addition to membrane scouring, in minimizing membrane fouling. The GAC in both the AFMBR (10 g) and the AOFMBR (6 g) was not replaced during this study (more than 200 days, including the acclimation and test periods), and there was no sign of reduced performance at the end of phase 4 due to the age of the carbon. While carbon replacement might be needed for operation over longer periods of time, the rate that carbon might need to be replaced cannot be estimated based on the results of this current study.

The TMP of 10.2 kPa that developed in the AFMBR is within the range of 5 kPa to 20 kPa used by others over a 100-d operation period without cleaning (15,26). A rapid increase in the TMP in the AOFMBR was observed in Phase 3, which usually would indicate sudden changes in the biofilm or cake layer structure (29). Sudden changes in TMP appear to occur more frequently in lab-scale membrane bioreactors than larger reactors (1,30). Even with this rapid TMP increase, the TMP of AOFMBR was still comparable to that of AFMBR. The initial TMP for AeMBR were higher than that of AFMBR and AOFMBR in both Phase 1 and 4, when the membrane was replaced by fresh one. The reason for this difference was likely due to the absence of the GAC for membrane scouring in the AeMBR, compared to the other two reactors. The

membrane flux of 11.6 L/m²-membrane-h in this study was close to that used in previous AFMBR studies (8-16 L/m²-membrane-h), and the TMP increase of the AFMBR in Phases 1 and 2 was also consistent with previous reports (12–14,31). The membrane flux set here was within a range typical of AnMBRs (10-40 L/m²-membrane-h) (6) and AeMBRs (4 -36 L/m²-membrane-h) (32).

5.4.2 Microbial community analysis

Phylum-level microbial community analyses in the AFMBRs have not been previously reported, and therefore comparisons cannot be made to previous studies for this reactor or the new AOFMBR. However, comparisons are possible to communities in conventional treatment systems. At phylum level, the dominant four phyla, *Proteobacteria*, *Bacteroidetes*, *Firmicutes*, and *Actinobacteria*, in the suspended biomass in the AOFMBR and AeMBR were the same four phyla as those identified in a previous study of 15 activated sludge samples collected from 14 treatment plants (33). The phyla with relative abundance above 5% in the suspended biomass of the AFMBR, *Proteobacteria*, *Bacteroidetes*, *Firmicutes*, and *Fusobacteria*, were also found dominant in an anaerobic moving bed biofilm reactor treating municipal wastewater (34). This suggests that the microbial communities in suspension at the genera level, resembled those communities from other aerobic and aerobic/anaerobic (moving bed) systems.

The GAC in the AFMBR and AOFMBR provides a more unique growth environment compared to the suspended cells. We observed a selective enrichment of *Geobacter* and certain methanogens (e.g. *Methanothrix* and *Methanospirillum*) in the GAC communities in the AFMBR. The abundance of these two groups on the GAC may be important, as *Geobacter* was shown to colonize GAC and conduct extracellular electron transfer to methanogens under anaerobic growth conditions (35,36). The transfer of extracellular electrons is particularly beneficial for acetoclastic

methanogens as acetate has to be activated first at the expense of adenosine triphosphate (ATP) in order to generate methane and carbon dioxide (37). This benefit could help explain the higher relative abundance of *Methanothrix*, an acetoclastic methanogen, on the GAC in the AFMBR.

The biofilm on the GAC in the AOFMBR, had a greater abundance of *Nitrospira* and *Nitrosomonas* compared to the suspended microbial communities in either the AOFMBR or the AeMBR. This suggests that nitrifying bacterial populations may have benefited from growth conditions on the GAC. Unfortunately, the enriched abundance of these microorganisms was not determined until the completion of the study, and nitrogen balances were not conducted as a part of this study. The comparatively higher relative abundance of *Nitrosomonas* and *Nitrospira* on the GAC in the AOFMBR, as well as the low concentrations of COD in the reactor effluent, suggest that having GAC in this system might produce conditions favorable for nitrification.

The suspended microbial communities in the AOFMBR also had a higher relative abundance of methane-oxidizing bacteria (e.g. *Methylomonas*, *Methylosarcina* and *Methylococcus*) compared to those in the AFMBR. The presence of the methane-oxidizing bacteria in the AOFMBR could indicate that methanogenesis may have occurred in this system, or they could just reflect growth of cells on dissolved methane present in the influent wastewater. The possibility of methane oxidation in this system may be an interesting area for further study.

5.4.3 Energy consumption

Although methane gas production was avoided in the AOFMBR, energy consumption was 4 times greater than that of the AFMBR. However, the presence of the GAC in the AOFMBR resulted in better membrane fouling control and better COD removal than the AeMBR. The minimum aeration intensity needed to effectively fluidize the GAC (6 g, 92 g/L) was $0.005 \text{ m}^3/\text{m}^2$ -cross section area-s, which is comparable to some AeMBRs (28,38,39). The

energy consumed by the AOFMBR and AeMBR was therefore similar to that of an AeMBR ($0.3\text{--}0.6\text{ kWh/m}^3$) (6) and activated sludge process ($0.3\text{--}0.6\text{ kWh/m}^3$) (40). However, the energy needed for AFMBR operation estimated here (0.06 kWh/m^3) and those reported by others ($0.019\text{ to }0.028\text{ kWh/m}^3$) (12,13) was about one tenth of that used by other types of AnMBRs ($0.25\text{--}1\text{ kWh/m}^3$) (6). One reason for the lower energy requirements of an AFMBR is that water recirculation is less energy intensive than gas sparging. Additional headlosses, for example, due to an increase in viscosity with MLSS accumulation, was not included in the calculations for the AFMBR, and thus the actual energy for that system is underestimated relative to the gas sparging systems.

Gas-phase methane produced in AFMBR was averaged $6.2 \pm 1.2\text{ L/m}^3$ –wastewater treated ($0.02\text{ m}^3\text{-CH}_4/\text{kg COD}$) in Phases 3 and 4. Although methane production overall was low compared to a previous AFMBR study (14), it was 36 times as high as a previous study using MFC effluent with the same AFMBR reactor design. The increased gas production observed here was most likely due to the higher influent COD in Phases 3 ($299 \pm 24\text{ mg/L}$) and 4 ($329 \pm 37\text{ mg/L}$) compared to the previous study (13) of $107 \pm 10\text{ mg/L}$. The methane production measured here, however, was 10 times lower than that typical of UASBs, CSTRs and AnMBRs treating various of wastewaters ($0.2\text{ to }0.4\text{ m}^3\text{-CH}_4/\text{kg COD}$) (41), which is a consequence of the different HRTs and influent CODs of AFMBR compared to these studies with other types of reactors.

It should be possible to reduce the energy used by the AOFMBR. Based on Stoke's Law, using GAC with a smaller size could reduce the needed aeration intensity needed to fluidize the media, as the settling velocity is dependent on particle size squared. Also, particles other than GAC could be used, but these materials might not be good adsorbents. Larger media has been found to be more useful for reducing fouling than smaller media (particle sizes ranging from $0.2\text{ to }2\text{ mm}$) (42). This suggests that there is an optimum particle size that can be chosen to balance energy demands with reduced membrane fouling. It might also be possible to use intermittent

aeration in the AOFMBR, which has been shown to have better fouling control under some operational conditions in AeMBRs (1).

5.5 Conclusions

An AOFMBR was developed by replacing recirculation in an AFMBR with aeration as the driving force for GAC fluidization, with a near-term goal of avoiding methane production and a long-term goal of reducing energy demands relative to AnMBRs and AeMBRs. Operation of the AOFMBR with two controls, the anaerobic AFMBR with GAC, and an AeMBR with aeration but no GAC, showed the following:

1. The effluent COD in the AOFMBR was maintained at the lowest concentrations compared to the other two reactors, with average maximum removal efficiencies of 92% (COD) and 87% (SCOD) for the high influent CODs in the last two Phases (averaging 299 ± 24 mg/L in Phase 3, and 329 ± 37 mg/L in Phase 4).
2. Effluent turbidity of the AOFMBR was steady and averaged 0.2 NTU, while the AFMBR had occasional spikes in the effluent turbidity.
3. Membrane fouling was better controlled in AOFMBR under three different influent CODs of 153 and 214 mg/L, with a TMP increase rate of only 80% compared to the AeMBR, and 43% compared to the AFMBR. SEM images also supported less membrane fouling in the presence of the GAC particles.
4. Eliminating recirculation by using air bubble in the AOFMBR compared to recirculation in the AFMBR did not result in a lower energy consumption for the AOFMBR. The use of intermittent aeration or optimization of the size and density of the media that is fluidized in the reactor could contribute lowering energy costs for operation.

5.6 References

1. Meng F, Chae S-R, Drews A, Kraume M, Shin H-S, Yang F. Recent advances in membrane bioreactors (MBRs): membrane fouling and membrane material. *Water Res.* 2009;43(6):1489–512.
2. Chang IS, Le Clech P, Jefferson B, Judd S. Membrane fouling in membrane bioreactors for wastewater treatment. *J Environ Eng.* 2002;128(11):1018–29.
3. Kimura K, Yamato N, Yamamura H, Watanabe Y. Membrane fouling in pilot-scale membrane bioreactors (MBRs) treating municipal wastewater. *Environ Sci Technol.* 2005;39(16):6293–9.
4. Fan B, Huang X. Characteristics of a self-forming dynamic membrane coupled with a bioreactor for municipal wastewater treatment. *Environ Sci Technol.* 2002 Dec 1;36(23):5245–51.
5. McCarty PL, Bae J, Kim J. Domestic wastewater treatment as a net energy producer-can this be achieved? *Environ Sci Technol.* 2011;45(17):7100–6.
6. Liao B-Q, Kraemer JT, Bagley DM. Anaerobic membrane bioreactors: applications and research directions. *Crit Rev Environ Sci Technol.* 2006;36(6):489–530.
7. Skouteris G, Hermosilla D, López P, Negro C, Blanco Á. Anaerobic membrane bioreactors for wastewater treatment: A review. *Chem Eng J.* 2012;198–199:138–48.
8. Xie K, Lin HJ, Mahendran B, Bagley DM, Leung KT, Liss SN, et al. Performance and fouling characteristics of a submerged anaerobic membrane bioreactor for kraft evaporator condensate treatment. *Environ Technol.* 2010;31(2012):511–21.
9. Vyrides I, Stuckey DC. Saline sewage treatment using a submerged anaerobic membrane reactor (SAMBR): Effects of activated carbon addition and biogas-sparging time. *Water Res.* 2009 Mar;43(4):933–42.

10. Sui P, Wen X, Huang X. Feasibility of employing ultrasound for on-line membrane fouling control in an anaerobic membrane bioreactor. *Desalination*. 2008 Jan;219(1–3):203–13.
11. Choo KH, Lee CH. Hydrodynamic behavior of anaerobic biosolids during crossflow filtration in the membrane anaerobic bioreactor. *Water Res*. 1998 Nov;32(11):3387–97.
12. Kim J, Kim K, Ye H, Lee E, Shin C, McCarty PL, et al. Anaerobic fluidized bed membrane bioreactor for wastewater treatment. *Environ Sci Technol*. 2011 Jan 15;45(2):576–81.
13. Ren L, Ahn Y, Logan BE. A two-stage microbial fuel cell and anaerobic fluidized bed membrane bioreactor (MFC-AFMBR) system for effective domestic wastewater treatment. *Environ Sci Technol*. 2014;48(7):4199–206.
14. Lee R, McCarty PL, Bae J, Kim J. Anaerobic fluidized membrane bioreactor polishing of baffled reactor effluent during treatment of dilute wastewater. *J Chem Technol Biotechnol*. 2015;90(3):391–7.
15. Bae J, Shin C, Lee E, Kim J, McCarty PL. Anaerobic treatment of low-strength wastewater: A comparison between single and staged anaerobic fluidized bed membrane bioreactors. *Bioresour Technol*. 2014;165(C):75–80.
16. Smith AL, Skerlos SJ, Raskin L. Anaerobic membrane bioreactor treatment of domestic wastewater at psychrophilic temperatures ranging from 15 °C to 3 °C. *Environ Sci Water Res Technol*. 2015;1(1):56–64.
17. Seib MD, Berg KJ, Zitomer DH. Reduced energy demand for municipal wastewater recovery using an anaerobic floating filter membrane bioreactor. *Environ Sci Water Res Technol*. 2016;2:290–7.

18. Kim K-Y, Yang W, Ye Y, LaBarge N, Logan BE. Performance of anaerobic fluidized membrane bioreactors using effluents of microbial fuel cells treating domestic wastewater. *Bioresour Technol.* 2016;208:58–63.
19. Cheng H, Xie Y, Villalobos LF, Song L, Peinemann K-V, Nunes S, et al. Antibiofilm effect enhanced by modification of 1,2,3-triazole and palladium nanoparticles on polysulfone membranes. *Sci Rep.* 2016 Apr;6:24289.
20. Harb M, Xiong Y, Guest J, Amy G, Hong P-Y. Differences in microbial communities and performance between suspended and attached growth anaerobic membrane bioreactors treating synthetic municipal wastewater. *Environ Sci Water Res Technol.* 2015;1(6):800–13.
21. Smith AL, Stadler LB, Love NG, Skerlos SJ, Raskin L. Perspectives on anaerobic membrane bioreactor treatment of domestic wastewater: A critical review. *Bioresour Technol.* 2012;122:149–59.
22. Bae J, Yoo R, Lee E, McCarty PL. Two-stage anaerobic fluidized-bed membrane bioreactor treatment of settled domestic wastewater. *Water Sci Technol.* 2013;68(2):394–9.
23. Brindle K, Stephenson T. The application of membrane biological reactors for the treatment of wastewaters. *Biotechnol Bioeng.* 1996;49(6):601–10.
24. Ying Z, Ping G. Effect of powdered activated carbon dosage on retarding membrane fouling in MBR. *Sep Purif Technol.* 2006;52(1):154–60.
25. Choo KHK-H, Lee C-HCH. Membrane fouling mechanisms in the membrane-coupled anaerobic bioreactor. *Water Res.* 1996;30(8):1771–80.
26. Shin C, McCarty PL, Kim J, Bae J. Pilot-scale temperate-climate treatment of domestic wastewater with a staged anaerobic fluidized membrane bioreactor (SAF-MBR). *Bioresour Technol.* 2014;159:95–103.

27. Satyawali Y, Balakrishnan M. Performance enhancement with powdered activated carbon (PAC) addition in a membrane bioreactor (MBR) treating distillery effluent. *J Hazard Mater.* 2009;170(1):457–65.
28. Johir MAH, Aryal R, Vigneswaran S, Kandasamy J, Grasmick A. Influence of supporting media in suspension on membrane fouling reduction in submerged membrane bioreactor (SMBR). *J Memb Sci.* 2011;374(1–2):121–8.
29. Zhang J, Chua HC, Zhou J, Fane AG. Factors affecting the membrane performance in submerged membrane bioreactors. *J Memb Sci.* 2006;284(1):54–66.
30. Xu L, Zhang G, Yuan G, Liu H, Liu J, Yang F. Anti-fouling performance and mechanism of anthraquinone/polypyrrole composite modified membrane cathode in a novel MFC-aerobic MBR coupled system. *RSC Adv.* 2015;5(29):22533–43.
31. Yoo R, Kim J, McCarty PL, Bae J. Anaerobic treatment of municipal wastewater with a staged anaerobic fluidized membrane bioreactor (SAF-MBR) system. *Bioresour Technol.* 2012;120:133–9.
32. Kim J, Kim K, Ye H, Lee E, Shin C, McCarty PL, et al. Anaerobic fluidized bed membrane bioreactor for wastewater treatment. *Environ Sci Technol.* 2011 Jan 15;45(2):576–81.
33. Zhang T, Shao M-F, Ye L. 454 Pyrosequencing Reveals Bacterial Diversity of Activated Sludge From 14 Sewage Treatment Plants. *ISME J.* 2012;6(6):1137–47.
34. Biswas K, Taylor MW, Turner SJ. Successional development of biofilms in moving bed biofilm reactor (MBBR) systems treating municipal wastewater. *Appl Microbiol Biotechnol.* 2014;98(3):1429–40.
35. Liu F, Rotaru A-E, Shrestha PM, Malvankar NS, Nevin KP, Lovley DR. Promoting direct interspecies electron transfer with activated carbon. *Energy Environ Sci.* 2012;5(10):8982.

36. Rotaru A-E, Shrestha PM, Liu F, Shrestha M, Shrestha D, Embree M, et al. A new model for electron flow during anaerobic digestion: direct interspecies electron transfer to *Methanosaeta* for the reduction of carbon dioxide to methane. *Energy Environ Sci.* 2014;7(1):408.
37. Jetten MSM, Stams AJM, Zehnder AJB. Isolation and characterization of acetyl-coenzyme A synthetase from *Methanothrix soehngenii*. *J Bacteriol.* 1989;171(10):5430–5.
38. Liu R, Huang X, Sun YF, Qian Y. Hydrodynamic effect on sludge accumulation over membrane surfaces in a submerged membrane bioreactor. *Process Biochem.* 2003;39(2):157–63.
39. Ueda T, Hata K, Kikuoka Y, Seino O. Effects of aeration on suction pressure in a submerged membrane bioreactor. *Water Res.* 1997;31(3):489–94.
40. Seib MD, Berg KJ, Zitomer DH. Reduced energy demand for municipal wastewater recovery using an anaerobic floating filter membrane bioreactor. *Environ Sci Water Res Technol.* 2016;2:290–7.
41. Visvanathan C, Abeynayaka A. Developments and future potentials of anaerobic membrane bioreactors (AnMBRs). *Membr Water Treat.* 2012;3(1):1–23.
42. Aslam M, McCarty PL, Bae J, Kim J. The effect of fluidized media characteristics on membrane fouling and energy consumption in anaerobic fluidized membrane bioreactors. *Sep Purif Technol.* 2014;132:10–5.

Chapter 6

Simultaneous nitrogen and organics removal using membrane aeration and effluent ultrafiltration in an anaerobic fluidized membrane bioreactor

Abstract

Dissolved methane and a lack of nutrient removal are two concerns for treatment of wastewater using anaerobic fluidized bed membrane bioreactors (AFMBRs). Membrane aerators were integrated into an AFMBR to form an Aeration membrane fluidized bed membrane bioreactor (AeMFMBR) capable of simultaneous removal of organic matter and ammonia without production of dissolved methane. Good effluent quality was obtained for domestic wastewater (193 ± 23 mg/L and 49 ± 5 mg-N/L) treatment, with no detectable suspended solids, $93 \pm 5\%$ of chemical oxygen demand (COD) removal to 14 ± 11 mg/L, and $74 \pm 8\%$ of total ammonia (TA) removal to 12 ± 3 mg-N/L. Nitrate and nitrite concentrations were always low (< 1 mg-N/L) during continuous flow treatment. Membrane fouling was well controlled by fluidization of the granular activated carbon (GAC) particles (transmembrane pressures maintained < 3 kPa). Analysis of the microbial communities suggested that nitrogen removal was due to nitrification and denitrification based on the presence of microorganisms associated with these processes.

6.1 Introduction

An anaerobic fluidized bed membrane bioreactor (AFMBR) was first developed as a post-treatment method for an anaerobic fluidized bed bioreactor (AFBR), achieving 87% removal of chemical oxygen demand (COD), 82% of soluble COD (SCOD), and ~100% of total suspended solid (TSS) (1). In addition, a low energy demand of 0.028 kWh/m³ was estimated for

the process, which is 10 times lower than that needed for treatment using anaerobic membrane bioreactor ($0.25\text{--}1\text{ kWh/m}^3$) (2). Membrane fouling is well controlled in an AFMBR by mechanical scouring due to fluidization of granular activated carbon (GAC) particles. Effective treatment has also been obtained using AFMBRs as a second process that followed treatment by other types of bioreactors. For example, the effluent of a microbial fuel cell (MFC) treating domestic wastewater was reduced to a COD of $16 \pm 3\text{ mg/L}$ and TSS of $< 1\text{ mg/L}$, at an AFMBR hydraulic retention time (HRT) of 1 h (3). Low effluent COD (11 mg/L) and negligible TSS were also achieved at an HRT of $\sim 1\text{ h}$ for effluent from an anaerobic baffled bioreactor (ARB) (4). The combined AFBR and AFMBR process was found to have an additional advantage of effective removal of pharmaceuticals from a wastewater (86-100%) (5). A disadvantage of AFMBR treatment, however, is that the effluent contains dissolved methane which would need to be removed prior to discharge (6). In addition, total nitrogen has not been reported to be reduced during AFMBR treatment, since a combination of anoxic and anaerobic conditions are required to achieve nitrification and denitrification.

Membrane-aerated bioreactors (MABRs) were developed to obtain efficient nitrogen removal through the growth of a biofilm on the aeration membranes. Oxygen is added by bubbleless gas transport through the membrane to the biofilm. Nitrification can occur in the stratified biofilm on the membrane, resulting in the release of nitrate which can reduce the concentration of organics by denitrification to levels needed to enable nitrification in the biofilm (7). Ammonia-oxidizing bacteria (AOB) have been identified in the deep biofilm layer near the membrane, while denitrifiers and heterotrophic bacteria grow on the outer layer (8). Stratified biofilm growth of nitrifiers and denitrifiers has also been confirmed using fluorescence in situ hybridization (7). Typically the biofilms on the membranes are 50 to 200 μm thick (9), which is usually deep enough to prevent oxygen transfer into the bulk liquid, thus maintaining anaerobic conditions in the solution (10). Membrane aerators immobilized with microorganisms were first

tested using synthetic wastewater (total organic carbon, TOC, 1000 mg/L and total nitrogen, TN, 58.5 mg-N/L) in batch mode (24 h), achieving a removal efficiency of 97.9% for TOC and 98.3% for TN with lumen pressure of 245 kPa (pure oxygen) (11). When treating organic-free synthetic wastewater (217 mg-N/L of ammonium) in continuous-flow mode, separate arrays of hollow fiber membranes (HFMs) that supplied pure bubbleless hydrogen and oxygen in a redox controlled bioreactor obtained a high ammonia removal flux (AR) of 5.8 g-N/m² membrane-d, with a nitrate and nitrite removal flux of 4.4 g-N/m²-d, at a pressure of 861 kPa (12). A total nitrogen removal flux (NRF) of 1.7 g-N/m²-d was achieved using an MABR supplied with air to treat COD-free wastewater (47.1 mM NH₃-N), with 75% removal of the influent nitrogen (7). Nitrogen and carbonaceous compounds in synthetic wastewater (TOC of 100 mg/L and TN of 25 g-N/m³) were simultaneously removed using an MABR supplied with air, showing a carbon removal flux (CRF) of 7.4 g-C/m²-d and NRF of 2.8 g-N/m²-d (13). One disadvantage of using MABRs is that they require relatively long hydraulic retention times (HRTs) compared to other processes. For example, HRTs can be as long as several days using air, for example 1 day (12), 4-6 days (7), 1.2-12 days (14) and 15 days (8). However, HRTs can be reduced to only ~1 to several hours few by using pure oxygen, for example 0.6 h (15), 6 h (13) and 1-10 h (16).

In order to achieve effective ammonia removal in an AFMBR, it was hypothesized that adding a membrane aeration module into the reactor could enable simultaneous removal of both carbonaceous and nitrogen compounds in a single aeration membrane fluidized bed membrane bioreactor (AeMFMBR). By infusing oxygen into the system, nitrogen could be removed through nitrification on aeration membranes, and denitrification by microorganisms on the aeration membranes or on GAC and in the mixed liquor. In addition, it was hypothesized that production of methane could be avoided through the use of the membrane aerators as nitrate could serve as the primary alternate electron acceptor. A bench-scale AeMFMBR was constructed by integrating two different modules, the membrane aerators and the membranes used for ultrafiltration of the

effluent, into a single reactor containing fluidized GAC. The performance of the AeMFMBR was initially examined using synthetic influent in fed-batch mode, and then by using synthetic or diluted domestic wastewaters in continuous flow mode. The mechanism of nitrogen removal was investigated through a microbial community analysis of the suspended biomass and the biomass on membrane aerators, and GAC.

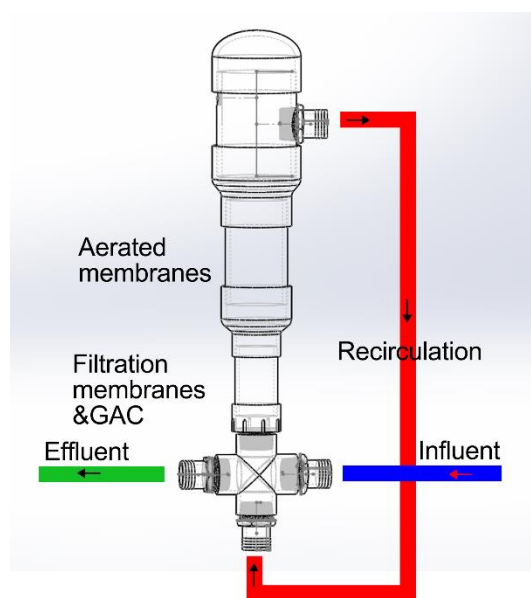


Fig. 6-1 Schematic of the AeMFMBR showing locations of the aeration and filtration membranes.

6.2 Material and Methods

6.2.1 Reactor setup

The AeMFMBR made of polyvinyl chloride (PVC, McMaster Carr) contained two chambers, one for filtration (lower section) and the other for aeration (upper section), with a total volume of 4.5 L (Fig. 6-1). The aeration membrane module contained 135 polyvinylidene fluoride (PVDF) HFMs (pore size of 0.1 μm , Kolon Inc., South Korea) that were sealed at one end. The ultrafiltration membrane module used to filter the wastewater had 54 PVDF HFMs. The

total surface area was estimated to be 0.08 m² for the aeration membrane module (18 m²/m³), and 0.03 m² for the filtration membranes (7 m²/m³). A magnetic water pump (50 px-x, 1100 GPH, Pan World, Japan) was used to keep the mixed liquor recirculated at a constant flowrate of 4.3 ± 0.9 L/min. Two peristaltic pumps (model no. 7523-90, Masterflex, Vernon Hills, IL) were used for influent and effluent pumping. A mass flow controller (0 to 10 LPM, Air/He/Ar, Cole-Parmer, US) was used to measure the air flowrate, and a pressure gauge (type 1490, Ashcroft, Stratford, CT) was used to measure the air pressure. GAC particles (45 g/L; DARCO MRX, 10 x 30 mesh, Norit Activated Carbon, Cabot, GA) were added into filtration chamber for biofilm growth and to control membrane fouling.

6.2.2 Operation

AeMFMBR operation was separated into six phases, with each phase used to sequentially examine the different aspects of the AeMFMBR components and test conditions, for example operation only with aeration membranes compared to operation with GAC and organic carbon in the feed, to identify the impact of the organic carbon on nitrogen removal. Each of these phases are identified with notation to indicate the specific aspects of operation, as follows: B for fed batch operation, or C for continuous flow operation; HN for high (~240 mg-N/L) and LN for low (50-80 mg-N/L) nitrogen concentrations; S for synthetic wastewater, and W for actual domestic wastewater; G for operation with GAC particles added to the reactor; U for operation with ultrafiltration of the effluent; and P for tests with a higher air pressure used in the aeration module compared to other tests (Table 6-1). For example, phase 3B-SG indicates phase 3 operation with fed batch conditions, a synthetic wastewater feed, and GAC fluidization (but no ultrafiltration of the effluent).

Table 6-1 Operational conditions of the reactors for the six phases.

Phase	Duration (day)	Mode	Wastewater	Air flow (mL/min)	COD (mg/L)	SCOD (mg/L)	TA (mg-N/L)
-------	----------------	------	------------	-------------------	------------	-------------	-------------

1B-HN	45	Batch	COD free	1.0 ± 0.2	-	-	236 \pm 9
2B-LN	25	Batch	COD free	1.0 ± 0.3	-	-	79 \pm 11
3B-SG	24	Batch	Synthetic	1.0 ± 0.2	162 \pm 3	162 \pm 3	73 \pm 7
4C-SGU	29	Continuous	Synthetic	1.0 ± 0.1	154 \pm 12	154 \pm 12	68 \pm 6
5C-WGU	38	Continuous	Domestic	1.2 ± 0.4	202 \pm 9	127 \pm 8	52 \pm 3
6C-WGUP	34	Continuous	Domestic	2.2 ± 0.2	193 \pm 23	107 \pm 17	49 \pm 5

The membrane aerator (air flowrate of 1 mL/min) was inoculated with sludge from a nitrification tank (Pennsylvania State University Wastewater Treatment Plant) and feed solution (40 mM NH_4HCO_3 , 14.3 mM NaCl, 3.7 mM KHCO_3 , 0.8 mM KHSO_4 , 1.25 mM KH_2PO_4 , 0.83 mM MgSO_4 , 1.23 mM CaCl_2 , and 0.11 mM FeCl_3) in a column with stirring for 50 days prior to phase 1B-HN. Each time the operational conditions were changed the reactor was operated for at least one week under the new conditions for reactor acclimation. The AeMFMBR was operated at a constant temperature room with 20 °C (minimum light source to avoid phototrophic growth).

In phase 1B-HN, membrane aerator module alone was tested for ammonia removal with the reactor operated in batch mode (two repeated cycles), using a COD-free medium, and a high concentration of ammonia (HN) for acclimation of the biofilm for nitrification (236 \pm 9 mg-N/L, [Table 6-1](#)). The feed solution contained 40 mM NH_4HCO_3 , 14.3 mM NaCl, 3.7 mM KHCO_3 , 0.8 mM KHSO_4 , 1.25 mM KH_2PO_4 , 0.83 mM MgSO_4 , 1.23 mM CaCl_2 , and 0.11 mM FeCl_3 (7). In all subsequent phases (2-6), lower nitrogen concentrations were used in the range of 49 to 79 mg-N/L, as indicated in [Table 6-1](#). In phase 2B-LN, the AeMFMBR was therefore operated under the same conditions as phase 1 except the total ammonia concentration in the feed solution was reduced to 79 \pm 11 mg-N/L.

In phases 3 through 6, GAC particles were added into the filtration chamber and only lower nitrogen concentrations were tested. In phases 3 and 4, glucose (0.075 g/L) and acetate (0.1 g/L) were added into the feed solution as a source of COD, producing a TCOD of ~150 mg/L. In phase 3B-SG, the reactor was therefore operated in batch mode (three repeated cycles) to examine the impact of a defined, synthetic wastewater on nitrogen removal, compared to no COD

in the influent in phase 2. The addition of GAC was used to provide a large surface area for biofilm growth.

In phases 4 through 6, the ultrafiltration membrane module was placed in the reactor, and the operation was switched to continuous flow, producing the combined conditions for complete AeMFMBR operation in all subsequent tests. In phase 4C-SGU, the reactor was fed synthetic wastewater at two different flowrates, with a 10 min on and 1 min off for membrane relaxation; 3.6 mL/min (7.2 L/m²·h), producing a net HRT of 20.5 h; and 1.8 mL/min (3.6 L/m²·h), to produce a longer HRT of 41 h.

For tests in phases 5 and 6, the feed was switched to a domestic wastewater obtained from the primary clarifier of the Pennsylvania State University Wastewater Treatment Plant and operated at the longer HRT of 41 h. The wastewater was diluted to a TCOD of ~200 mg/L using distilled water, and the total ammonia (TA) concentration was adjusted to ~50 mg-N/L by adding ammonium bicarbonate, to simulate COD removal by an upstream process (such as an MFC) with no nitrogen removal. For phase 5C-WGU, the reactor operation was therefore the same as that in phase 4 except the synthetic wastewater was replaced by a diluted wastewater with a similar TA concentration. In phase 6C-WGUP, the lumen pressure (P) was increased to 4-5 kPa from 2-3 kPa in the first 5 phases to increase air flowrate in order to try to increase the ammonia removal rate. A low lumen pressure was applied in this study to make sure an axoic environment was maintained in the AeMFMBR.

6.2.3 Analytical methods

TCOD and SCOD were measured using commercial kits (COD digestion vials, low range and high range, Hach). Three-day headspace biochemical oxygen demand (HBOD) tests were used to analyze the reactor effluent and mixed liquor concentrations, where the HBOD₃ is approximately equal to a BOD₅ measured using standard methods (17). Total ammonia

(Nitrogen-ammonia reagent Set, high range, Hach), nitrite (NitraVer X nitrogen-nitrate reagent set, high range, Hach) and nitrate (NitriVer 3 TNT reagent set, nitrogen-nitrite, low range, Hach) concentrations were measured for the effluent and the liquid inside the AeMFMBR. Mixed liquor suspended solids (MLSS) was quantified based on total suspended solid (TSS) following standard methods (method 2540D, with filters having with a pore size of 1.5 μm ; GE Whatman) using a sample volume of ~ 50 mL. Dissolved oxygen (DO) was monitored using an oxygen meter (NeoFox oxygen monitoring kit with probe, Ocean optics, US). Dissolved methane for the effluent and mixed liquor were measured based on gases desorbed from solution as previously described (3), except 4 mL of headspace was left for air while transferring the sample to serum bottle (10 mL) instead of filling serum bottle without leaving a headspace. Transmembrane pressure (TMP) of the ultrafiltration membrane was monitored using a pressure transducer (TDH 31, Transducer Direct, US). The pH and conductivity of the diluted wastewater were measured using a probe and meter (Seven-Multi, Mettler-Toledo International Inc.).

Microorganisms were sampled from the aeration membranes at the end of phase 2B-LN and 4C-SGU, and from GAC particles and the suspended biomass in 4C-SGU. DNA was extracted from the samples following the Power Soil DNA isolation kit protocol with some modifications to improve DNA extraction (Mo Bio Laboratories, Inc) (18). Bead tubes with 0.1 mm glass beads were used instead of the garnet bead-beating tube in the original kit. The sample (GAC, centrifuged suspended solids from mixed liquor sample or aeration membranes cut into small pieces) and 750 μL bead solution were added to the bead tube, and tubes were mixed using a bead mill (Bead Ruptor 12 Homogenizer, Kennesaw, GA) for 45 s instead of using a vortexer, followed by centrifugation at $10,000 \times g$ for 1 minute, and incubation at 4 $^{\circ}\text{C}$ for 10 minutes. The extracted DNA was then sequenced by DNASense (Denmark). Briefly, DNA samples were amplified by polymerase chain reaction (PCR). The forward 515F (5'-GTGYCAGCMGCCGCGGTA-3') and reverse 805R (5'-GACTACHVGGGTATCTAATCC-3')

tailed primers were designed for targeting the V4 region of bacterial and archaeal 16S rRNA gene (18). The resulting amplicons were then purified, and single read sequenced (251bp) on MiSeq (Illumina). Taxonomy was assigned using the RDP classifier in QIIME (19), using the MiDAS database v.2.1.2 (20). Principle component analysis (PCA) was generated based on the relative abundance of operational taxonomic units (OTUs) with OTUs (unit vector) >5% present shown as axes. Square-root transformed Bray-Curtis similarities (BCS) were calculated between samples.

The oxygen transfer efficiency (OTE) was calculated assuming complete nitrification (total ammonium converted to nitrate) using the set air flowrate and measured AR as:

$$OTE = \frac{nAR_f A m_{O_2}}{0.23 m_N \rho Q_{air}} \quad (6-1)$$

where n the stoichiometric ratio of ammonia and oxygen (4), AR_f is ammonia removal flux (g-N/m² d), A the membrane aerator area (0.03 m²), m_{O_2} the molecular weight of oxygen gas (32 g/mol), 0.23 the mass fraction of oxygen in air, m_N is the molecular weight of nitrogen (14 g/mol), ρ the density of air at 20 °C (1.205×10^3 g/m³) and Q_{air} the airflow rate (m³/d). The Student-T test was used to assess differences in COD and ammonia removals among phases, with the differences considered to be significant for $p \leq 0.05$.

6.3 Results and Discussion

6.3.1 Nitrogen removal with COD-free synthetic wastewater

In the initial operation of the reactor (phase 1B-HN) with a high initial ammonia concentration of 236 ± 9 mg-N/L, the AR was 0.4 ± 0.02 g/m²-d (Fig. 6-2, Fig. D-S1), resulting in a total nitrogen removal efficiency of $72 \pm 2\%$ over a period of 20 days. When the ammonia concentration was reduced to 79 ± 11 mg-N/L in the next phase (2B-LN) the rate was only slightly

lower at 0.3 ± 0.06 g-N/m²-d (Fig. 6-2), indicating that the feed concentration had little impact on the rate of removal (Fig. D-S2). The TN concentration at the end of cycle in phase 2B-LN was <5 mg-N/L, indicating the membrane aeration could effectively reduce TN to a low concentration. These two ARs were lower than those previously reported for MABRs treating inorganic ammonium using air, which ranged around 1.7 g-N/m²-d (~30-50 kPa) (7) to 2 g-N/m²-d (21). The lower rate here was probably due to the low lumen pressure (2 kPa) and the low ambient temperature (20 °C) compared to these previous studies.

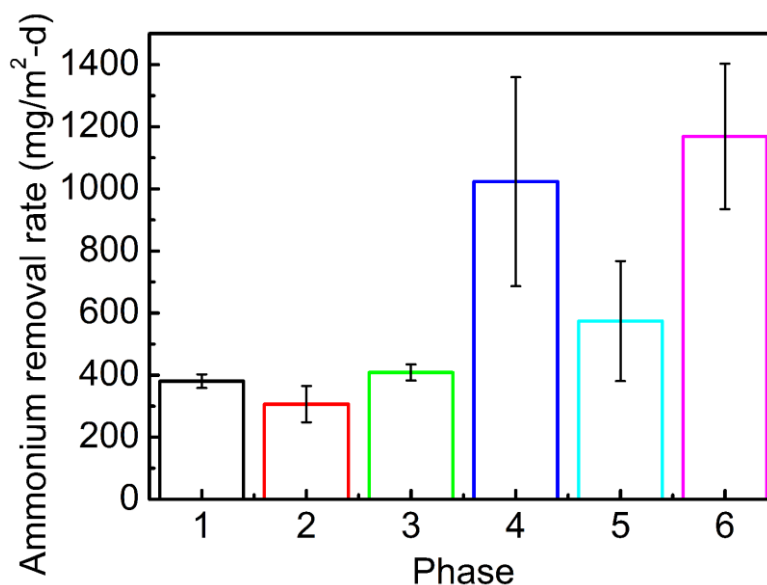


Fig. 6-2 Comparison of ammonia removal rate (AR) in each of the six phases of operation (phase 1B-HN, 2B-LN, 3B-SG, 4C-SGU, 5C-WGU and 6C-WGUP).

The nitrite concentrations during the operation were always low (Fig. D-S1 and D-S2), with 0.6 ± 0.6 mg-N/L for phase 1B-HN (Table 6-2) and 0.8 ± 0.7 mg-N/L for phase 2B-LN (Table 6-2). The nitrate concentrations were also low, with 1.8 ± 1.4 mg-N/L for phase 1B-HN and 1.6 ± 1.4 mg-N/L for phase 2B-LN (Table 6-2). The low nitrite and nitrate accumulated indicated that ammonium oxidation to nitrite was the limiting step in nitrification. Although the feed did

not contain any appreciable COD, the measured TCOD in mixed liquor in phase 2B-LN was 41 ± 23 mg/L. The COD was believed to be generated by autotrophic nitrifiers, consistent with a previous study treating COD-free synthetic wastewater (22), where COD was also found to be produced, likely by the generation and release of soluble microbial products (SMP) into the solution.

Table 6-2 Nitrate and nitrite concentration, total ammonia removal and TCOD/SCOD removal during the six phases of operation.

Phase	Nitrite (mg-N/L)	Nitrate (mg-N/L)	Removal Efficiency	TCOD removal efficiency	SCOD removal efficiency
1B-HN	0.6 ± 0.6	1.8 ± 1.4	$72 \pm 2\%$	-	-
2B-LN	0.8 ± 0.7	1.6 ± 1.4	$94 \pm 1\%$	-	-
3B-SG	0.7 ± 0.9	0.9 ± 0.3	$81 \pm 12\%$	-	-
4C-SGU	0.08 ± 0.06	0.6 ± 0.4	$65 \pm 16\%$	$75 \pm 12\%$	-
5C-WGU	0.02 ± 0.01	0.4 ± 0.1	$64 \pm 14\%$	$75 \pm 8\%$	$64 \pm 14\%$
6C-WGUP	0.02 ± 0.01	0.5 ± 0.1	$74 \pm 8\%$	$93 \pm 5\%$	$89 \pm 7\%$

6.3.2 COD and nitrogen removals using synthetic wastewater

In phase 3B-SG when COD was added as a synthetic wastewater (162 ± 3 mg-COD/L) and GAC particles were used, COD and nitrogen were degraded simultaneously with membrane aeration. The AR of 0.4 ± 0.03 g/m²-d (Fig. 6-2) obtained in phase 3B-SG was similar to that in phase 1B-HN and 2B-LN, despite the addition of the organic matter into the feed solution. Nitrate and nitrate concentrations remained low (<1 mg-N/L) (Fig. D-S3), consistent with phases 1B-HN and 2B-LN. Organic matter was degraded to a low concentration of 25 ± 19 mg-COD/L (Fig. D-S4). However, compared with the nearly linear decrease in ammonia in the first three phases, the COD removal rate decreased over time, with a very rapid initial decrease in COD followed by a slower rate of removal over time.

When the filtration membrane was introduced into the system in phase 4C-SGU, and the AeMFMBR was switched from fed-batch mode to continuous flow operation at an HRT of 20.5 h (4C-SGU1), the average AR increased by 1.5 times to 1.0 ± 0.3 g/m²-d (Fig. 6-2). The TA

concentration inside the AeMFMBR was similar to that in the effluent (Fig. 6-3), indicating the filtration membrane did not impact retention of soluble ammonia. An average of $25 \pm 8\%$ removal of nitrogen was obtained, with effluent TN of 51 ± 1 mg-N/L (Fig. 6-3). In order to increase nitrogen removal, the HRT was increased to 41 h (4C-SGU2), leading to $55 \pm 1\%$ of TA removal, with an effluent TA of 37 ± 1 mg-N/L. The ARs obtained in 4C-SGU at the two different HRTs (1.0 ± 0.4 g/m²-d at 20.5 h, and 1.1 ± 0.2 g-N/m²-d at 41 h) were not significantly different (T-test, $p = 0.6$), indicating that the AR was not dependent on the HRT.

There was no significant increase in COD removal efficiency (T-test, $p = 0.4$) when the HRT was increased in phase 4C-SGU from 20.5 h ($77 \pm 12\%$) to 41 h ($70 \pm 11\%$). The average effluent TCOD was 39 ± 19 mg/L, which would be below the standard discharge standard for BOD₅ of 30 mg/L assuming a typical ratio of 2:1 COD:BOD₅ ratio (23).

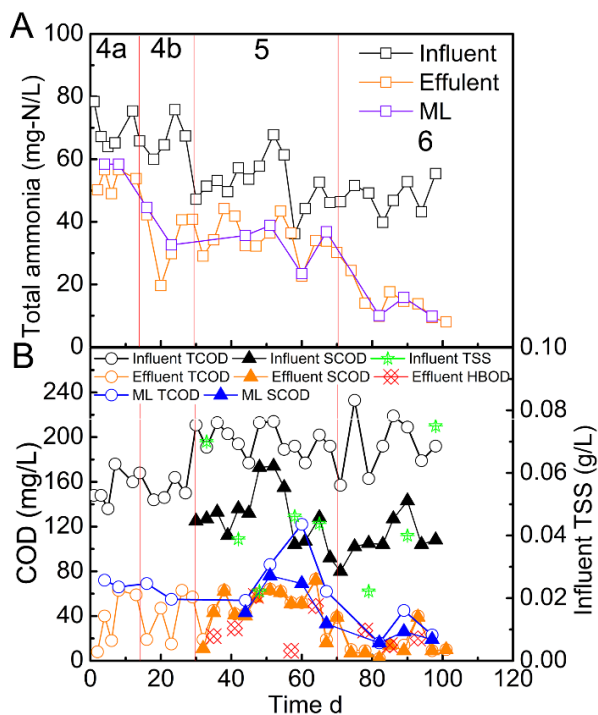


Fig. 6-3 (A) Total ammonia (TA) concentration of the influent, effluent, and the mixed liquor during continuous mode operation (phase 4C-SGU, 5C-WGU and 6C-WGUP); (B) TCOD,

SCOD, HBOD, and TSS of the influent, effluent and the mixed liquor. Two different HRTs were used in phase 4C-SGU with 4a (20.5 h) and 4b (41 h).

6.3.3 COD and nitrogen removal using diluted domestic wastewater

When domestic wastewater was treated instead of the synthetic wastewater in phase 5C-WGU, the AR was reduced by 40% to 0.6 ± 0.2 g/m²-d (Fig. 6-2). The difference was likely due to the form of nitrogen, which was only NH₄HCO₃ in phases 1B-HN to 4C-SGU, but a mixture of organic nitrogen and this ammonium salt (~40%) in 5C-WGU. In addition, domestic wastewater may contain inhibitors for nitrifying bacteria. The overall nitrogen removal was $33 \pm 9\%$, with an effluent TA concentration of 36 ± 5 mg-N/L (Fig. 6-3). Only small concentrations of nitrate (0.02 ± 0.01 mg-N/L) and nitrite (0.4 ± 0.1 mg-N/L) were measured in the treated effluent.

When the aeration pressure in phase 6C-WGUP was increased from 2 to 4-5 kPa, the AR (1.2 ± 0.2 g/m²-d, Fig. 6-2) was twice that obtained in 5C-WGU (0.6 ± 0.2 g-N/m²-d, T-test, $p = 0.002$). A lower effluent TA of 12 ± 3 mg-N/L (Fig. 6-3) was obtained, with a TA removal efficiency of $74 \pm 8\%$ that was significantly higher than that in 5C-WGU (T-test, $p < 0.001$). The effluent nitrate (0.02 ± 0.01 mg-N/L) and nitrite (0.4 ± 0.1 mg-N/L) concentrations remained low and were not significantly different from those in 5C-WGU (T-test, $p > 0.4$), indicating the ammonia oxidation was still the limiting step for nitrification in 6-DWHA/C. The TA concentration inside the AeMFMBR was similar to that in the effluent in both phases 5C-WGU and 6C-WGUP (Fig. 6-3), while the nitrate and nitrite concentration inside the AeMFMBR were slightly higher than those in the effluent (Fig. D-S5).

COD was effectively degraded, with an effluent TCOD of 49 ± 16 mg/L and SCOD of 47 ± 17 mg/L in phase 5C-WGU (Fig. 6-3), resulting in removal efficiency of $75 \pm 8\%$ for TCOD and $64 \pm 14\%$ for SCOD. In phase 6C-WGUP with the higher aeration rate, COD removal was further improved with an effluent TCOD of 14 ± 11 mg/L and SCOD of 13 ± 11 mg/L, indicating

that the increase in air flux enhanced both COD removal and nitrogen removal. The removal efficiencies reached $93 \pm 5\%$ for TCOD, and $89 \pm 7\%$ based on SCOD in 6C-WGUP (Table 6-2). The similar effluent TCOD and SCOD in 5C-WGU and 6C-WGUP (Fig. 6-3) indicated good solids removal with the filtration membrane. This was further confirmed by TSS tests, where no TSS were detected in the effluent, with influent TSS of diluted domestic wastewater ranging from 20 mg/L to 80 mg/L (Fig. 6-3).

6.3.4 Transmembrane pressure, DO and dissolved methane

Membrane fouling was well mitigated in the AeMFMBR by using fluidized GAC particles, with a maximum TMP of 3 kPa (Fig. 6-4) during continuous-mode of operation. There was a decrease in TMP in phase 4C-SGU with a longer HRT, indicating that a longer HRT reduced fouling due to the decreased flux. This result was consistent with a previous study where shorter HRTs led to larger membrane fouling (24).

In phase 5C-WGU when the synthetic wastewater was switched to actual wastewater, the TMP was still low (0.4 ± 0.3 kPa). However, the TMP increased to 1.1 ± 0.4 kPa when air flowrate was doubled in phase 6C-WGUP. The MLSS of the AeMFMBR in 6C-WGUP (70 ± 3 mg-TSS/L) (Fig. 6-3) was significantly higher than that in 5C-WGU (30 ± 10 mg-TSS/L) (T-test, $p = 0.01$). The increase in MLSS could help explain the increase in TMP in 6C-WGUP. The TCOD and SCOD inside the reactor were higher than those in the effluent (Fig. 6-3), suggesting that a cake layer formed on the filtration membrane that could have contributed to the removal of COD, as suggested by others (18,25).

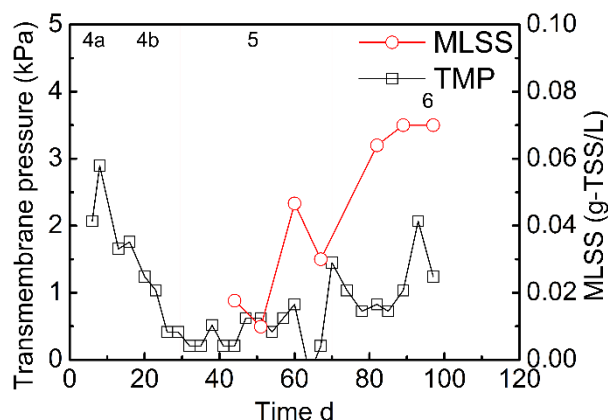


Fig. 6-4 Transmembrane pressure and mixed liquor suspended solids in phase 4C-SGU, 5C-WGU and 6C-WGUP. Two different HRTs were used in phase 4C-SGU with 4a (20.5 h) and 4b (41 h).

There was no measurable DO (0 mg/L) in the AeMFMBR during continuous mode operation period, indicating the fluid environment in the AeMFMBR was anaerobic. Although the DO in the mixed liquor of the AeMFMBR remained zero (i.e. anaerobic conditions), dissolved methane was never detected in either the mixed liquor or effluent samples possibly because methanogenic archaea (relative abundance <0.01%) were not enriched in the system. This result is different from that obtained in a previous AFMBR study where a COD to methane conversion of 10% resulted in a dissolved methane concentration of 1.5 mL/L (3).

The OTE during continuous flow mode operation was calculated using Eq. 6-1 and the calculated ammonia flux and air flow to be high, with $82 \pm 16\%$ for phase 5C-WGU, and $74 \pm 9\%$ for 6C-WGUP when treating diluted domestic wastewater. These high OTEs indicated that most of the oxygen was consumed for nitrogen removal even with the introduction of organic matter. The rest of the oxygen in the air supply was believed to be consumed by heterotrophs on the membrane aerator surface, since the DO was maintained near zero.

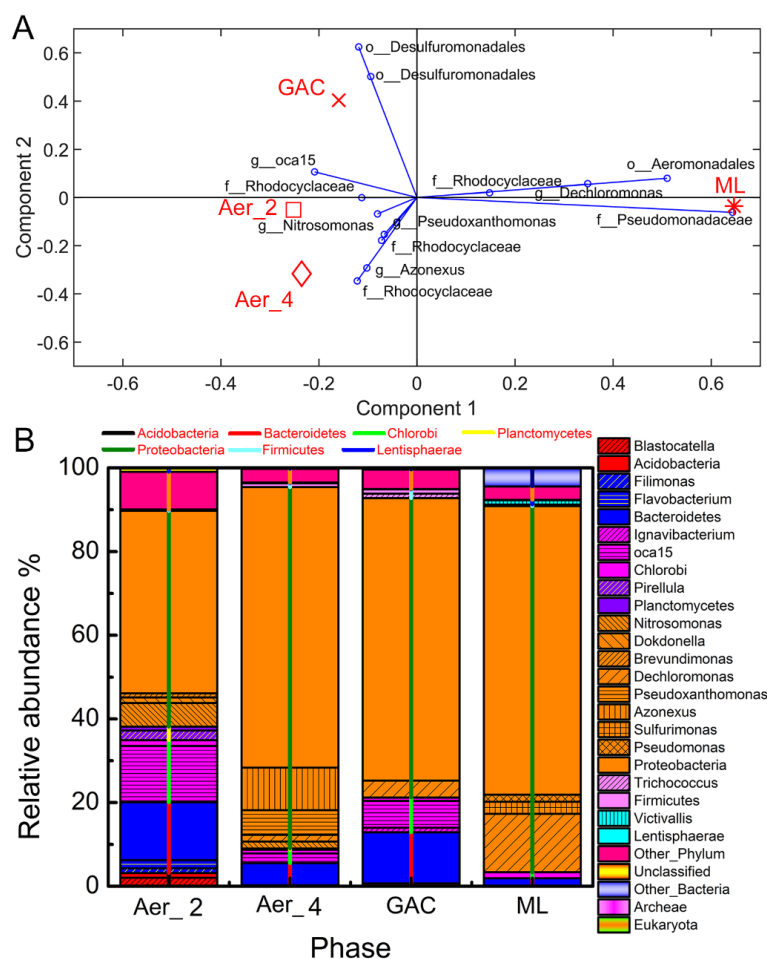


Fig. 6-5 Community analysis of membrane aerator in phase 2B-LN (Aer_2) and GAC, mixed liquor (ML), and the membrane aerator in phase 4C-SGU (Aer_4). (A) Principal component analysis based on OTUs relative abundance. Microbial community presented with first two principal components with OTUs relative abundance >5% shown as the axes. The axes pointing at the sample indicates the high relative abundance; (B) microbial community analysis based on the relative abundance on the genus level. Only the genera with a relative abundance higher than 1% were shown (with pattern), while the other genera were included based on phylum level (pure color and vertical lines). Archaea (<0.01%) and Eukaryota were shown at the Kingdom level.

6.3.5 Microbial community analyses

The microbial community samples formed four distinct groups as they did not cluster with each other based on a PCA analysis (Fig. 6-5A). The BCS of the membrane aerator samples in phases 2B-LN and 4C-SGU was 46%, indicating the community changed after organics were introduced. The BCS between the membrane aerator and GAC in 4C-SGU was 57%, higher than that between membrane aerator and the mixed liquor (37%).

In phase 2B-LN, the ammonia removal for membrane aerators treating COD-free synthetic wastewater was likely due to biological nitrification and denitrification, based on the microbial community analysis of the membrane aerator. *Nitrosomonas* (6%) was one of the dominant genera (Fig. 6-5B) on the membrane aerator in phase 2B-LN. Members of this genus are commonly found in activated sludge process (26,27), and were reported to be present in the biofilm on membrane aerator in other several studies (7,28) as the AOB converting ammonia to nitrite. In addition, OTU_28 was shown to have a relative abundance of 6% (*Rhodocyclaceae* family), with 96% sequence similarity to *Dechloromonas denitrificans* which was reported as denitrifying bacteria (28). No anammox genera were found on the membrane aerator sample.

The microbial community of membrane aerator in phase 4C-SGU with synthetic wastewater changed compared with that in phase 2-LN/B with no COD in the feed, although ammonia removal was still occurring by nitrification and denitrification. The *Rhodocyclaceae* became the dominant biofilm family (47%) on the membrane aerator when the organics were introduced. Within the *Rhodocyclaceae* family, *Azonexus* (10%) (Fig. 6-5B) was the dominant genus, which includes denitrifying bacteria species such as *Azonexus caeni* (29) and *Azonexus hydrophilus* (30). *Nitrosomonas* were also dominant on membrane aerator in 4C-SGU (2%). In contrast, members of the genus *Nitrosomonas* were not detected in the mixed liquor and were present at very low relative abundance (0.2%) on GAC. The family of *Comamonadaceae*, whose

members were reported as denitrifying bacteria (31), also had a high relative abundance of 6%. In addition, *Pseudoxanthomonas* was shown to have a high relative abundance of 6%, and bacteria in this genus have been reported to stabilize the sludge structure in a sequencing batch reactor achieving partial nitrification (32).

Both the mixed liquor and GAC probably also contributed to denitrification, indicated by the high relative abundance of the denitrifying genus *Dechloromonas* on the GAC (5%) and in the mixed liquor (14%) samples (Fig. 6-5B) (28,33). Other than *Dechloromonas*, other OTUs belonging to the *Rhodocyclaceae* family were found with a high relative abundance of 11% in GAC and 12% in ML. Obligate or facultative anaerobes, such as *Geobacter metallireducens* (OTU_19, similarity of 99%) (34), *Geobacter hydrogenophilus* (OTU_136, similarity of 99%) (35) and *Aeromonas rivipollensis* (OTU_17, similarity of 99%) (36), were shown to have a significant relative abundance (>13%) on the GAC and mixed liquor samples, indicating an anoxic environment was maintained in the AeMFMBR, consistent with the result of the DO measurements.

The genus *Oca15* belonging to the order *Ignavibacteriales* was found to colonize with a relatively high abundance the membrane aerator in phase 2B-LN (14%) and 4C-SGU (2%) tests, and the GAC in phase 4C-SGU (6%). *Oca15* was previously found in a wastewater treatment plant treating textile wastewater (37), but it has not been well studied. The colonization of *Oca15* on the growth media was quite interesting and could be worth investigating in a future study.

6.3.6 Overall assessment and future studies

Based on the microbial community analysis, ammonia removal was most likely due to biological nitrification and denitrification. The lack of any dissolved oxygen or methane, or visible gas bubbles, suggests that air stripping was not a factor in ammonia removal in the AeMFMBR. In order to rule out the effect of air stripping for ammonia removal, an abiotic test

was conducted using membrane aerators to strip an ammonium bicarbonate solution (80 mg-N/L). No noticeable ammonia removal was shown during the first 20-day stripping (bubbleless addition of the air) (Fig. D-S6). In addition, there was no decrease in TN even when sparging tests were conducted with a gas diffuser using air.

Although the HRT of the AeMFMBR was shorter than those reported in some other MABR tests (several days using air) (7,8,12,14), and comparable with a hybrid systems combining anaerobic baffled reactor with membrane aerator (40 h) (28), the HRT was still a little too long to be feasible as a post-treatment technique. According to the COD and nitrogen removal in the AeMFMBR, it is indicated that the nitrogen removal had a slower rate than COD removal. The slow nitrogen removal rate was likely due to the low lumen pressure applied in this study for maintaining an anaerobic environment for mixed liquor, supported by the DO measurement and microbial community analysis. In order to reduce the HRT, increased lumen pressure or larger surface area should be used in future tests to increase the rates of nitrification using membrane aerators. In these future studies, a balance could be found between maintaining an anaerobic environment and applied lumen pressure to maximize the AR.

6.4 Conclusions

The operation of the AeMFMBR at an HRT of 41 h produced a good effluent quality with a TN of 12 ± 3 mg-N/L and COD of 14 ± 1 mg/L, and non-detectable dissolved oxygen or methane. Nitrate and nitrite concentrations in the effluent were <1 mg-N/L. High removal efficiencies were obtained for both COD ($93 \pm 5\%$) and ammonia ($74 \pm 8\%$). Membrane fouling was well mitigated with a TMP <3 kPa. Analysis of the microbial communities supported a mechanism of ammonia removal in the AeMFMBR based on nitrification and denitrification in the presence or absence of added COD.

6.5 References

1. Kim J, Kim K, Ye H, Lee E, Shin C, McCarty PL, et al. Anaerobic fluidized bed membrane bioreactor for wastewater treatment. *Environ Sci Technol*. 2011 Jan 15;45(2):576–81.
2. Liao B-Q, Kraemer JT, Bagley DM. Anaerobic membrane bioreactors: applications and research directions. *Crit Rev Environ Sci Technol*. 2006;36(6):489–530.
3. Ren L, Ahn Y, Logan BE. A two-stage microbial fuel cell and anaerobic fluidized bed membrane bioreactor (MFC-AFMBR) system for effective domestic wastewater treatment. *Environ Sci Technol*. 2014;48(7):4199–206.
4. Lee R, McCarty PL, Bae J, Kim J. Anaerobic fluidized membrane bioreactor polishing of baffled reactor effluent during treatment of dilute wastewater. *J Chem Technol Biotechnol*. 2015;90(3):391–7.
5. Dutta K, Lee MY, Lai WWP, Lee CH, Lin AYC, Lin CF, et al. Removal of pharmaceuticals and organic matter from municipal wastewater using two-stage anaerobic fluidized membrane bioreactor. *Bioresour Technol*. 2014;165(C):42–9.
6. Yoo R, Kim J, McCarty PL, Bae J. Anaerobic treatment of municipal wastewater with a staged anaerobic fluidized membrane bioreactor (SAF-MBR) system. *Bioresour Technol*. 2012;120:133–9.
7. Gilmore KR, Terada A, Smets BF, Love NG, Garland JL. Autotrophic nitrogen removal in a membrane-aerated biofilm reactor under continuous aeration: a demonstration. *Environ Eng Sci*. 2013;30(1):38–45.
8. Terada A, Hibiya K, Nagai J, Tsuneda S, Hirata A. Nitrogen removal characteristics and biofilm analysis of a membrane-aerated biofilm reactor applicable to high-strength nitrogenous wastewater treatment. *J Biosci Bioeng*. 2003;95(2):170–8.

9. Casey E, Glennon B, Hamer G. Review of membrane aerated biofilm reactors. *Resour Conserv Recycl.* 1999;27(1–2):203–15.
10. Casey E, Glennon B, Hamer G. Oxygen mass transfer characteristics in a membrane-aerated biofilm reactor. *Biotechnol Bioeng.* 1999;62(2):183–92.
11. Hirasa O, Ichijo H, Yamauchi A. Preparation of new support for immobilization of activated sludges. *J Ferment Bioeng.* 1991;71(5):376–8.
12. Smith DP, Rector T, Reid-Black K, Hummerick M, Strayer R, Birmele M, et al. Redox control bioreactor: A unique biological water processor. *Biotechnol Bioeng.* 2008;99(4):830–45.
13. Hibiya K, Terada A, Tsuneda S, Hirata A. Simultaneous nitrification and denitrification by controlling vertical and horizontal microenvironment in a membrane-aerated biofilm reactor. *J Biotechnol.* 2003;100(1):23–32.
14. Gilmore KR, Little JC, Smets BF, Love NG. Oxygen transfer model for a flow-through hollow-fiber membrane biofilm reactor. *J Environ Eng.* 2009;135(9):806–14.
15. Pankhania M, Stephenson T, Semmens MJ. Hollow fibre bioreactor for wastewater treatment using bubbleless membrane aeration. *Water Res.* 1994;28(10):2233–6.
16. Brindle K, Stephenson T, Semmens MJ. Nitrification and oxygen utilisation in a membrane aeration bioreactor. *J Memb Sci.* 1998;144:197–209.
17. Logan BE, Patnaik R. A gas chromatographic-based headspace biochemical oxygen demand test. *Water Environ Res.* 1997;69(2):206–14.
18. Ye Y, LaBarge N, Kashima H, Kim K-Y, Hong P-Y, Saikaly PE, et al. An aerated and fluidized bed membrane bioreactor for effective wastewater treatment with low membrane fouling. *Environ Sci Water Res Technol.* 2016;2(6):994–1003.

19. Caporaso JG, Kuczynski J, Stombaugh J, Bittinger K, Bushman FD, Costello EK, et al. QIIME allows analysis of high-throughput community sequencing data. *Nat Methods*. 2010;7(5):335–6.
20. McIlroy SJ, Kirkegaard RH, McIlroy B, Nierychlo M, Kristensen JM, Karst SM, et al. MiDAS 2.0: an ecosystem-specific taxonomy and online database for the organisms of wastewater treatment systems expanded for anaerobic digester groups. *Database*. 2017;2017(1).
21. Semmens MJ, Dahm K, Shanahan J, Christianson A. COD and nitrogen removal by biofilms growing on gas permeable membranes. *Water Res*. 2003;37(18):4343–50.
22. Rezania B, Oleszkiewicz JA, Cicek N. Hydrogen-dependent denitrification of water in an anaerobic submerged membrane bioreactor coupled with a novel hydrogen delivery system. *Water Res*. 2007;41(5):1074–80.
23. Hays S, Zhang F, Logan BE. Performance of two different types of anodes in membrane electrode assembly microbial fuel cells for power generation from domestic wastewater. *J Power Sources*. 2011;196(20):8293–300.
24. Huang Z, Ong SL, Ng HY. Submerged anaerobic membrane bioreactor for low-strength wastewater treatment: effect of HRT and SRT on treatment performance and membrane fouling. *Water Res*. 2011;45(2):705–13.
25. Smith AL, Stadler LB, Love NG, Skerlos SJ, Raskin L. Perspectives on anaerobic membrane bioreactor treatment of domestic wastewater: A critical review. *Bioresour Technol*. 2012;122:149–59.
26. Wagner M, Loy A, Nogueira R, Purkhold U, Lee N, Daims H. Microbial community composition and function in wastewater treatment plants. *Antonie Van Leeuwenhoek*. 2002;81(1–4):665–80.

27. Zhang T, Shao M-F, Ye L. 454 Pyrosequencing reveals bacterial diversity of activated sludge from 14 sewage treatment plants. *ISME J.* 2012;6(6):1137–47.
28. Hu S, Yang F, Liu S, Yu L. The development of a novel hybrid aerating membrane-anaerobic baffled reactor for the simultaneous nitrogen and organic carbon removal from wastewater. *Water Res.* 2009;43(2):381–8.
29. Quan Z-X, Im W-T, Lee S-T. *Azonexus caeni* sp. nov., a denitrifying bacterium isolated from sludge of a wastewater treatment plant. *Int J Syst Evol Microbiol.* 2006;56(5):1043–6.
30. Chou J-H, Jiang S-R, Cho J-C, Song J, Lin M-C, Chen W-M. *Azonexus hydrophilus* sp. nov., a *nifH* gene-harboring bacterium isolated from freshwater. *Int J Syst Evol Microbiol.* 2008;58(4):946–51.
31. Adav SS, Lee D-J, Lai J-Y. Microbial community of acetate utilizing denitrifiers in aerobic granules. *Appl Microbiol Biotechnol.* 2010;85(3):753–62.
32. Wan C, Sun S, Lee DJ, Liu X, Wang L, Yang X, et al. Partial nitrification using aerobic granules in continuous-flow reactor: Rapid startup. *Bioresour Technol.* 2013;142:517–22.
33. Tago K, Ishii S, Nishizawa T, Otsuka S, Senoo K. Phylogenetic and functional diversity of denitrifying bacteria isolated from various rice paddy and rice-soybean rotation fields. *Microbes Environ.* 2011;26(1):30–5.
34. Schleinitz KM, Schmeling S, Jehmlich N, von Bergen M, Harms H, Kleinstaubler S, et al. Phenol degradation in the strictly anaerobic iron-reducing bacterium *Geobacter metallireducens* GS-15. *Appl Environ Microbiol.* 2009;75(12):3912–9.
35. Kerin EJ, Gilmour CC, Roden E, Suzuki MT, Coates JD, Mason RP. Mercury methylation by dissimilatory iron-reducing bacteria. *Appl Environ Microbiol.* 2006;72(12):7919–21.
36. Marti E, Balcázar JL. *Aeromonas rivipollensis* sp. nov., a novel species isolated from aquatic samples. *J Basic Microbiol.* 2015;55(12):1435–9.

37. Meerbergen K, Van Geel M, Waud M, Willems KA, Dewil R, Van Impe J, et al.
Assessing the composition of microbial communities in textile wastewater treatment plants in comparison with municipal wastewater treatment plants. *Microbiologyopen*. 2017;6(1).

Chapter 7

Future studies

In this dissertation, I examined the use of buffer in MFC/MEC and the use of membrane bioreactor as the post-treatment for MFC effluent. I evaluated the effect of buffer charge on the air cathode performance in MFC, showing that the cationic buffer can enhance the cathodic current by improved transport with migration (Chapter 3). An innovative polymer buffer was developed with higher buffer capacity than the conventional buffer (50 mM PBS), resulting in a higher hydrogen production rate than that with PBS and a good buffer retention with the use of CEM, AEM and UFM (Chapter 4). In addition, the post-treatment of MFC effluent was assessed by comparing AOFMBR, AFMBR and MBR treating diluted domestic wastewater, concluding that AOFMBR had a better treatment performance in terms of COD removal under high influent COD (~300 mg/L) and membrane fouling control (Chapter 5). Integrating AFMBR and membrane aerator as AeMFMBR achieved simultaneous COD and nitrogen removal with low effluent COD and total ammonia (Chapter 6). Although those aspects in use of buffer in MFC/MEC and membrane bioreactor for post-treatment have been addressed, future studies will be required to optimize the buffer and post-treatment of MFC/MEC.

1. The effect of buffer charge needs to be investigated in MFCs or MECs and simulated with a time-dependent model. The Nernst-Planck equation and my results in Chapter 3 suggested that the use of a cationic buffer in the catholyte could increase cathode

- performance by enhanced buffer transport, but the extent of this influence needs to be investigated. In addition, the buffer transport in the catholyte correlates with pH, species concentration, concentration gradient, buffer charge and electric field, which tend to change over the operation cycle. Therefore, a time-dependent model simulating the ion transport is worth being developed to quantitatively analyze the effect of buffer charge on cathode performance.
2. An inexpensive approach for buffer capacity regeneration needs to be developed for the MEC catholyte. The MEC catholyte pH tends to increase during operation due to the production of hydroxide ion by HER, which reduces the potential for hydrogen production according to Nernst equation. The replacement of catholyte buffer is required to achieve stable hydrogen production. Therefore, a cheap approach for buffer capacity regeneration would be helpful to reduce the cost of buffer replacement.
 3. The AOFMBR needs to be improved by reducing the energy needed for aeration. The AOFMBR achieved better COD removal and had less membrane fouling than the AFMBR, but the energy cost was 4 times as high energy as the AFMBR. An optimization of the AOFMBR aeration process to reduce energy cost while maintaining similar performance is worth exploring.
 4. GAC scouring with a different driving forces (rising air bubbles and recirculation) needs to be examined to investigate their similar or different contributions to membrane fouling control. The interaction between the scouring media and membrane is likely quite

- complicated. A future study focusing on the scouring effect with gas fluidization as the driving force could contribute to a better understanding of mechanisms for membrane fouling mitigation.
5. Optimization of AeMFMBR will be needed to reduce its HRT by shrinking the reactor size and adjusting aeration while remaining low DO. Good COD and total ammonia removal were simultaneously accomplished by an AeMFMBR, but it required a relatively long HRT of 42 h. A significant reduction in HRT is required for this to be competitive with other approaches. A reduction could likely to be achieved by increasing the specific membrane surface area (membrane area per reactor volume) and aeration rate (gas pressure could be increased),

Appendix A

Effect of buffer charge on performance of air-cathodes used in microbial fuel cells

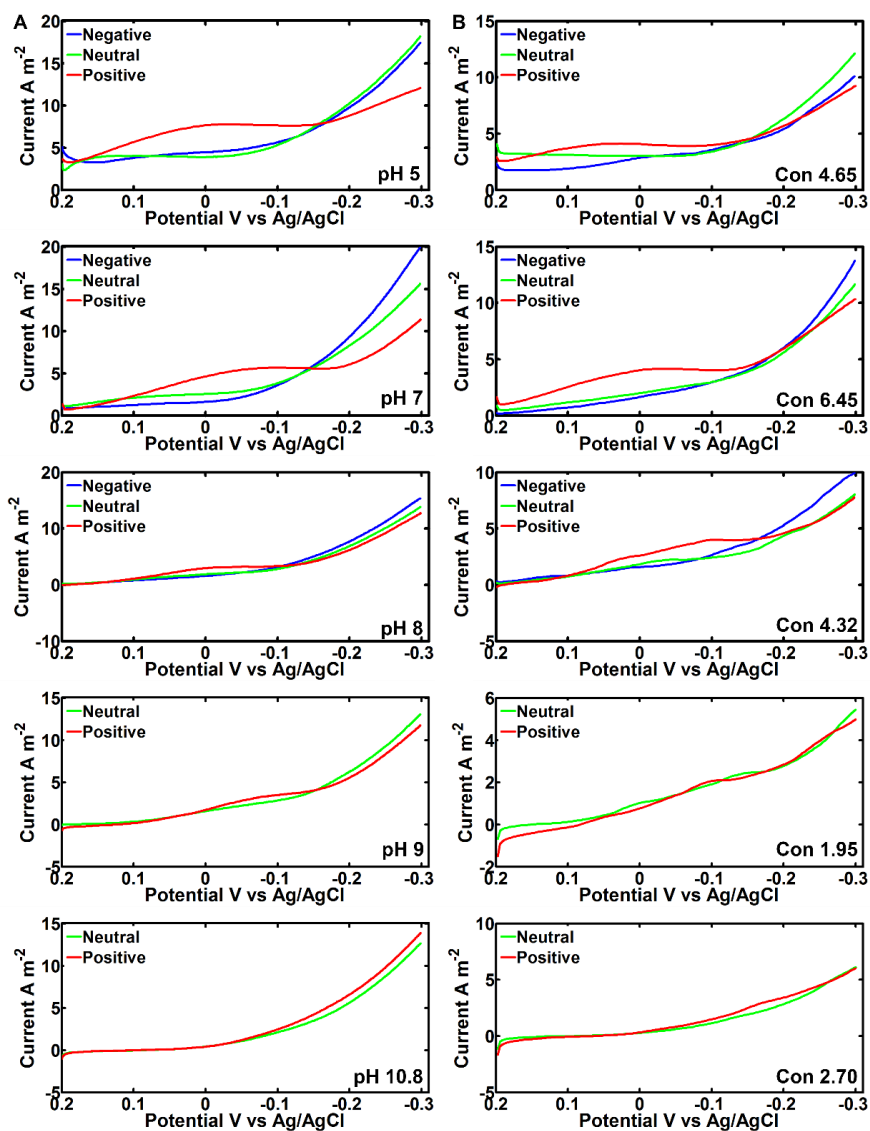


Fig. A-S1 LSVs for buffers of three groups with pKa and pH 5, 7, 8, 9, 10.8. The conductivity of the buffer solution is A. 7 mS/cm, B. LC (at the lower right corner)

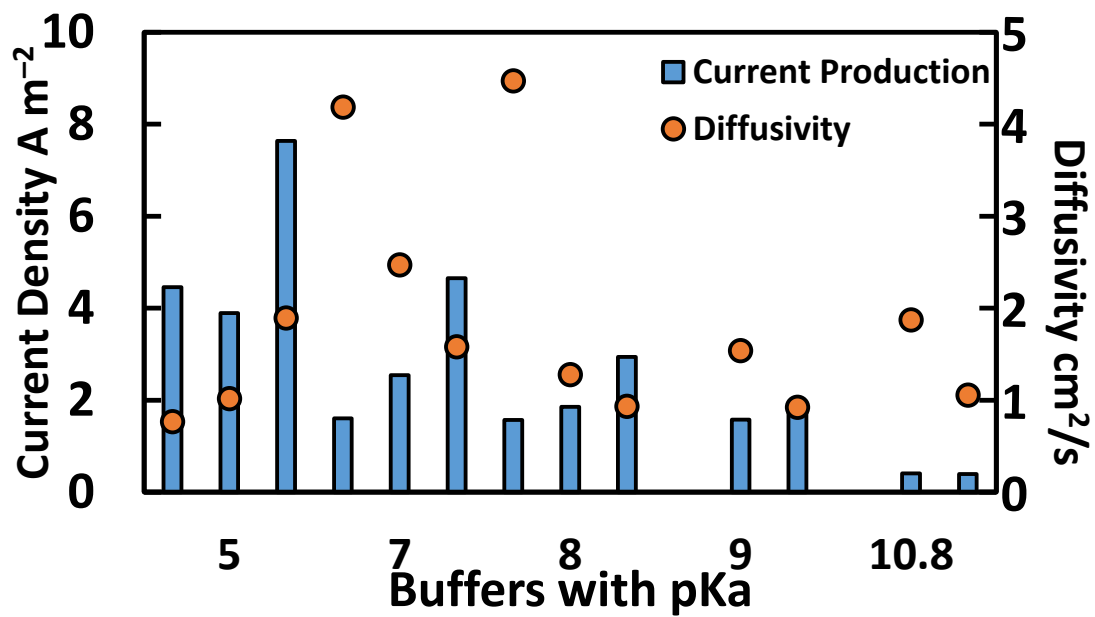


Fig. A-S2 The relationship between diffusivity and cathodic current

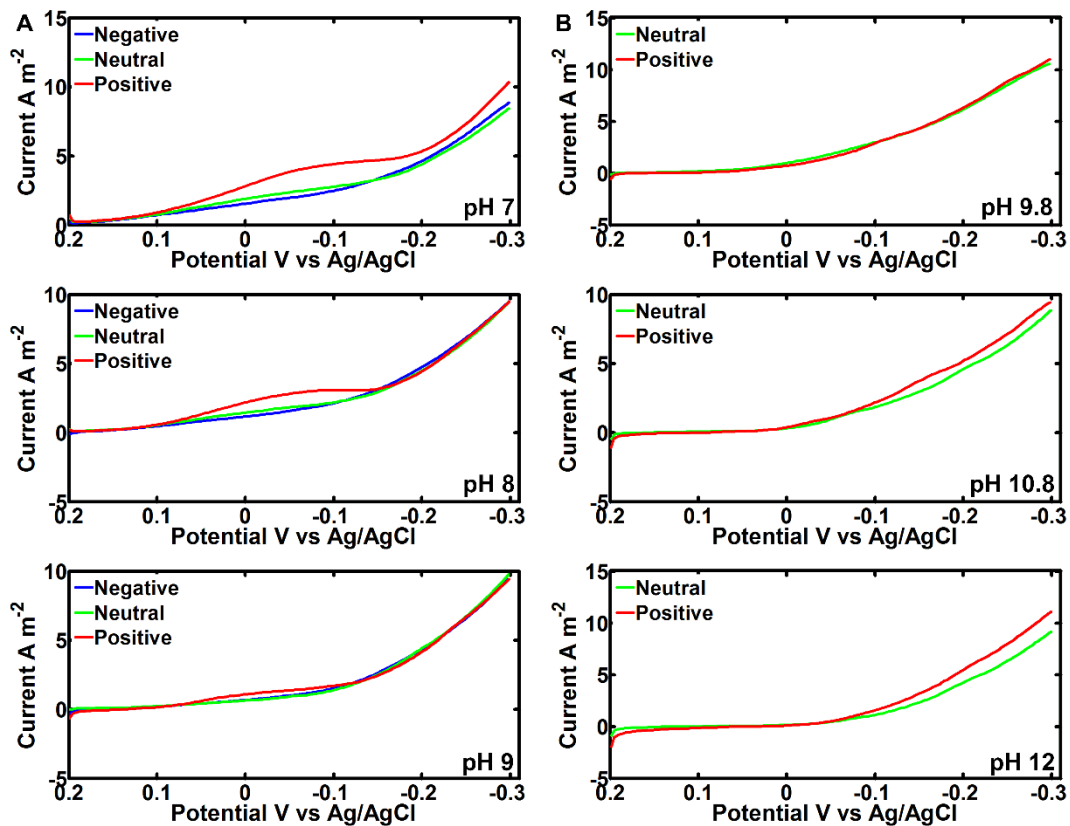


Fig. A-S3 LSVs for cathode buffered by buffers with A. pKa 8, pH adjusting to 7, 8, and 9, and conductivity of 5.5 mS/cm; B. pKa 10.8, pH adjusting to 9.8, 10.8 and 12, and conductivity of 4.9 mS/cm.

Appendix B

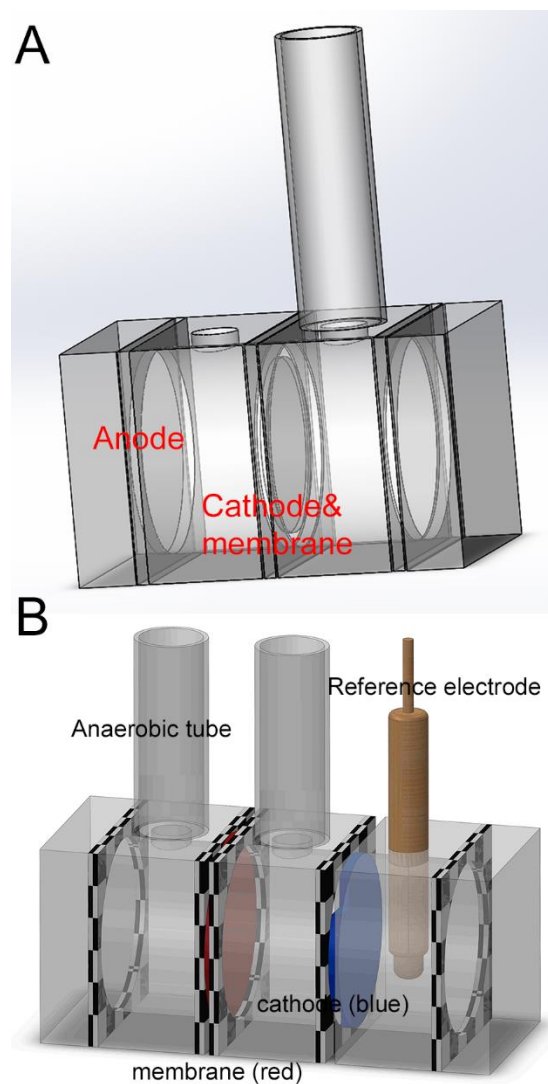
The importance of OH^- transport through anion exchange membrane in microbial electrolysis cells

Fig. B-S1 (A) the structure for MEC (4 cm wide) with 2 cm electrode spacing, resulting in anode and cathode volume of 13 mL; (B) electrochemical half cells with anode chamber of 13 mL and cathode chamber of 26 mL. The cathode was incised to ventilate produced hydrogen gas from reference electrode chamber to the chamber with anaerobic tube for gas sample collection.

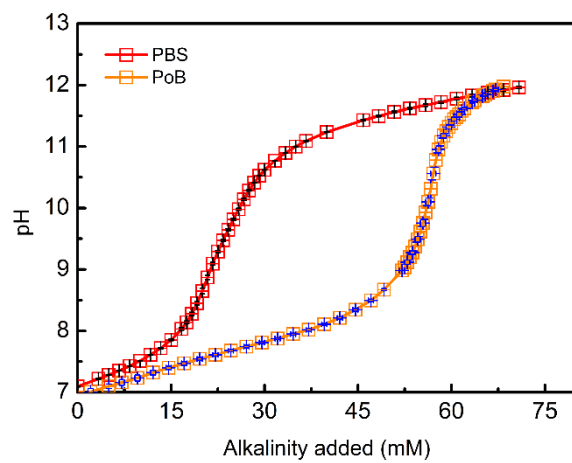


Fig. B-S2 Titration curves showing the buffer capacities of the PBS and PoB solutions.

Details for MW distribution test of the polymer buffer

The MW distribution test was carried out using the protocol below (*Bruce E. Logan, Environmental Transport Process, John Wiley & Sons, 2012, p.71*):

1. The concentration of the original polymer buffer solution was tested as C_0 . The total volume was V_0 .

2. Permeate was collected from the ultrafiltration cell with different ultrafiltration membranes with cut-off of 2 K, 10 K, 30 K and 100 K. The volume and its TOC concentration was monitored. A set of volume and TOC can be obtained as V_1, V_2, V_3, \dots (L) and the corresponding TOC concentration of C_1, C_2, C_3, \dots (mg L^{-1})

3. The cumulative mass of TOC can be calculated using the volumes and the TOC concentration as:

$$M_i = \sum_1^i V_i C_i \quad (\text{B-1})$$

4. The cumulative volume of permeate can be calculated as:

$$V_{a,i} = \sum_1^i V_i \quad (\text{B-2})$$

5. The TOC concentration could pass through the ultrafiltration $C_{r,0}$ can be obtained by non-linear fitting using cumulative masses and volumes:

$$M_i = \frac{C_{r,0}}{V_0^{P_c-1}} [V_0^{P_c} - (V_0 - V_f)^{P_c}] \quad (\text{B-3})$$

where $C_{r,0}$ is the original concentration that can pass through the membrane, P_c is filtration coefficient, and V_f is the filtrate volume.

6. The percentage of the chemicals has MW smaller than the membrane pore size is:

$$p_{smaller} = \frac{C_{r,0}}{C_0} \times 100\% \quad (\text{B-4})$$

7. The percentage of the chemicals has MW larger than the membrane pore size is:

$$p_{larger} = \left(1 - \frac{C_{r,0}}{C_0}\right) \times 100\% \quad (\text{B-5})$$

8. With a set of membranes with different cut off, the distribution can be obtained.

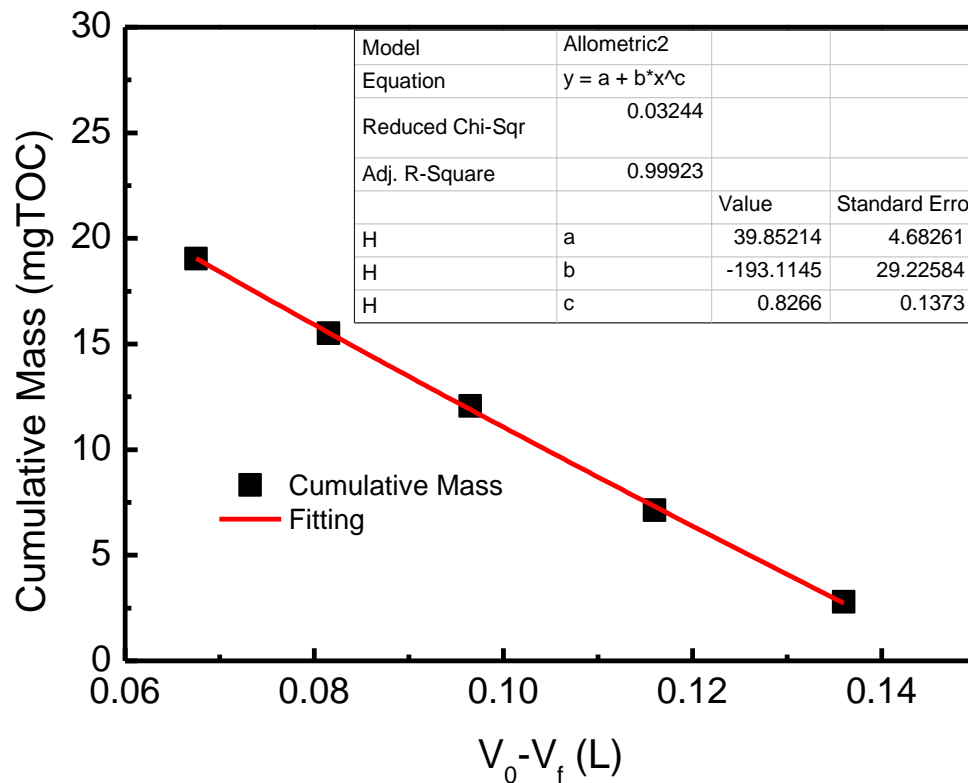
An example of 100 K membrane:

$V_0=151$ mL, $C_0=260$ mg/L, $V_0=151$ mL

Filtrate volume, V_f (mL)	TOC (mg/L)	Cumulative mass (mg)
15	186	2.8

30	217	7.1
49.5	253	12.1
64.5	229	15.5
78.5	252	19.0

The data were plotted using Cumulative mass vs. $(V_0 - V_f)$, and then fitted using non-linear fitting method, Allometric2, in the Origin 8.5 pro.



The P_c and $C_{r,0}$ obtained from fitting:

$$C_{r,0} = 268 \text{ mg/L}$$

$$P_c = 0.83$$

The percentage (<100 KDa) is:

$$p_{smaller} = \frac{C_{r,0}}{C_0} \times 100\% = 100\%$$

Appendix C

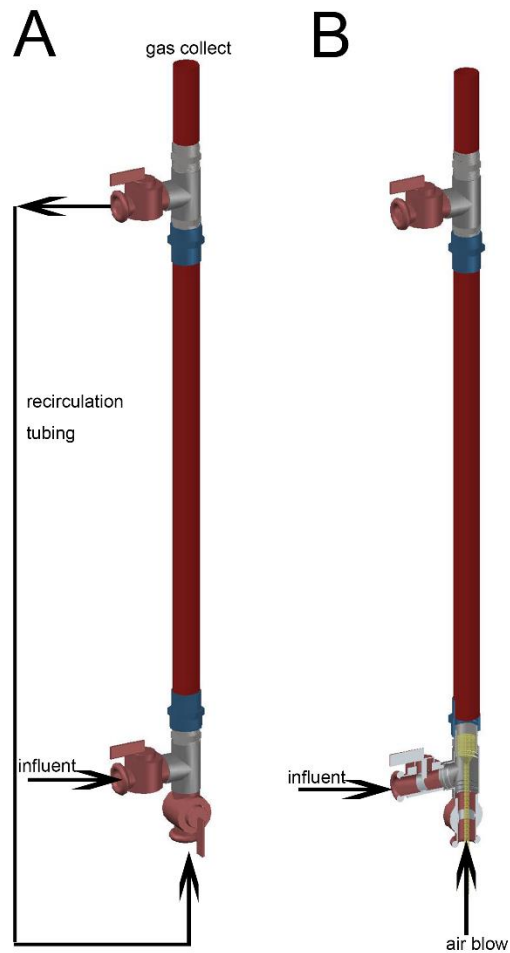
An aerated and fluidized bed membrane bioreactor for effective wastewater treatment with low membrane fouling

Fig. C-S1 Reactor configuration A. AFMBR, B. AOFMBR and AeMBR. AeMBR and AOFMBR had the same reactor configuration except no GAC was added into AeMBR

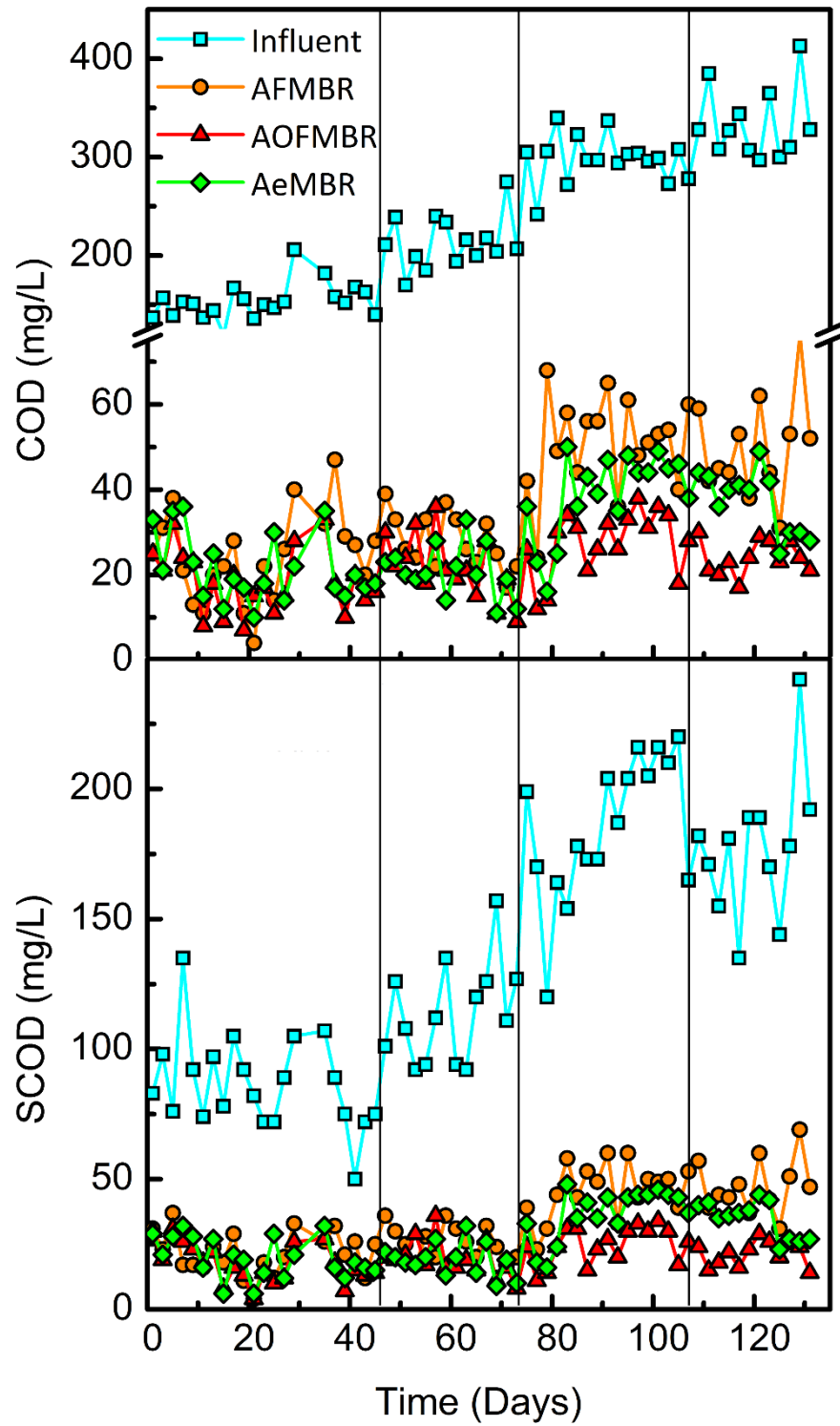


Fig. C-S2 The effluent COD and SCOD over time

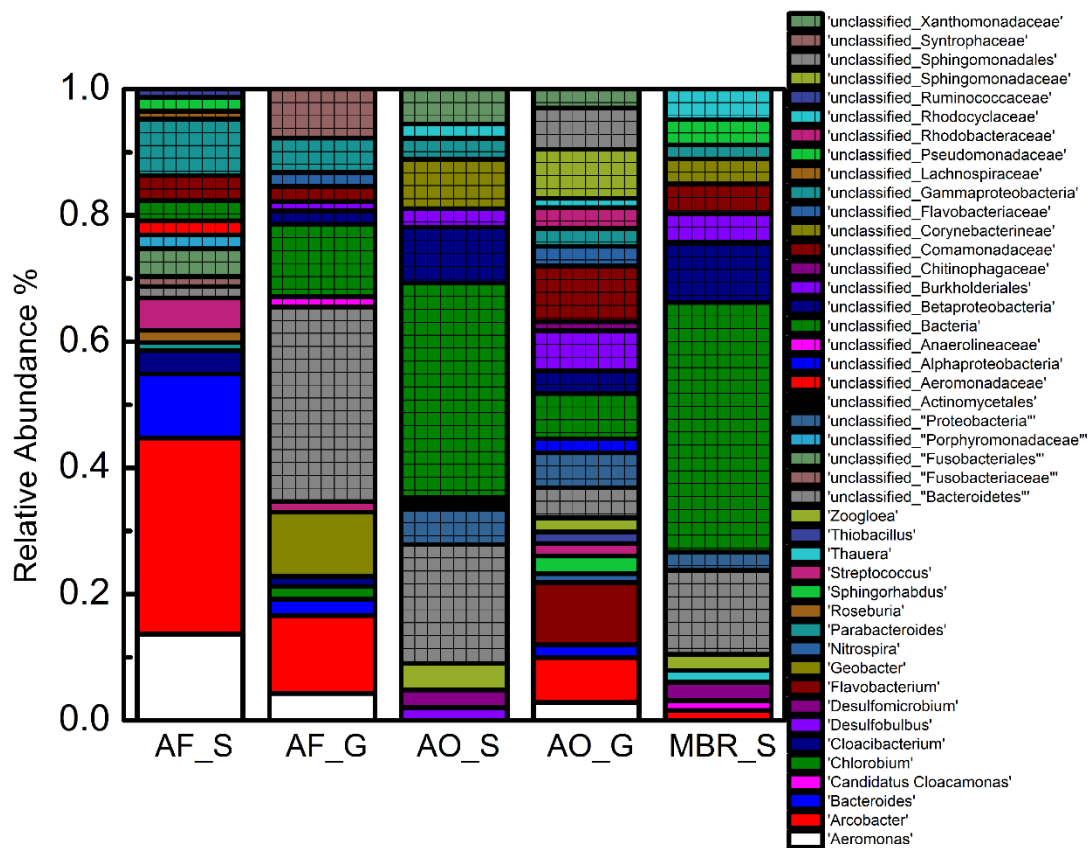


Fig. C-S3 Analysis of the microbial communities in the solution (S) and on the GAC (G) in the AOFMBR (AO), AFMBR (AF) and AeMBR (MBR) reactors based on relative abundance at the genus level (removing genera at <1% abundance)

Energy calculations for the AFMBR and AOFMBR

The energy used by the AFMBR was estimated as described previously [182], except as noted below:

1. Influent pumping energy

The head increase due to the influent pumping is

$$H_L = h + \frac{v^2}{2g} = h + \frac{\left(\frac{Q}{A}\right)^2}{2g} = (0.5 \text{ m}) + \frac{\left(\frac{\left(\frac{0.85 \frac{\text{cm}^3}{\text{min}}\right) \frac{1 \text{ min}}{60 \text{ s}} \frac{1 \text{ m}}{100 \text{ cm}}}{\left(\frac{\pi}{4}\right)(0.6 \text{ cm})^2}\right)^2}{(2)\left(9.8 \frac{\text{m}}{\text{s}^2}\right)} = 0.5 \text{ m} \quad (\text{C-1})$$

where $h = 0.5 \text{ m}$ is the height difference between the pump and water surface level, and $v = 5 \times 10^{-4} \text{ m/s}$ is the velocity of the influent, calculated from the inlet diameter of 0.6 cm and influent flow rate of $0.85 \text{ cm}^3/\text{min}$. H_L is the headloss of the influent pumping.

The power and energy cost normalized to treated wastewater for influent pumping energy:

$$W_i = \rho g H_L Q = \left(1000 \frac{\text{kg}}{\text{m}^3}\right) \left(9.8 \frac{\text{m}}{\text{s}^2}\right) (0.5 \text{ m}) \left(0.85 \frac{\text{cm}^3}{\text{min}}\right) \frac{1 \text{ m}^3}{10^6 \text{ cm}^3} \frac{1 \text{ min}}{60 \text{ s}} \frac{1 \text{ W}}{\frac{1 \text{ kg m}^2}{\text{s}^3}}$$

$$= 7.0 \times 10^{-5} \text{ W} \quad (\text{C-2})$$

$$W_i^N = \frac{W_i}{Q} = \frac{(7.0 \times 10^{-5} \text{ W}) \frac{1 \text{ kW}}{1000 \text{ W}}}{\left(0.85 \frac{\text{cm}^3}{\text{min}}\right) \frac{1 \text{ m}^3}{10^6 \text{ cm}^3} \frac{60 \text{ min}}{1 \text{ h}}} = 0.0014 \frac{\text{kWh}}{\text{m}^3} \quad (\text{C-3})$$

where $H_L = 0.5 \text{ m}$ is the total headloss of the influent pumping, and $\rho = 1000 \text{ kg/m}^3$ is the density of the wastewater, and $Q = 0.85 \text{ cm}^3/\text{min}$ is the flow rate of influent, E_i represents the power required for influent pumping, and E_i^N is the normalized influent pumping energy cost for treating 1 m^3 wastewater.

2. Effluent pumping energy

The transmembrane pressure on day 75 was chosen for this calculation as this was at the end of phase 2 where the TMP increase remains slow and linear, although other pressures could similarly be used to make this calculation.

The energy for effluent pumping energy:

$$W_e = \Delta P Q = (9 \times 10^3 \text{ Pa}) \left(0.85 \frac{\text{cm}^3}{\text{min}}\right) \frac{1 \text{ m}^3}{10^6 \text{ cm}^3} \frac{1 \text{ min}}{60 \text{ s}} \frac{1 \frac{\text{kg}}{\text{m s}^2}}{1 \text{ Pa}} \frac{1 \text{ W}}{1 \frac{\text{kg m}^2}{\text{s}^3}} = 1.3 \times 10^{-4} \text{ W} \quad (\text{C-4})$$

$$W_e^N = \frac{W_e}{Q} = \frac{(1.3 \times 10^{-4} \text{ W}) \frac{1 \text{ kW}}{1000 \text{ W}}}{\left(0.85 \frac{\text{cm}^3}{\text{min}}\right) \frac{1 \text{ m}^3}{10^6 \text{ cm}^3} \frac{60 \text{ min}}{1 \text{ h}}} = 0.0026 \frac{\text{kWh}}{\text{m}^3} \quad (\text{C-5})$$

where $\Delta P = 9000 \text{ Pa}$ is the transmembrane pressure, and $\rho = 1000 \text{ kg/m}^3$ is the density of the wastewater, and $Q = 0.85 \text{ cm}^3/\text{min}$ is the effluent flow rate. E_e represents the power required for effluent pumping, and E_e^N is the normalized effluent pumping energy cost for treating 1 m^3 wastewater.

3. Recirculation pumping energy

The headloss of GAC fluidization:

$$\Delta P = g(\rho_c - \rho_g)(1 - \varepsilon)h = \left(9.8 \frac{\text{m}}{\text{s}^2}\right) \left[(1300 - 1000) \frac{\text{kg}}{\text{m}^3}\right] (1 - 0.75)(0.3 \text{ m}) \frac{1 \text{ Pa}}{1 \frac{\text{kg}}{\text{m s}^2}}$$

$$= 220.5 \text{ Pa} \quad (\text{C-6})$$

$$H_L = \frac{\Delta P}{\rho g} = \frac{(220.5 \text{ Pa}) \frac{1 \frac{\text{kg}}{\text{m}^3}}{1 \text{ Pa}}}{(1000 \frac{\text{kg}}{\text{m}^3})(9.8 \frac{\text{m}}{\text{s}^2})} = 0.0225 \text{ m} \quad (\text{C-7})$$

where $\rho_c = 1300 \text{ kg/m}^3$ is the density of the GAC particle, and $\rho_g = 1000 \text{ kg/m}^3$ is the density of the wastewater, and $h = 0.3 \text{ m}$ is the bed height in our reactor design, and $\varepsilon = \frac{\text{void volume}}{\text{void volume} + \text{media volume}} = 1 - \frac{\text{The settled bed height}}{\text{fluidized bed height}} = \frac{(30-7.5) \text{ cm}}{(30) \text{ cm}} = 0.75$ is the porosity of GAC fluidization, and ΔP presents the pressure drop caused by GAC fluidization, and H_L is the corresponding headloss.

The headloss of the two tee connectors calculated by Darcy–Weisbach equation (not included in the previous study) (K value derived from *Water Transmission and Distribution WSO: Principles and Practices of Water Supply Operations, 2014, page 114*):

$$H_L = K \frac{v^2}{2g} = K \frac{(Q/A)^2}{2g} = (2.4) \frac{\left(\frac{(250 \frac{\text{cm}^3}{\text{min}}) \frac{1 \text{ m}^3}{10^6 \text{ cm}^3} \frac{1 \text{ min}}{60 \text{ s}}}{(\frac{\pi}{4})(1.5 \text{ cm})^2} \right)^2}{(2)(9.8 \frac{\text{m}}{\text{s}^2})} = 7.1 \times 10^{-5} \text{ m} \quad (\text{C-8})$$

where $K = 2.4$ is the friction coefficient for tee connectors, and $v = 2.4 \text{ cm/s}$ is the recirculation velocity (calculated with the recirculation flow rate of $250 \text{ cm}^3/\text{min}$ and the crosssection diameter of 1.5 cm). H_L is the total headloss for the two tee connectors.

The headloss by flowing through the reactor estimated by Hazen-Williams Equation (not included in the previous study) (C value was obtained from *Optimal Design of Water Distribution Networks, 2004, page 116*):

$$H_L = \left(\frac{Q_r}{0.278CD^{2.63}} \right)^{\frac{1}{0.54}} L = \left(\frac{(250 \frac{\text{cm}^3}{\text{min}}) \frac{1 \text{ min}}{60 \text{ s}}}{(0.278 \frac{\text{m}^{0.37}}{\text{s}})(140)(1.5 \text{ cm} \frac{1 \text{ m}}{100 \text{ cm}})^{2.63}} \right)^{\frac{1}{0.54}} \quad (0.5 \text{ m})$$

$$= 4.8 \times 10^{-5} \text{ m} \quad (\text{C-9})$$

where $Q_r = 250 \text{ cm}^3/\text{min}$ is the recirculation flow rate of, and $D = 1.5 \text{ cm}$ is the diameter of the pipe, and $C = 140$ (assumed) is Hazen-Williams constant. H_L is the headloss due to GAC fluidization.

The energy for maintaining GAC fluidization was calculated as:

$$W_r = \rho g H_{L, \text{total}} Q_r$$

$$= \left(1000 \frac{\text{kg}}{\text{m}^3} \right) \left(9.8 \frac{\text{m}}{\text{s}^2} \right) (0.0225 \text{ m} + 7.1 \times 10^{-5} \text{ m} + 4.8 \times 10^{-5} \text{ m}) \left(250 \frac{\text{cm}^3}{\text{min}} \right) \frac{1 \text{ min}}{60 \text{ s}} \frac{1 \text{ m}^3}{10^6 \text{ cm}^3} \frac{1 \text{ W}}{1 \frac{\text{kg m}^2}{\text{s}^3}}$$

$$= 9.2 \times 10^{-4} \text{ W} \quad (\text{C-10})$$

$$W_r^N = \frac{W_r}{Q} = \frac{(9.2 \times 10^{-4} \text{ W}) (\frac{1 \text{ kW}}{1000 \text{ W}})}{(0.85 \frac{\text{cm}^3}{\text{min}}) \frac{1 \text{ m}^3}{10^6 \text{ cm}^3} \frac{60 \text{ min}}{1 \text{ h}}} = 0.019 \frac{\text{kWh}}{\text{m}^3} \quad (\text{C-11})$$

where $Q_r = 250 \text{ cm}^3/\text{min}$ is the recirculation flow rate, and $H_{L, \text{total}} = 0.0226 \text{ m}$ is the total headloss (calculated by summing up all the headloss), and $\rho = 1000 \text{ kg/m}^3$ is the density of the wastewater, , $Q = 0.85 \text{ cm}^3/\text{min}$ is the influent flow rate. E_r represents the power required for

recirculation pumping, and E_r^N is the normalized recirculation pumping energy cost for treating 1 m³ wastewater.

The influent and effluent pumping energy of AOFMBR and AeMBR were calculated with the same method as AFMBR. Influent pumping energy was estimated to be 0.0014 kWh/m³ for both reactors, and the effluent pumping energy, 0.0013 kWh/m³ (AOFMBR) and 0.0022 kWh/m³ (AeMBR) (TMP of 4.5 kPa in AOFMBR and 7.5 kPa in AeMBR, day 75).

The air blower energy was estimated using:

$$W_a = \rho g H_L Q_a = \left(1000 \frac{\text{kg}}{\text{m}^3}\right) \left(9.8 \frac{\text{m}}{\text{s}^2}\right) (0.3 \text{ m}) \left(240 \frac{\text{cm}^3}{\text{min}}\right) \frac{1 \text{ min}}{60 \text{ s}} \frac{1 \text{ m}^3}{10^6 \text{ cm}^3} \frac{1 \text{ W}}{1 \frac{\text{kg m}^2}{\text{s}^3}}$$

$$= 0.012 \text{ W} \quad (\text{C-12})$$

$$W_a^N = \frac{W_a}{Q} = \frac{(0.012 \text{ W}) \left(\frac{1 \text{ kW}}{1000 \text{ W}}\right)}{\left(0.85 \frac{\text{cm}^3}{\text{min}}\right) \frac{1 \text{ m}^3}{10^6 \text{ cm}^3} \frac{60 \text{ min}}{1 \text{ h}}} = 0.24 \frac{\text{kWh}}{\text{m}^3} \quad (\text{C-13})$$

where $P = 30 \text{ cm}$ is the head at air inlet, and $Q_a = 240 \text{ cm}^3/\text{min}$ is the air flow rate, and $Q = 0.85 \text{ cm}^3/\text{min}$ is the flow rate. E_a represents the power required for air blowing, and E_a^N is the normalized energy cost of aeration for treating 1 m³ wastewater.

Table C-S1 The effluent COD, SCOD and removal efficiencies (average \pm SD) for the three reactors in the 131-day of operation for the four phases.

		COD (mg/L)	SCOD (mg/L)	COD removal (%)	SCOD removal (%)
Phase 1	AOFMBR	18 \pm 7	17 \pm 8	88 \pm 4	80 \pm 9
	AeMBR	22 \pm 8	20 \pm 8	86 \pm 5	77 \pm 9
	AFMBR	24 \pm 10	22 \pm 8	84 \pm 6	75 \pm 11
Phase 2	AOFMBR	18 \pm 7	17 \pm 8	90 \pm 3	82 \pm 2
	AeMBR	22 \pm 8	20 \pm 8	84 \pm 4	76 \pm 7
	AFMBR	24 \pm 10	22 \pm 8	90 \pm 3	82 \pm 7
Phase 3	AOFMBR	18 \pm 7	17 \pm 8	91 \pm 2	86 \pm 3
	AeMBR	22 \pm 8	20 \pm 8	87 \pm 3	80 \pm 5
	AFMBR	24 \pm 10	22 \pm 8	83 \pm 3	85 \pm 6
Phase 4	AOFMBR	18 \pm 7	17 \pm 8	93 \pm 2	88 \pm 3
	AeMBR	22 \pm 8	20 \pm 8	88 \pm 3	80 \pm 4
	AFMBR	24 \pm 10	22 \pm 8	85 \pm 3	76 \pm 5

Table C-S2 Examination of whether the effluent CODs among the reactors (AF-AFMBR, AO-AOFMBR, MBR-AeMBR) were significantly different. When p values (based on the Student's T-test) were smaller than 0.03, the effluents were not considered to be significantly different. Comparisons are made on the data shown in Figure 5-1.

	AF/AO	AO/MBR	AF/MBR
Phase 1	0.03	0.09	0.22
Phase 2	0.007	0.40	0.001
Phase 3	<0.001	0.002	0.002
Phase 4	<0.001	<0.001	0.002

Reference

Ren, L., Ahn, Y., Logan, B.E., 2014. A two-stage microbial fuel cell and anaerobic fluidized bed membrane bioreactor (MFC-AFMBR) system for effective domestic wastewater treatment. *Environ. Sci. Technol.* 48, 4199–4206.

Appendix D

Simultaneous nitrogen and organics removal using membrane aeration and effluent ultrafiltration in an anaerobic fluidized membrane bioreactor

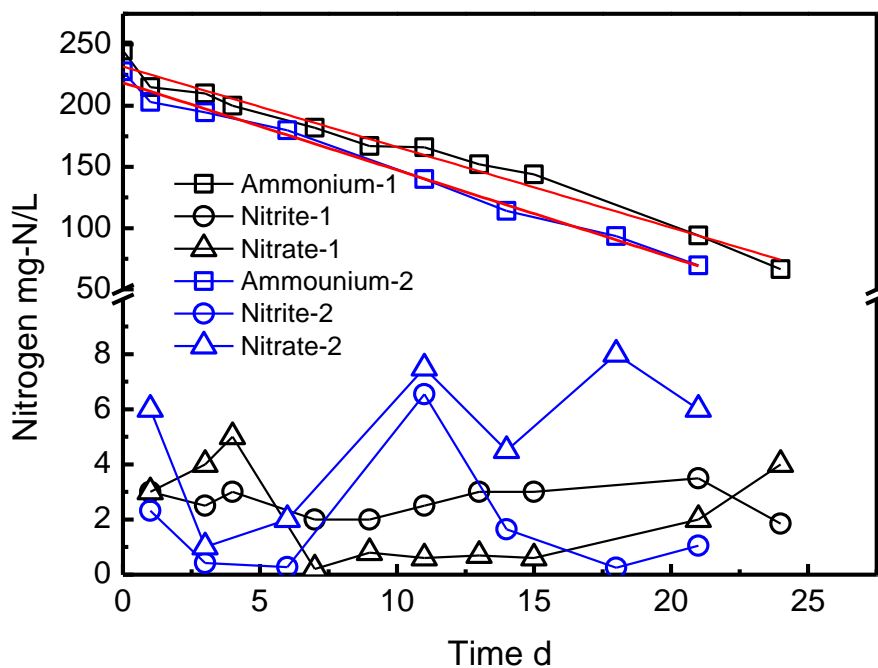


Fig. D-S1 The ammonia, nitrate and nitrite concentration in phase 1B-HN (batch mode repeated two times, synthetic wastewater with 236 ± 9 mg-N/L)

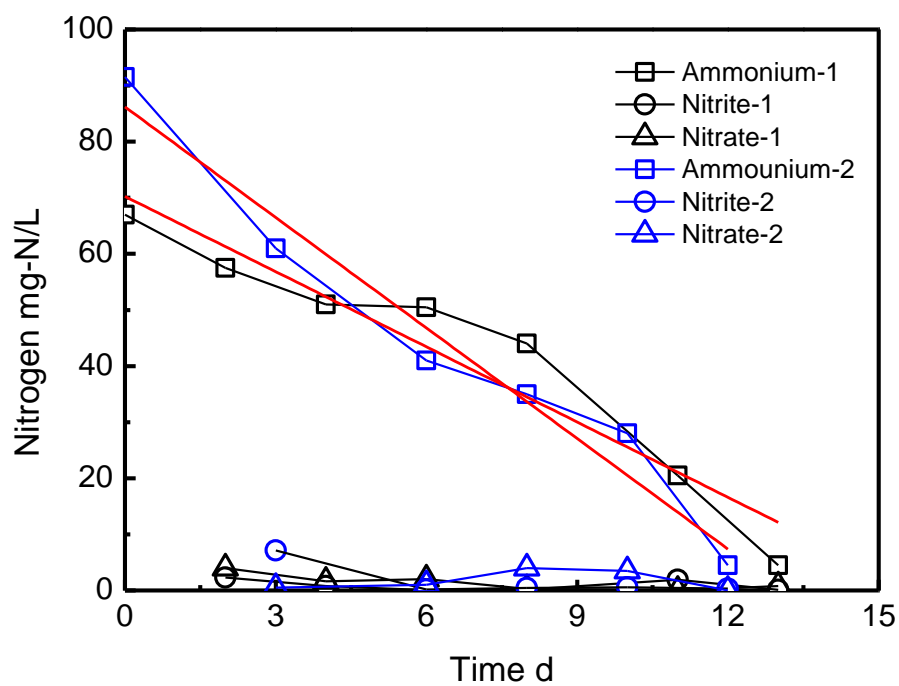


Fig. D-S2 Ammonia, nitrate and nitrite concentration in phase 2B-LN (batch mode repeated two times, COD-free synthetic wastewater with 79 ± 11 mg-N/L)

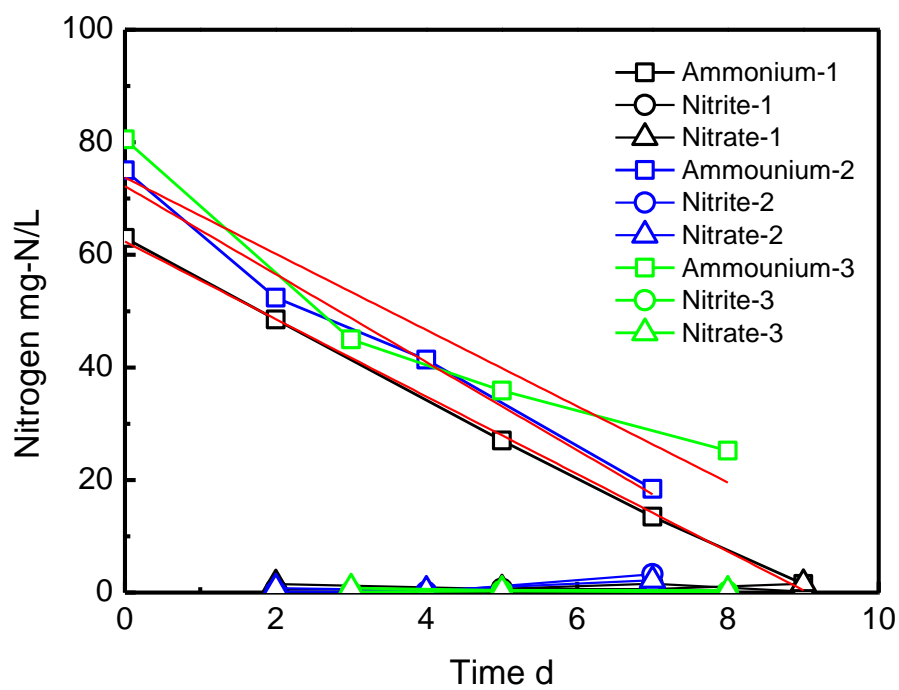


Fig. D-S3 Ammonia, nitrite and nitrate concentration in phase 3B-SG (batch mode repeated three times, synthetic wastewater with 73 ± 7 mg-N/L)

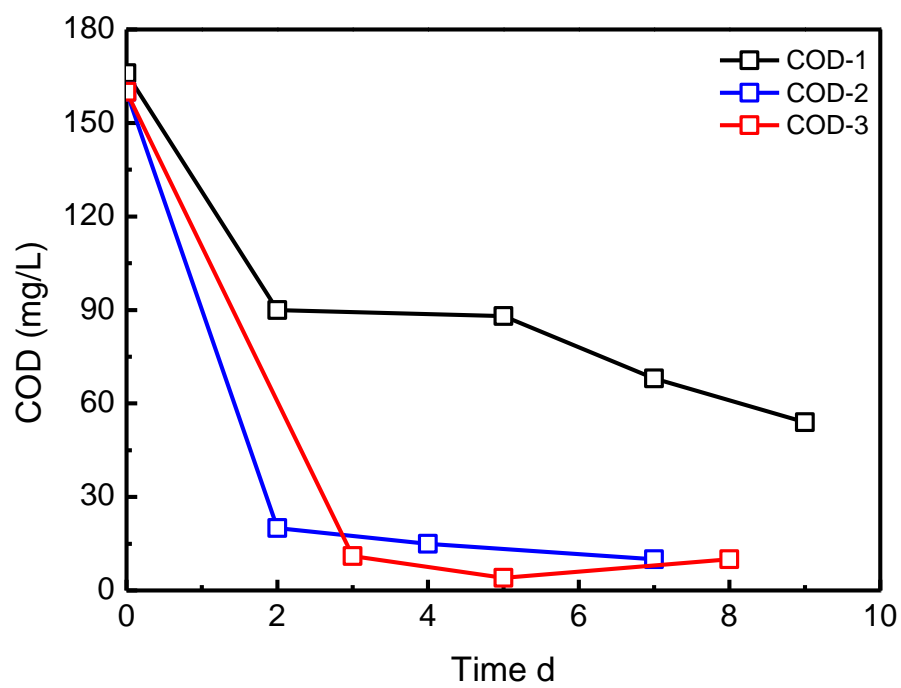


Fig. D-S4 Triplicate COD removal test in phase 3B-SG.

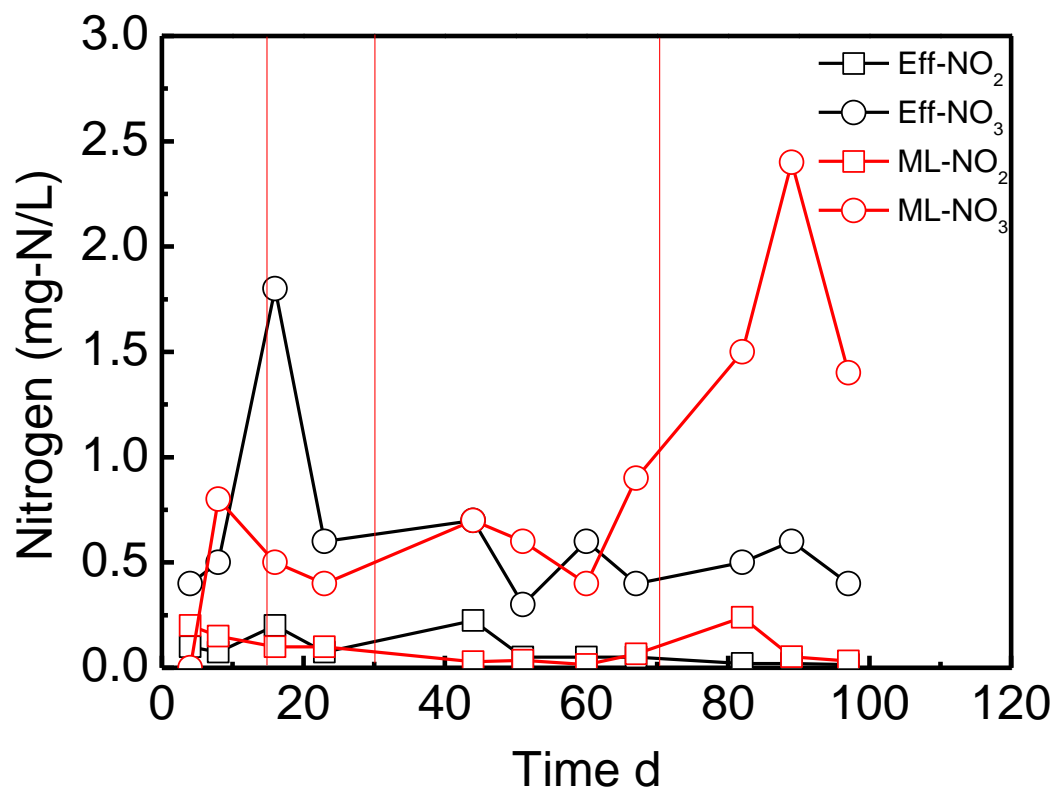


Fig. D-S5 Nitrite and nitrate concentrations in the effluent and mixed liquor (ML) during continuous flow operation (phases 4C-SGU, 5C-WGU and 6C-WGUP).

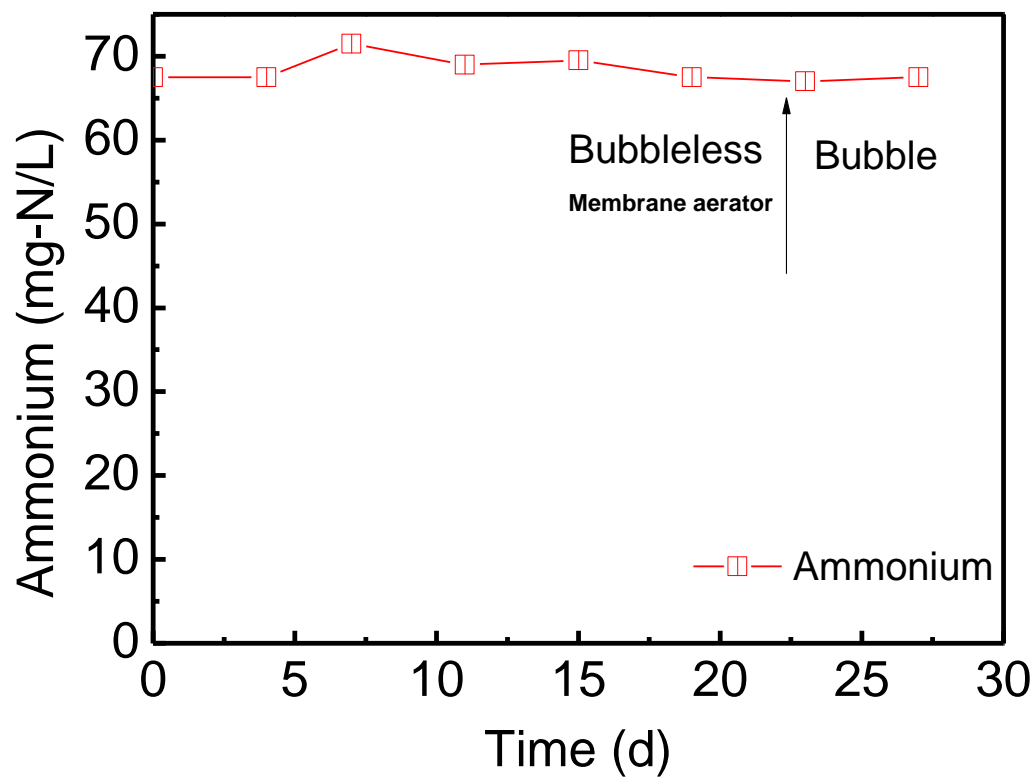


Fig. D-S6 Bubbleless and bubble abiotic air stripping test.

VITA

Yaoli Ye

Education

B.S. Energy and Environment Systematic Engineering, Zhejiang University, China, 2007–2011

M.S. Thermal Engineering, Zhejiang University, China, 2011–2014

Ph.D. Environmental Engineering, The Pennsylvania State University, USA, 2014–present

Journal publications

Cheng, S., Ye, Y., Ding, W., & Pan, B. (2014). Enhancing power generation of scale-up microbial fuel cells by optimizing the leading-out terminal of anode. *Journal of Power Sources*, 248, 931-938.

Ye, Y., Zhu, X., & Logan, B. E. (2016). Effect of buffer charge on performance of air-cathodes used in microbial fuel cells. *Electrochimica Acta*, 194, 441-447.

Ye, Y., LaBarge, N., Kashima, H., Kim, K. Y., Hong, P. Y., Saikaly, P. E., & Logan, B. E. (2016). An aerated and fluidized bed membrane bioreactor for effective wastewater treatment with low membrane fouling. *Environmental Science: Water Research & Technology*, 2(6), 994-1003.

Ye, Y., Pascal E. Saikaly, and B. E. Logan. "Simultaneous nitrogen and organics removal using membrane aeration and effluent ultrafiltration in an anaerobic fluidized membrane bioreactor." *Bioresource Technology* (2017). *Accepted*.

Conference presentations

An aerated and fluidized bed membrane bioreactor for effective wastewater treatment with low membrane fouling. Oral in the 88th Pennsylvania Water Environment Association Annual Technical Conference, The Pennsylvania State University, University Park, PA, USA, June, **2016**.

Honors and Awards

2016 PennTec 88 th Annual Technical Conference & Exhibition, Student research award

2014 National scholarship for graduate students

2014 Outstanding graduates in Zhejiang Province

2012 Chen Kefa second-grade scholarship, Zhejiang University